Global-local separated representations based on the Proper Generalized Decomposition

Carlos Sandino de Benito

UNIVERSITE BRETAGNE SCIENCES LOIRE POUR L'INGENIEUR

CENTRALE NANTES

THESE DE DOCTORAT DE

L'ÉCOLE CENTRALE DE NANTES
COMUE UNIVERSITE BRETAGNE LOIRE

ECOLE DOCTORALE N° 602
Sciences pour l'Ingénieur
Spécialité : *Mécanique des Solides, des Matériaux, des Structures et des Surfaces*

Par
Carlos SANDINO

Global-local separated representations based on the Proper Generalized Decomposition

Thèse présentée et soutenue à Nantes, le 13/12 /2019
Unité de recherche : EA 7471, Institut de Calcul Intensif (ICI)

Rapporteurs avant soutenance :

Amine AMMAR	Professeur des Universités, ENSAM Angers
Pierre JOYOT	Maître de Conférences, ESTIA

Composition du Jury :

Président :	Mazen SAAD	Professeur des Universités, Ecole Centrale de Nantes
Examinateurs :	Amine AMMAR	Professeur des Universités, ENSAM Angers
	Marianne BERINGHIER	Maître de Conférences, ISAE-ENSMA
	Pierre JOYOT	Maître de Conférences, ESTIA
	Mazen SAAD	Professeur des Universités, Ecole Centrale de Nantes
Invitée :	Luisa SILVA	Chargé de Recherche HDR, Ecole Centrale de Nantes
Dir. de thèse :	Francisco CHINESTA	Professeur des Universités, Arts et Métiers ParisTech
Co-encadrant de thèse :	José Vicente AGUADO	Ingénieur de Recherche, Ecole Centrale de Nantes

Contents

Table of figures

Introduction

The Proper Generalized Decomposition (PGD) has emerged as an alternative approach for building separated representations which are obtained through the use of *a priori* unknown functions of the coordinates of the problem. It represents a successful method for calculating approximations of solutions of multidimensional problems due to the fact that it involves an important decrease on the numerical complexity when compared to solving a full-model, as it reduces considerably the degrees of freedom of the problem.

One of the main advantages of the PGD method, with respect to other model reduction methods, lies in its adequacy to compute space separated representations in Cartesian-like domains. For instance, the PGD space separated representation allow calculating 3D high-fidelity solutions of plate or shells while keeping a computational complexity characteristic of 2D solvers. It seems appropriate to focus this numerical tool on the development of new approaches that allow us to improve its performance for more complex geometries. The main objective of this thesis is to generalize space separated representations to non-Cartesian domains, by introducing the notion of Global-Local separated representations. Global-Local separated representations are constructed by carrying out a partition of the domain into subdomains and can be understood as a multiplicative decomposition in which the local modes capture the solution at the finer scale, while the global modes solve the coarser scale. In other words, the solution can be obtained by particularising a generic local solution for every subdomain of the partition.

Although this thesis is only concerned with the numerical analysis and implementation of the proposed technique, numerous applications of engineering interest can be devised. For instance, this space separation scheme could be an interesting alternative method when addressing multi-scale models defined in fractal geometries, laminates and multi-fibre models in composite manufacturing, models with local features of interest, or models containing inclusions or different materials along the domain.

Chapter 1 introduces the basics of Model Order Reduction (MOR) by carrying out a summarised definition of several well-known techniques. More specifically, after a short review of *a posteriori* MOR techniques, the Proper Generalized Decomposition, is described and discussed.

Once the fundamentals of MOR techniques and more specifically, the PGD, have been introduced, Chapter 2 is devoted to review the state of the art on the use of MOR to compute space separated representations. The motivation of the thesis is also presented in this chapter, stressing the necessity of a new separation scheme. To this aim, two strategies are proposed.

The first proposal is presented in Chapter 3, which is dedicated to a new Global-Local PGD procedure for partitioned domains. This methodology is based on the partition of unity and its objective is to enrich coarse meshed FEM solutions by using the PGD approach. It builds a separated representation that provides the local enrichment, without neither the use of a priori knowledge of the solution nor the implementation of auxiliary local problems to determine the enrichment. To this aim, the construction of the PGD separated representation is carried out by means of two PGD variables defined over the global and local levels. The first PGD variable (global) is defined over the coarse mesh described by the domain partition. The other PGD variable (local) represents the enrichment and is defined over a fine meshed support. Thus, by satisfying the partition of unity, the coupling of both discretization levels allows this enrichment to be reproduced along the whole domain.

In order to address the need of incorporating MOR techniques into pre-existing simulation platforms, a second strategy is introduced in Chapter 4. This proposal is devoted to a less intrusive Global-Local PGD scheme. The starting point of this PGD is the use of discrete operators which are assembled by means of standard mesh-based techniques in order to use the PGD as an algebraic iterative solver. Continuity on the boundaries of the partition does not need to be imposed explicitly, as it comes as a built-in property of the discrete operators.

Chapter 1

Basics of Model Order Reduction methods

The use of Model Order Reduction (MOR) methods has emerged from the need of dealing with new challenges in science and engineering, for which the use of standard mesh-based methods may fail. MOR methods represent a good alternative for solving multiparametric and multidimensional problems, in order to decrease the computational burden, mainly due to the high number of degrees of freedom in such higher dimensional spaces. In this chapter, a summarised definition of several well-known techniques is carried out in order to describe the fundamentals of the Model Order Reduction (MOR). More specifically, after a short review of *a posteriori* MOR techniques, the Proper Generalized Decomposition, which is the primary focus of this thesis, is described and discussed.

Contents

1.1 Some limitations of standard discretization techniques

Numerical simulation is widely used for solving problems in engineering that involve physics phenomena, and whose behaviour can be described by means of partial differential equations (PDE). This kind of engineering problems includes structural analysis, heat transfer, electromagnetism, fluid flow, mass transport, among many others.

Many numerical methods have been proposed over the last decades. All of them are based on the notion of *discretization*, that is, writing a discrete set of equations that solve the original continuous model approximatively. Generally speaking, the accuracy of the solution increases as the number of degrees of freedom grows, whether they are mesh-based methods, meshless methods or particle methods. Therefore, the computational burden can become in many cases a remarkable limitation. Due to this issue, simulation requires very often a relatively large amount of computing resources. The impressive progress of high performance computing platforms represents a good alternative for alleviating this issue [35, 36, 102]. However, in this thesis we explore MOR as a means of devising more efficient representations of the solution.

Some of the challenges of numerical simulation with standard discretization techniques are:

- **Solving problems defined over a high-dimensional space or multi-parametric problems**. High-dimensional models, such as models defining quantum chemistry [24, 69] or kinetics of complex fluids [15], suffer the concept of the *curse of dimensionality* [11]: the computational complexity increases exponentially as the problem dimensions do. If we want to solve a problem defined over a space domain of dimension N by using a mesh-based discretization method with M nodes along each coordinate, the total number of nodes of the problem reaches M^N. The *curse of dimensionality* also occurs when addressing multi-parametric models [20, 57, 90], for which the number of parameters under consideration constitutes a major limitation.

- **Problems defined over degenerated geometries**, i.e. at least one of the characteristic dimensions of the problem is several orders of magnitude smaller than the other dimensions. This is the case of bar, plate or shell geometries, commonly used in structures. Some well-known hypotheses allow the domain to be turned into a lower dimension problem, which can be solved easily. However, for complex geometries such simplification cannot be carried out, and therefore, they usually require of extremely fine meshes that may increase considerably the complexity of the problem.

- **Multi-scale problems**. Regarding space domains, it is difficult to address different scales in order to achieve an accurate solution, for instance, in problems consisting

of metamaterials whose structure is defined at the microscale. In order to deal with these problems, several methods have been implemented, like the homogenization [81]. Moreover, when considering models whose spectrum of characteristic times is extremely wide, standard incremental discretization techniques can yield very time-consuming simulations: such as reaction-diffusion models of the degradation of plastic materials [43], processes involving microwaves [65, 101, 110] or ultrasounds or solid mechanics models with strongly non-linear and coupled constitutive equations involving many scales and different characteristic times.

- **The need of real-time simulation**: applications such as augmented reality [9, 54, 55], haptic surgery applicators [33, 77, 86, 98, 99, 118] control, manufacturing identification or reconfiguration of malfunctioning systems.

The Finite Element Method (FEM) will be used as a reference method throughout the entire thesis. This choice is motivated by the fact that FEM has become a *de facto* standard for numerical simulation in many industrial sectors. Also, we will consider the question of intrusiveness, i.e. how to integrate the MOR methods developed in this thesis, into the existing finite element codes.

1.2 Model Order Reduction

Model Order Reduction (MOR) provides a mathematical basis to reduce the numerical complexity of the model at hand. It is based on the idea of replacing standard approximation spaces by appropriate low-dimensional approximations. This approximation should able to capture the features of interest of a solution obtained with a high-fidelity simulation tool while satisfying the accuracy requirements and preserving basic properties of the original systems, such as consistency, stability and convergence.

MOR methods can be classified according to the need to be fed with a simulation database to build the lower approximation space or not:

- ***A posteriori* methods**. The construction of the reduced-order model is carried out after computing a relatively low amount of solutions obtained by a high-fidelity model. The Proper Orthogonal Decomposition [26, 71, 93] and the Reduced Basis Methods [74, 96] are the most representative *a posteriori* techniques.

- ***A priori* methods**. The approximate solution of the full model is not required to build the reduced model. The Proper Generalized Decomposition [5, 29, 30, 32], which is largely analysed in this thesis, is included in this class.

1.2.1 *A posteriori* techniques

1.2.1.1 The Proper Orthogonal Decomposition (POD)

The Proper Orthogonal Decomposition (POD) is a MOR technique that constructs an approximate description of high-dimensional problems which lies in a much lower dimension with respect to the original problem. It is built by taking advantage of previously computed samples of the high-fidelity solution, from which a reduced orthogonal basis is extracted. This method is also known as the Principal Component Analysis (PCA) [58], the Karhunen-Loève Decomposition (KLM) [72] or the Singular Value Decomposition (SVD), and has been widely used in problems concerning heat transfer simulation [14], Navier-Stokes flows [21], chemistry [91], among others.

For instance, we can assume a problem represented by an elliptic PDE and defined over a parametric domain (for a parameter μ). We can write the usual notation of computational mechanics for the weak form, based on [1], in order to find $u \in V$ (an appropriate approximation space), such that:

$$a(\mu; u, w) = f(\mu; w) \tag{1.1}$$

for every $w \in V$ and the parameter $\mu \in I_\mu$. Bilinear and linear forms are denoted by $a(\,\cdot\,,\,\cdot\,) : V \times V \to \mathbb{K}$ and $f(\,\cdot\,) : V \to \mathbb{K}$, respectively. The objective of the POD is to obtain a solution of the parametric problem that can be expressed in a low-dimension separated representation described as:

$$u(\mu) \approx \sum_{i=1}^{M} \alpha_i(\mu)\Phi_i \tag{1.2}$$

where $\alpha_i(\mu)$ is a parameter-dependent coefficient for each mode and $\{\Phi_i\}_{i=1}^{M}$ is a set of orthogonal basis vectors extracted from a database of pre-computed solutions of the original, high-fidelity model. The POD forms a subspace $\mathcal{S} := \operatorname{span}\{\phi_i\}_{i=1}^{M}$ whose dimension is expected to be considerably smaller than that of the original model.

The starting point of this technique is the sampling, i.e the extraction of the snapshots representing a certain amount of solutions of the problem [53]. The selection of an appropriate set of snapshots determines the capability of reproducing the original solution by using the orthonormal basis. A collection of m snapshots is denoted as $\{U_i\}_{i=1}^{m}$. The scalar product between elements of V is denoted as $\langle\ ,\ \rangle_V$. By removing the mean, the snapshot collection can be written as $\{\hat{U}_i\}_{i=1}^{m}$, where $\hat{U}_i = U_i - U_{\text{mean}}$.

The POD basis is the orthonormal set $\Phi_M = \{\Phi_1 \cdots \Phi_M\}$ (with $M \leq m \ll n$). The elements of the basis are ordered as the decreasing sequence of the squared of their corresponding singular values that minimizes the sum of the squared projection errors ε_{POD} over

all the orthonormal sets $[\phi_1 \cdots \phi_M]$ of $\mathcal{S}$ ($\langle \phi_k, \phi_l \rangle_V = \delta_{kl}$):

$$\Phi_M = \arg \min_{\phi_1 \cdots \phi_M} \sum_{j=1}^{m} \left\| \hat{U}_j - \sum_{j=1}^{M} \left\langle \hat{U}_j, \phi_j \right\rangle_V \phi_j \right\|_V^2 \tag{1.3}$$

It can be shown that the optimum value of the above functional corresponds to:

$$\varepsilon_{POD} = \sum_{j=M+1}^{m} \sigma_j^2, \tag{1.4}$$

σ_j being the j-th singular value associated with the singular vectors not included in the basis. Moreover, the truncation error, i. e. the value used to determine the order of the orthonormal basis ($M \leq m$), can be defined by:

$$\epsilon_{POD} = \frac{\sum_{j=M+1}^{j=m} \sigma_j^2}{\sum_{j=1}^{j=m} \sigma_j^2}. \tag{1.5}$$

It is important to remark the difference between this relative error and the error with respect to the full model solution. The error committed via truncation represents the amount of precomputed information that is not taken into consideration by choosing the first M components of the reduced basis. The error with respect to the full model will depend on the capability of the snapshots to capture the essential characteristics of the high-fidelity solution, which reveals the importance of choosing an appropriate sampling technique.

Once the reduced basis Φ_M has been extracted, the parameter-dependent coefficients $\{\alpha_i(\mu)\}_{i=1}^{M}$ can be easily obtained by using a Galerkin projection of the full problem (Eq. (1.1)) onto the reduced subspace:

$$\sum_{i=1}^{M} a(\mu; \Phi_i, \Phi_j)\, \alpha_i(\mu) = f(\mu; \Phi_j), \quad \forall j. \tag{1.6}$$

The solution provided by the POD is the best approximation that can be obtained by using the previously computed information, which means that the main challenge of POD-based techniques lies in selecting appropriate sampling methods that capture the necessary information. If the snapshots are not able to capture all the details related to the full-model solution, the reduced basis will not be accurate enough to reproduce an approximate solution for the whole required parameter range.

1.2.1.2 The Reduced Basis Method (RBM)

The Reduced Basis Method [75, 96] is a technique that follows the approach of the POD and addresses the limitations of this method. It introduces a more efficient sampling strategy

that updates the reduced basis by introducing the concept of the error estimator. In order to illustrate this technique, we can assume a reduced basis extracted from problem Eq. (1.1), already consisting of M terms, as follows:

$$\Phi = \{\Phi_1, \cdots, \Phi_M\}. \tag{1.7}$$

In order to expand the reduced basis, the calculation of the residual obtained with the approximated solution provided by the basis Φ is carried out:

$$r_M(\mu) = \sum_{i=1}^{M} a(\mu; \Phi_i, w)\alpha_i(\mu) - f(\mu; w), \tag{1.8}$$

for $w \in V$ (with V representing the space of the high-fidelity problem).

The norm of the residual can be defined as the error indicator for this technique, which will actually guide the sampling process. If both the bilinear form $a(\ ,\ )$ and the linear form $f(\ )$ are affine with respect to the parameter μ, it can be shown that the norm of the residual can be computed at a small computational cost (the operators can be precomputed offline). Therefore, the residual can be easily calculated for the so-called *train points*, covering the whole range of μ. It is important to remark that the residual norm is the simplest error indicator, but other techniques, such as the Successive Constraint Method (SMC), have been developed in order to obtain better error estimators in the framework of the RBM. The interested reader can refer to [27, 60, 61].

Once the residual has been evaluated for the train points, the objective is to identify the value for which this estimator is maximized, as follows:

$$\tilde{\mu} = \arg \max_{\mu \in \mathcal{P}_{train}} \|r_M(\mu)\|^2. \tag{1.9}$$

Then, the solution is evaluated for $\tilde{\mu}$ using the high-fidelity model. This computed solution $u(\tilde{\mu})$ is the new snapshot, which is added to the reduced basis as a new term, usually orthogonalized with respect to the previous elements of the basis using a Gram-Schmidt procedure.

1.2.2 *A priori* techniques: The Proper Generalized Decomposition (PGD)

The approximate solutions provided by *a posteriori* model order reduction techniques have involved an important advance in terms of computational cost and solving parametric problems. Nevertheless, the need for precomputed data for constructing the reduced basis is an important impediment to the application of these techniques in problems with a lack of previous knowledge.

Regarding *a priori* techniques, low-rank tensor approximations constitute a family of increasingly popular techniques due to its generality and success in science and technology.

The interested reader can refer to [51] for a list of applications. This approximation includes Canonical [25, 56], Tucker [111] and Hierarchical Tucker [52] representations, among others.

Another interesting technique that avoids the knowledge of information concerning the full-model solution and represents the main focus of this thesis is the Proper Generalized Decomposition (PGD). This method [5, 29, 30, 32] has emerged as an alternative approach for building separated representations which are obtained through the use of *a priori* unknowns functions of coordinates of the problem.

The PGD is based on previous works developed by Ladevèze [67, 68, 85, 88, 92], who proposed an approach to build space-time separated representations for transient problems in the LATIN solver framework (Non-linear Large Time Increment). These separated representations can be defined as

$$u(\mathbf{x}, t) \approx \sum_{i=1}^{M} X_i(\mathbf{x}) T_i(t), \tag{1.10}$$

where the solution can be approximated by a finite sum of functional products depending on the geometric coordinates of the problem ($X_i(\mathbf{x})$) and the time ($T_i(t)$).

Based on this approach, the PGD authors proposed a separated representation based on Eq. (1.10), where the approximated solution of the unknown field $u(x_1, \ldots, x_d)$ can be represented as

$$u(x_1, \ldots, x_d) \approx \sum_{i=1}^{M} F_i^1(x_1) \times \cdots \times F_i^d(x_d) \tag{1.11}$$

where now, the functions $F_i^1(x_1), \ldots, F_i^d(x_d)$ are unknown *a priori*. These functions are defined over the domains Ω_i where each coordinate of the problem is defined (geometric coordinates, time, material properties, boundary conditions...), building a parametric space where the solution can be represented and avoiding the exponential complexity with respect to the problem dimensions. The PGD obtains the solution by splitting the full-model problem into d lower dimension problems defined over each coordinate.

In summary, the main advantages of the PGD are:

- The PGD approximated solution is obtained by constructing a separated representation from *a priori* unknown functions.
- The separated representation of the solution is built by the successive addition of new terms (enrichments) to the finite sum, i.e. the approximation space is enriched in every step.
- The parameters of the problem can be added as extra coordinates.
- The separated representation of the parametric solution is computed offline, which means that the online phase only concerns the particularization for the desired set of parametric values.

- There is an important decrease in the numerical complexity of the PGD when compared to solving a full-model. Using a standard mesh-based discretization technique for a problem defined over d dimensions with n nodes for each dimension, the number of degrees of freedom is n^d. For a PGD separated representation consisting of M terms, the number of unknowns is $M \times n \times d$.

1.2.2.1 PGD formulation

The PGD can be applied to a PDE system defined over a multi-dimensional domain consisting of several coordinates. In this illustrative case, and for the sake of clarity, we develop the PGD formulation for a generic problem with two separated coordinates, denoted by μ_1 and μ_2. We consider a generic variational formulation, as in Eq. (1.1):

$$a(u, v) = b(w), \tag{1.12}$$

where the objective is to find $u \in V := V_{\mu_1} \otimes V_{\mu_2}$ (a tensor product space), for every $w \in V$.

The aim of the PGD is to compute an approximation of the solution of the problem represented by Eq. (1.12), in the form of a separated representation. If we consider that this approximation is defined as a sum of M functions products of unknown functions depending on the coordinates μ_1 and μ_2 (separated representation of order M), it can be written following Eq. (1.11):

$$u(\mu_1, \mu_2) \approx \sum_{i=1}^{M} u_i^{\mu_1} u_i^{\mu_2}, \tag{1.13}$$

where $u_i^{\mu_1}$ and $u_i^{\mu_2}$ are the pair of functions that the PGD computes in every enrichment (also called *modes*). In other words, these modes build the basis in which the approximated solution is represented. For this purpose, two finite dimensional approximation spaces are defined from the modes:

$$V_{\mu_1} := \text{span}\left\{ v_i^{\mu_1} = \frac{u_i^{\mu_1}}{\|u_i^{\mu_1}\|}, 1 \leq i \leq M \right\} \quad \textit{and} \quad V_{\mu_2} := \text{span}\left\{ v_i^{\mu_2} = \frac{u_i^{\mu_2}}{\|u_i^{\mu_2}\|}, 1 \leq i \leq M \right\}, \tag{1.14}$$

both of dimension M. Thus, we can introduce the following subset of the tensor product space $V := V_{\mu_1} \otimes V_{\mu_2}$:

$$S_M := \left\{ v \in V : \quad v = \sum_{i=1}^{M} \alpha_i v_i^{\mu_1} v_i^{\mu_2}, \quad \textit{with} \quad v_i^{\mu_1} \in V_{\mu_1}, v_i^{\mu_2} \in V_{\mu_2} \quad \alpha_i \in \mathbb{K} \right\}. \tag{1.15}$$

We can denote u^M, the rank-M separated representation of the solution, as an element of S_M. The concept of PGD enrichment lies in the progressive construction of S_M, as it is obtained from the previous approximation subspace, i.e. $S_M = S_{M-1} + S_1$ (for $M \geq 2$), and consequently, the approximation spaces are nested, i.e. $S_{M-1} \subset S_M$. Hence, when a new pair of functions (u^{μ_1}, u^{μ_2}) are computed, their corresponding approximation spaces

V_{μ_1} and V_{μ_2} are updated by normalizing these new functions. The enriched approximation of the solution, obtained from u^M, reads:

$$u^{M+1} = u^M + u^{\mu_1} u^{\mu_2} = \sum_{i=1}^{M+1} \alpha_i v_i^{\mu_1} v_i^{\mu_2}. \tag{1.16}$$

This update is obtained by solving:

$$a(u^{\mu_1} u^{\mu_2}, w) = r(u^M, w) = b(w) - a(u^M, w), \tag{1.17}$$

for every $w \in V$. As the calculation of both u^{μ_1} and u^{μ_2} represents a non-linear problem, assuming an elliptic problem, Eq. (1.17) can be turned into an equivalent non-linear optimization problem:

$$\min_{u_s, u_\mu} \mathcal{J}(u^{\mu_1}, u^{\mu_2}) := \frac{1}{2} a(u^{\mu_1} u^{\mu_2}, u^{\mu_1} u^{\mu_2}) - r(u^M, u^{\mu_1} u^{\mu_2}). \tag{1.18}$$

The strategy for obtaining the new pair of functions is illustrated in Section 2. Its convergence has been proven in [42] for different types of problems, as well as the compactness of the solution, as the PGD generalizes POD in some cases.

1.3 Algebraic formulation of the PGD

For reasons that will be made clear in Chapter 4, we give here also an algebraic formulation of the PGD method [1]. To this end, we will make use of tensor product spaces to formulate the problem. Given $V_{\mu_1} := \text{span}\left\{v_{1\leq i\leq m}^{\mu_1}\right\}$ and $V_{\mu_2} := \text{span}\left\{v_{1\leq j\leq n}^{\mu_2}\right\}$, the tensor product space defined by both spaces is

$$V := \text{span}\left\{v_i^{\mu_1} v_j^{\mu_2}, \quad for \quad 1 \leq i \leq m \quad and \quad 1 \leq j \leq n\right\}, \tag{1.19}$$

and therefore, an element of the space V can be obtained as follows:

$$u = \sum_{i=1}^{m} \sum_{j=1}^{n} u_{ij} v_i^{\mu_1} v_j^{\mu_2}, \tag{1.20}$$

where u_{ij} are the weights. Now, we can apply the Galerkin method to Eq. (1.12), with the consequent discretization of the problem. Eq. (1.12) can be rewritten as:

$$\langle A(u), w\rangle = \langle b, w\rangle, \tag{1.21}$$

where $\langle \cdot, \cdot \rangle$ denotes an inner product on V, A is a linear operator defined by $A : V \to V$ and b is an element of V. Using a Galerkin approach, where w is approximated in the same

tensor space as the solution, the terms of Eq. (1.21) are rewritten as:

$$\begin{aligned}\langle A(u), w\rangle &= \sum_{i=1}^{m}\sum_{j=1}^{n}\sum_{k=1}^{m}\sum_{l=1}^{n} u_{ij}\left\langle A(v_i^{\mu_1}v_j^{\mu_2}), v_k^{\mu_1}v_l^{\mu_2}\right\rangle w_{kl}\\ \langle b, w\rangle &= \sum_{i=1}^{m}\sum_{j=1}^{n}\sum_{k=1}^{m}\sum_{l=1}^{n} b_{ij}\left\langle v_i^{\mu_1}v_j^{\mu_2}, v_k^{\mu_1}v_l^{\mu_2}\right\rangle w_{kl}\end{aligned} \tag{1.22}$$

Example 1.1 (*Structure of the problem*). W e can consider that A is the laplacian operator, s represent the space coordinates and the parameter d is the diffusivity coefficient ($A(\,\cdot\,) = \lambda\,\Delta(\,\cdot\,)$). Then, for $1 \le i, k \le m$ and $1 \le j, l \le n$ we have

$$\begin{aligned}\langle A(v_i^s v_j^\lambda), v_k^s v_l^\lambda\rangle = \langle \Delta v_i^s, v_k^s\rangle_s \langle \lambda v_j^\lambda, v_l^\lambda\rangle_\lambda \quad &\rightsquigarrow \quad \boldsymbol{K}_s \otimes \boldsymbol{D}_\lambda,\\ \langle v_i^s v_j^\lambda, v_k^s v_l^\lambda\rangle = \langle v_i^s, v_k^s\rangle_s \langle v_j^\lambda, v_l^\lambda\rangle_\lambda \quad &\rightsquigarrow \quad \boldsymbol{M}_s \otimes \boldsymbol{M}_\lambda,\end{aligned} \tag{1.23}$$

where $\boldsymbol{K}_s$, $\boldsymbol{M}_s$ are the diffusion (laplacian-like) matrix and the mass matrix in the physical domain, respectively. $\boldsymbol{D}_\lambda$, $\boldsymbol{M}_\lambda$ are a sort of weighted mass matrix and the mass matrix itself in the parametric domain, respectively. We denote by "$\otimes$" the Kronecker product.

Notice that it is possible to write Eq. (1.23) thanks to the fact that the operator A is linear and admits a separated representation, called an *affine decomposition*. In general, for linear problems this requirement is not difficult to satisfy. Moreover, the inner product in tensor product spaces has the following property: for $u = u^{\mu_1}u^{\mu_2}$ and $v = v^{\mu_1}v^{\mu_2}$, we have $\langle u, v\rangle = \langle u^{\mu_1}, v^{\mu_1}\rangle_{\mu_1}\langle u^{\mu_2}, v^{\mu_2}\rangle_{\mu_2}$, where $\langle\,\cdot\,,\,\cdot\,\rangle_{\mu_1}$ and $\langle\,\cdot\,,\,\cdot\,\rangle_{\mu_2}$ are inner products on V_{μ_1} and V_{μ_2}, respectively. The norm inherits the same property.

Thus, (1.21) can be written now in the following algebraic form:

$$\boldsymbol{w}^H \boldsymbol{A}\boldsymbol{u} = \boldsymbol{w}^H \boldsymbol{f}, \tag{1.24}$$

where $\boldsymbol{w}$ and $\boldsymbol{u}$ are vectorizations of their corresponding tensors and $\boldsymbol{w}^H$ denotes the conjugate-transpose of $\boldsymbol{w}$. In the previous example, $\boldsymbol{A} = \boldsymbol{K}_s \otimes \boldsymbol{D}_\lambda$ and $\boldsymbol{f} = (\boldsymbol{M}_s \otimes \boldsymbol{M}_\lambda)\boldsymbol{b}$, where $\boldsymbol{b}$ is a vectorization of its corresponding tensor.

In general, $\boldsymbol{A}$, for the separated representation of u based on the coordinates μ_1 and μ_2 can be rewritten in the following separated form, using T and R terms, respectively:

$$\begin{aligned}\boldsymbol{A} &= \sum_{i=1}^{T} \boldsymbol{A}_i^{\mu_1} \otimes \boldsymbol{A}_i^{\mu_2}\\ \boldsymbol{f} &= \sum_{i=1}^{R} \boldsymbol{f}_i^{\mu_1} \otimes \boldsymbol{f}_i^{\mu_2},\end{aligned} \tag{1.25}$$

or, more generally, for D coordinates of the problem:

$$\begin{aligned} \boldsymbol{A} &= \sum_{i=1}^{T} \otimes_{j=1}^{D} \boldsymbol{A}_i^j \\ \boldsymbol{f} &= \sum_{i=1}^{R} \otimes_{j=1}^{D} \boldsymbol{f}_i^j \end{aligned} \tag{1.26}$$

Hence, following this formulation, the rank-M PGD separated form of the approximation of the solution, based on the coordinates μ_1 and μ_2 can be written as:

$$\boldsymbol{u}^M = \sum_{i=1}^{M} \boldsymbol{u}_i^{\mu 1} \otimes \boldsymbol{u}_i^{\mu 2}, \tag{1.27}$$

or, for D coordinates:

$$\boldsymbol{u}^M = \sum_{i=1}^{M} \otimes_{j=1}^{D} \boldsymbol{u}_i^j, \tag{1.28}$$

We can suppose that, after M successive corrections of the solution (enrichments), a new rank-one enrichment is computed as follows ($\mathcal{C}_1$ representing the set of elementary tensors of rank one):

$$\begin{aligned} \boldsymbol{u}^{M+1} &= \boldsymbol{u}^M + \boldsymbol{u}, \\ \text{with} \quad \boldsymbol{u} \in \text{vect}(\mathcal{C}_1) \quad &\Leftrightarrow \quad \boldsymbol{u} = \boldsymbol{u}^1 \otimes \cdots \otimes \boldsymbol{u}^D, \end{aligned} \tag{1.29}$$

which satisfies:

$$\boldsymbol{A}\boldsymbol{u} \approx \boldsymbol{f} - \boldsymbol{A}\boldsymbol{u}^M. \tag{1.30}$$

Finally, in order to obtain the new enrichment, Eq. (1.30) is turned into the following non-linear optimization problem [6, 42]:

$$\min_{\boldsymbol{u} \in \text{vect}(\mathcal{C}_1)} \frac{1}{2}\langle \boldsymbol{A}\boldsymbol{u}, \boldsymbol{u} \rangle + \frac{1}{2}\langle \boldsymbol{A}\boldsymbol{u}^M, \boldsymbol{u} \rangle - \langle \boldsymbol{f}, \boldsymbol{u} \rangle. \tag{1.31}$$

By solving Eq. (1.31) with an appropriate alternating direction strategy, the PGD constructs a separated representation by solving several low-dimensional problems when compared to the full-model problem.

Chapter 2

Space separated representations: state of the art

The objective of this chapter is to review MOR techniques for building space separated representations in Cartesian-like or partitioned domains. Both *a posteriori* and *a priori* MOR approaches are covered. The analysis presented in this chapter provides a better understanding of the PGD formulation applied to Cartesian domains, when compared to standard mesh-based techniques. Limitations will also be analysed.

Based on this, the motivation and objectives of this thesis will be given; that is, to generalize space separated representations to non-Cartesian domains by introducing the notion of Global-Local separated representation. This objective, inspired by multi-scale approaches, Domain Decomposition and methods based on the partition of unity, proposes the use of partitioned domains in order to build separated representations that solve the limitations of the standard PGD in terms of intrusiveness and geometry constraints.

Contents

2.1 PGD space separated representations in cartesian-like domains

The PGD has been presented as a successful technique for calculating approximations of solutions of multidimensional problems. In particular, it is possible to construct that kind of approximation by considering the separation (whenever possible) of the coordinates of the domain in the physical space (i.e. the geometry). The motivation of using space separated representations is to solve 3D models as a sequence of 1D problems in parallelepiped domains, or as a sequence of 2D plus 1D problems in extruded domains.

Nevertheless, the space separated representations associated with the PGD approach present an important limitation: they are built by using variables associated with Cartesian geometries. This reduces considerably the applicability of this method for capturing solutions defined over domains consisting of non-Cartesian geometries. Therefore, it seems appropriate to address this numerical tool to new approaches that allow us to broaden its applicability.

After revisiting some space separation schemes, this chapter is devoted to introducing the main objective of this thesis: to create a new PGD separation strategy in order to generalize the space separated representations for solving problems defined over non-Cartesian domains.

To this aim, the first step is the definition of space separated representation. For instance, following Eq. (1.11), a full separated form provided by the Proper Generalized Decomposition for a 3D domain reads:

$$u(x,y,z) \approx \sum_{i=1}^{M} F_i^x(x) F_i^y(y) F_i^z(z) \tag{2.1}$$

for the domain $\Omega = \Omega_x \times \Omega_y \times \Omega_z$. This separated form allows solving the problem defined over the 3D domain Ω as a sequence of three 1D problems, which reduces the complexity of the problem and consequently, the computational cost of the solution. This kind of approach has been applied in some examples shown in [50].

In Fig. 2.1, some domain geometries and their corresponding proposal for separated representation are plotted. As mentioned before, the full space separated representation is achieved by splitting a problem defined over a 3D domain (for instance, a cube) in order to obtain three problems with a 1D complexity. When this separated form is not possible or it is not interesting in view of the particular geometry of the problem, other separations can be proposed. One such case is that of degenerated geometries, for which it seems more interesting to implement separated representations where some of the Cartesian coordinates are grouped.

2.1.1 Degenerated domains

One of the most employed applications of PGD space separated representations is the calculation of solutions in degenerated geometric domains. In this kind of domains, at least

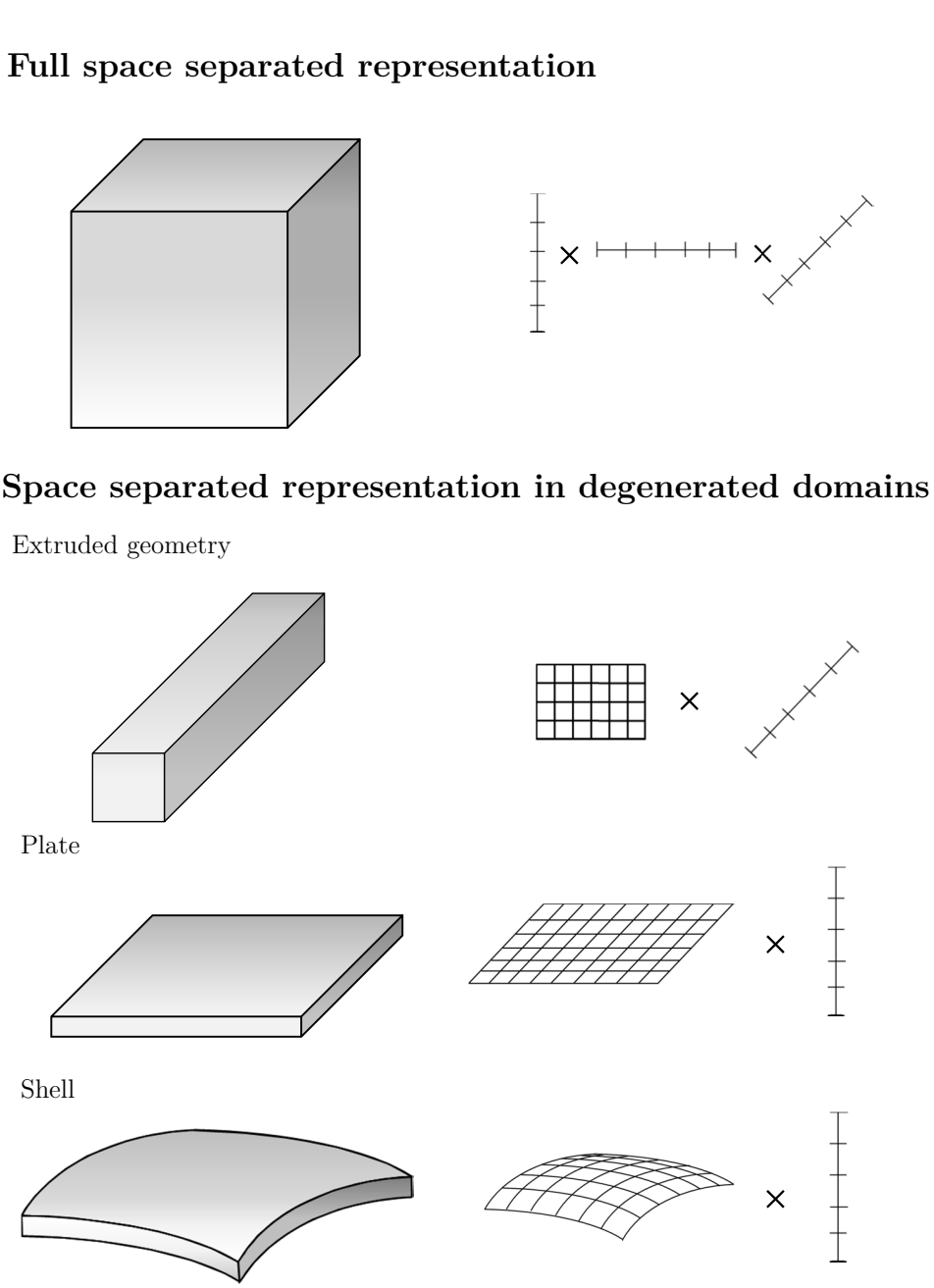

Figure 2.1: Scheme representing examples of space separated representations.

one of the characteristic dimensions is much smaller than the others, i.e. several orders of magnitude of difference between the dimensions. These configurations are extensively found in industrial research and their computational processing by means of standard mesh-based discretization techniques can be a difficult issue to resolve.

This is the case, for instance, of plate or shell-like domains, which are typical elements of structures and materials manufacturing. In this kind of geometries, the thickness is quite smaller than the rest of the dimensions, but frequently captures an important amount of relevant information in terms of material behaviour. Thus, in order to compute all this relevant information, these geometries usually require an extremely fine mesh along the thickness, which considerably increases the degrees of freedom and consequently, the computational cost of the problem. Therefore, due to the need for development of new techniques for solving this issue, this kind of geometric configurations became an important research focus for the application of the PGD.

PGD-based separated representations split the physical space into several lower dimensional domains, where the *smaller* dimensions are treated separately from the rest of the dimensions. Thus, problems defined over 3D dimensions can be solved from a sequence of 2D and 1D problems.

One important space separated representation associated with a degenerated geometry is the so-called *in-plane-out-of-plane* PGD, where the separated form is constructed by dividing the 3D domain into two subdomains, concerning the *plane* and the *thickness* ($\Omega = \Omega_\pi \times \Omega_\perp$ with $\Omega_\pi \subset \mathbb{R}^2$ and $\Omega_\perp \subset \mathbb{R}$).

Thus, an approximation of the 3D solution can be obtained as described in Eq. (2.2): a finite sum of products of two functions depending on the coordinates of the *plane* and the *thickness* respectively.

$$u(x, y, z) \approx \sum_{i=1}^{M} F_i^\pi(x, y) F_i^\perp(z). \tag{2.2}$$

This separated representation, which is more appropriate for plate or shell domains than a full space separated representation, has been vastly studied by Bognet et al. in several studies in the framework of composite materials. In [16], this technique was presented and applied to thermoelastic problems defined in plate geometries, where the full 3D model can be solved with 2D characteristic computational complexity. Thus, the PGD was successfully applied to composite plates and honeycomb composites, and the orientation of the composite plies was introduced as an extra coordinate without affecting the solvability of the problem. Moreover, this study reveals the decrease of the computational time that the *in-plane-out-of-plane* PGD represents when compared to FEM based 3D discretizations, especially when the number of degrees of freedom increases along the thickness.

Following the same research line, this approach was applied to shell geometries in [17] and both previous studies (for plates and shells respectively) were adapted to thermal models, solid and fluids mechanics and electromagnetic problems in [18]. The same approach was

extensively considered in structural plate and shell models in [44, 113, 114, 115, 116, 117]. With respect to other structural applications, a parametric 3D elastic solution of beams involved in frame structures was proposed in [19].

The *in-plane-out-of-plane* was also extended to many different physics, e.g. squeeze flows of Newtonian and Non-Newtonian fluids in laminates in [48], flows in stratified porous media in [28], and non-linear viscoplastic flows in plate domains in [22]. Moreover, this technique was enriched with discontinuous functions for representing cracks in [49], delamination in [79] and thermal contact resistances in [31].

2.1.2 Construction of the PGD for space separated representations

In order to illustrate the process of building a separated representation in the framework of the PGD, we propose a simple example following the *in-plane-out-of-plane* approach. We can consider the Poisson equation

$$\Delta u(x,y,z) + f(x,y,z) = 0, \tag{2.3}$$

where the unknown temperature field is defined over a 3D plate domain $\Omega = \Omega_\pi \times \Omega_\perp$ with $\Omega_\pi \subset \mathbb{R}^2$ and $\Omega_\perp \subset \mathbb{R}$. For the sake of simplicity, the points $(x,y,z) \in \Omega$ are expressed as $(x,y,z) = (\boldsymbol{x},z)$, with $\boldsymbol{x} = (x,y) \in \Omega_\pi$ and $z \in \Omega_\perp$. Homogeneous Dirichlet boundary conditions are imposed and the constant source term f is applied to the whole domain Ω.

The objective of the PGD is to obtain a separated representation of an approximate solution of the unknown temperature field $u(\boldsymbol{x},z)$ as indicated in Eq. (1.11), i.e. as a finite sum of products of functions depending on coordinates of the plane Ω_π and the thickness $\Omega_\perp$ respectively. This separated representation can be written as

$$u(\boldsymbol{x},z) \approx \sum_{i=1}^{M} F_i^\pi(\boldsymbol{x}) F_i^\perp(z) \tag{2.4}$$

where F_i^π and $F_i^\perp$ represent the functions depending on coordinates $\boldsymbol{x}$ and z respectively and M is the number of terms of the functional product necessary to reproduce the unknown field.

The first step for building the separated representation is the description of the weighted residual form of Eq. (2.3):

$$\int_{\Omega_\pi \times \Omega_\perp} u^* \left(\Delta^\pi u + \frac{\partial^2 u}{\partial z^2} + f \right) d\Omega_\pi \, d\Omega_\perp = 0, \tag{2.5}$$

where Δ^π represents the in-plane Laplace operator.

The fact of constructing the approximate solution by adding new terms (enrichments) to the previous solution allows writing the separate form for the step M as follows

$$u^M(\boldsymbol{x},z) = u^{M-1}(\boldsymbol{x},z) + F_M^\pi(\boldsymbol{x}) F_M^\perp(z) = \sum_{i=1}^{M-1} F_i^\pi(\boldsymbol{x}) F_i^\perp(z) + F_M^\pi(\boldsymbol{x}) F_M^\perp(z) \tag{2.6}$$

with $u^{M-1}(\boldsymbol{x},z)=\sum_{i=1}^{M-1}F_i^{\pi}(\boldsymbol{x})F_i^{\perp}(z)$ representing the approximate solution for the previous enrichment step and functions F_M^{π} and $F_M^{\perp}$ being unknown. In order to obtain these functions, an iterative approach is implemented. $u^{M,p}$ represents the approximation at the enrichment step M and the iteration p:

$$u^{M,p}(\boldsymbol{x},z)=u^{M-1}(\boldsymbol{x},z)+F_{M,p}^{\pi}(\boldsymbol{x})F_{M,p}^{\perp}(z) \tag{2.7}$$

Thus, the iteration for calculating the functions $F_{M,p}^{\pi}(\boldsymbol{x})$ and $F_{M,p}^{\perp}(z)$ can be carried out, following the *alternating direction strategy* [29]. For this purpose, we can assume that $F_{M,p}^{\pi}(\boldsymbol{x})$ can be calculated from $F_{M,p-1}^{\perp}(z)$ (obtained at the previous iteration $p-1$). Now, Eq. (2.7) reads

$$u^{M,p}(\boldsymbol{x},z)=u^{M-1}(\boldsymbol{x},z)+F_{M,p}^{\pi}(\boldsymbol{x})F_{M,p-1}^{\perp}(z) \tag{2.8}$$

and consequently $F_{M,p}^{\pi}(\boldsymbol{x})$ is the only unknown function. If we consider the weight function

$$u^{*}(\boldsymbol{x},z)=F_{M}^{\pi *}(\boldsymbol{x})F_{M,p-1}^{\perp}(z) \tag{2.9}$$

and substitute Eq. (2.8) and Eq. (2.9) into Eq. (2.5), we obtain:

$$\begin{aligned}\int_{\Omega_\pi\times\Omega_\perp} F_M^{\pi *}F_{M,p-1}^{\perp}\left(\Delta^{\pi}F_{M,p}^{\pi}F_{M,p-1}^{\perp}+F_{M,p}^{\pi}\frac{\partial^2 F_{M,p-1}^{\perp}}{\partial z^2}\right)d\Omega_\pi\, d\Omega_\perp = \\ -\int_{\Omega_\pi\times\Omega_\perp} F_M^{\pi *}F_{M,p-1}^{\perp}\sum_{i=1}^{M-1}\left(\Delta^{\pi}F_i^{\pi}F_i^{\perp}+F_i^{\pi}\frac{\partial^2 F_i^{\perp}}{\partial z^2}\right)d\Omega_\pi\, d\Omega_\perp \\ -\int_{\Omega_\pi\times\Omega_\perp} F_M^{\pi}*F_{M,p-1}^{\perp}f\, d\Omega_\pi\, d\Omega_\perp\end{aligned} \tag{2.10}$$

As can be observed in Eq. (2.10), all terms integrated over $\Omega_\perp$ are known and can be computed, Eq. (2.10) resulting in a 2D integration over Ω_π:

$$\begin{aligned}\int_{\Omega_\pi} F_M^{\pi *}\left(\alpha^{\pi}\Delta^{\pi}F_{M,p}^{\pi}+\beta^{\pi}F_{M,p}^{\pi}\right)d\Omega_\pi = \\ -\int_{\Omega_\pi} F_M^{\pi *}\sum_{i=1}^{M-1}\left(\gamma_i^{\pi}\Delta^{\pi}F_i^{\pi}+\delta_i^{\pi}F_i^{\pi}\right)d\Omega_\pi-\int_{\Omega_\pi}F_M^{\pi *}\xi^{\pi}\, d\Omega_\pi\end{aligned} \tag{2.11}$$

where coefficients α^{π}, β^{π}, γ_i^{π}, δ_i^{π} and ξ^{π} result from the 1D integrations over $\Omega_\perp$. Considering the discretization of the domain Ω_π, Eq. (2.11) can be easily solved, obtaining the function $F_{M,p}^{\pi}$ (for more details, the interested reader can refer to [29]).

The same scheme is applied for calculating $F_{M,p}^{\perp}$ from $F_{M,p}^{\pi}$, by substituting Eq. (2.7) and the following weight function

$$u^{*}(\boldsymbol{x},z)=F_{M,p}^{\pi}(\boldsymbol{x})F_{M}^{\perp *}(z) \tag{2.12}$$

into Eq. (2.5), resulting in:

$$\int_{\Omega_\pi \times \Omega_\perp} F^\pi_{M,p} F^{\perp *}_M \left(\Delta^\pi F^\pi_{M,p} F^\perp_{M,p} + F^\pi_{M,p} \frac{\partial^2 F^\perp_{M,p}}{\partial z^2} \right) d\Omega_\pi \, d\Omega_\perp =$$
$$- \int_{\Omega_\pi \times \Omega_\perp} F^\pi_{M,p} F^{\perp *}_M \sum_{i=1}^{M-1} \left(\Delta^\pi F^\pi_i F^\perp_i + F^\pi_i \frac{\partial^2 F^\perp_i}{\partial z^2} \right) d\Omega_\pi \, d\Omega_\perp$$
$$- \int_{\Omega_\pi \times \Omega_\perp} F^\pi_{M,p} F^{\perp *}_M f \, d\Omega_\pi \, d\Omega_\perp \tag{2.13}$$

Finally, in Eq. (2.13), all terms integrated over Ω_π are known and can be computed, Eq. (2.13) resulting in a 1D integration over $\Omega_\perp$:

$$\int_{\Omega_\perp} F^{\perp *}_M \left(\alpha^\perp \frac{\partial^2 F^\perp_{M,p}}{\partial z^2} + \beta^\perp F^\perp_{M,p} \right) d\Omega_\perp =$$
$$- \int_{\Omega_\perp} F^{\perp *}_M \sum_{i=1}^{M-1} \left(\gamma^\perp_i \frac{\partial^2 F^\perp_i}{\partial z^2} + \delta^\perp_i F^\perp_i \right) d\Omega_\perp - \int_{\Omega_\perp} F^{\perp *}_M \xi^\perp \, d\Omega_\perp \tag{2.14}$$

with $\alpha^\perp$, $\beta^\perp$, $\gamma^\perp_i$, $\delta^\perp_i$ and $\xi^\perp$ resulting from the terms associated with the 2D integration over Ω_π. Thus, $F^\perp_{M,p}$ can be obtained with a previous discretization of the domain $\Omega_\perp$.

For each step of the iteration, the error is computed by calculating :

$$\varepsilon_p = \frac{\left\| F^\pi_{M,p}(\boldsymbol{x}) F^\perp_{M,p}(z) - F^\pi_{M,p-1}(\boldsymbol{x}) F^\perp_{M,p-1}(z) \right\|^2}{\left\| F^\pi_{M,p-1}(\boldsymbol{x}) F^\perp_{M,p-1}(z) \right\|^2} < \epsilon \tag{2.15}$$

When the value of ε_p achieves a suitable tolerance ϵ, the corresponding enrichment step M has been fulfilled and the product of the functions $F^\pi_M(\boldsymbol{x})$ and $F^\perp_M(z)$ is included in the separated form as a new term.

Finally, by computing an appropriate measure of the error, the end of the enrichment process is achieved when this error becomes small enough. For instance, the PGD error can be calculated as the relative weight of the new mode with respect to all the modes obtained as follows

$$\varepsilon_{PGD} = \frac{\left\| F^\pi_M(\boldsymbol{x}) F^\perp_M(z) \right\|^2}{\left\| \sum_{i=1}^{M} F^\pi_i(\boldsymbol{x}) F^\perp_i(z) \right\|^2} \tag{2.16}$$

When the suitable value for ε_{PGD} is achieved, the approximation of the solution takes the form of Eq. (2.4), i.e. a finite sum of functional products depending on the parameters of the problem (in this case, the coordinates $\boldsymbol{x}$ and z), this separated form being obtained without computing *a priori* information associated with the full-model solution.

Moreover, this approximation represents an important gain in terms of computational cost. For instance, a 3D FEM model corresponding to the 2D (plane) and 1D (thickness)

meshes employed in this example, i.e. $\Omega^h = \Omega^h_\pi \times \Omega^h_\perp$ (Ω^h represents the meshed 3D domain and Ω^h_π and $\Omega^h_\perp$ are the 2D and 1D meshed domains of the PGD, respectively), would need to solve a system with $n = N_{\boldsymbol{x}} \times N_z$ unknown values. If a fine mesh is used to solve the problem, the complexity of the problem increases considerably. Nevertheless, this PGD example solves a sequence of 2D and 1D uncoupled problems, which means that the number of unknown values is $n_{PGD} = M \times (N_{\boldsymbol{x}} + N_z)$, i.e. a considerably smaller amount of unknowns when compared to the FEM model (provided that M is sufficiently small), especially when fine meshes are required to capture the through-thickness behavior.

2.2 Model Order Reduction techniques in partitioned domains

In this section, some MOR techniques based on the use of partitioned domains are analysed.

2.2.1 *A posteriori* techniques

The Reduced Basis Element Method [74], which represents an important reference for this study, is based on the combination of a reduced basis discretization and the domain decomposition method [95, 97]. The basic idea is to split the domain into several subdomains and construct a reduced basis for these subdomains by considering representative geometric snapshots. The global solution is obtained by coupling the individual basis solutions via Lagrange multipliers.

This method was subsequently applied to a thermal fin problem in [75]. The objective is to take advantage of the repetitive configuration of the problem in order to easily reproduce the solution of some generic blocks along the whole domain. For this purpose, the domain is split into subdomains that are similar to several generic domains. The subdomains are considered as the deformation of one or a few of reference generic domains. These reference domains are *filled* with reduced basis functional spaces that are mapped to each subdomain together with the geometry. The solution of each subdomain is obtained as a linear combination of the precomputed solution mapped from the reference domain onto each particular subdomain and the matching between the subdomains solution is carried out by means of Lagrange multipliers. In [73], this approach was extended to the steady Stokes equation. The same approach was recently applied in [64] to the thermal simulation of integrated circuits by using a multiblock POD model and in [80] to the transient thermal simulation of integrated circuits by means of a POD-based reduced basis element technique.

These interesting studies deal with the challenge of building separated representations by using partitions of the domain in order to take advantage of the repetitive geometry or configuration of the problem, which is intimately related to the object of study of this thesis. Nevertheless, the need for precomputed information for constructing the reduced

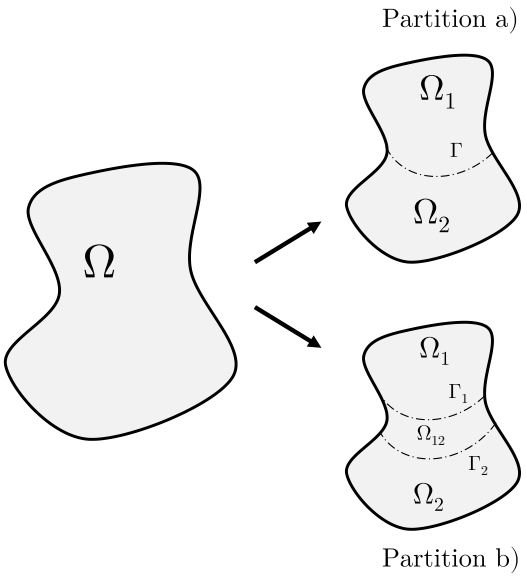

Figure 2.2: Partition of domain Ω: a) disjoint subdomains, b) overlapping subdomains.

basis represents an important limitation in terms of applicability. This situation reveals the necessity of *a priori* approaches in order to address this challenge.

2.2.2 *A priori* techniques

Regarding the construction of space separated representations inspired by the partition of the domain, the combination of the domain decomposition method (DD) [95, 97] and the PGD represents an interesting approach. The DD is a technique that can be used in any discretization method for partial differential equations. It reformulates any boundary-value problem on a partition of the computational domain into several subdomains. This allows obtaining a more efficient way to calculate the solution by using parallel computer platforms, as every subdomain can be solved independently, with the boundary conditions which represent the interaction between subdomains. It represents a very useful technique when different kinds of differential equations are applied to each subdomain.

Thus, the basic idea of the DD technique is the partition of the domain into several parts. Fig. 2.2 represents the two different ways for splitting a generic domain Ω. The first way a) is obtained by dividing the domain into two disjoint subdomains (Ω_1 and Ω_2) with a common boundary Γ. The second way b) consists in a partition of two overlapping subdomains (Ω_1 and Ω_2), with a shared region Ω_{21} and two boundaries (Γ_1 and Γ_2).

With respect to the objective of this thesis, some interesting techniques have implemented

the combination of DD and PGD for partitioned domains or repetitive topologies in order to build a more efficient separation strategy compared to full space PGD techniques.

For instance, a method for coupling FEM and PGD is proposed in [3] for the treatment of localized behaviour of model solutions. More specifically, the PGD is enriched with finite elements for describing discontinuities, this technique also being used for the treatment of boundaries for coupling subdomains in the framework of domain decomposition techniques.

Other interesting work is presented in [59], in which the authors introduced an efficient combination of DD and PGD for parametrised elliptic problems with complex geometries, taking advantage of the repetitive configuration of some domains and carrying out an appropriate partition into subdomains. Thus, a PGD approximate solution is obtained in each subdomain in terms of the solution at the interface. The evaluation of the approximation in each subdomain is a simple function evaluation given the interface values.

In [83], another combination of PGD and DD is proposed for addressing problems in complex domains where the PGD full space separated representation or the sequence of 2D and 1D problems cannot be applied even after the use of mapping techniques to simplify the geometry. To this aim, this study proposes a DD strategy based on the use of the PGD and the Arlequin coupling strategy [13], for splitting the physical space and adding parameters as extra coordinates. Thus, a PGD approximation is applied to calculate the solution at every subdomain of the partition and the Lagrange multiplayer that enforces the equality of the solution at every overlapping region. The Arlequin strategy is also used in [84] for multimodel problems in order to combine PGD reduced models for the simulation of structures involving localized geometrical details. To this aim, the LATIN algorithm [67, 68, 85, 88, 92] is introduced to solve the problem in a decoupled manner and the PGD approach is then used to solve every model.

With respect to other approaches outside the framework of Domain Decomposition, the concept of partitioning in the framework of the PGD has been used in [10] for the calculation of a PGD approximation with a constant partition of the time domain, for the case of a moving source in a transient heat transfer problem. Another interesting approach is based on the use of wavelets for approximating the functions involved in separated representations for multi-scale solutions [70]. More recently, the partition of unity has been introduced in [62, 63] for building PGD separated representations based on different levels of discretization.

2.3 Motivation of the thesis

2.3.1 Partitioned domains: the Global-Local scheme

After the previous summary of MOR techniques based on space separated representations, it seems necessary to progress on the adaptation of this method to different geometries in order to properly capture the relevant information of models defined over some particular

domains.

Some techniques have been introduced in this chapter in order to emphasize the importance of the simplification of the geometry when building separated representations, by grouping some of the coordinates of the problem in view of its geometry. These approaches split the problem into lower-dimension problems, the separated representation being constructed by following the so-called (in the context of this thesis) *standard* PGD point of view, i.e. by using the discretization of each lower-dimension domain. Nevertheless, sometimes the geometry or the configuration of some problems suggests the necessity of building separated representations not related to the Cartesian coordinates.

Such is the case of domains consisting of geometric patterns, multi-scale problems, repetitive structures or domains consisting of different materials or parts. All these cases, suggest the need of developing an MOR technique for taking advantage of these configurations. This issue has already been addressed by using *a posteriori* MOR techniques but it still remains a challenge when using *a priori* approaches.

Taking into consideration the approaches presented in Section 2.2, the aim of this thesis is to develop a technique that is able to solve problems with a new PGD scheme based on partitioning, without using an extra technique for coupling the solution of all the subdomains. For this purpose, the Global-Local PGD is introduced. This approach is based on the idea that the solution in each subdomain of the partition is obtained by particularising a generic local solution.

Thus, after splitting the domain into several subdomains, the standard point of view is substituted by a separation based on the definition of two variables: the local variable, associated with a fine mesh and the global variable, which represents the partition. This point of view contributes to the considerable reduction of degrees of freedom that the PGD approach implies.

2.3.2 The Partition of Unity: coupling discretization levels

When addressing problems applied to domains with particular local features or repetitive structures with standard mesh-based approaches, FEM approaches based on the partition of unity such as the Generalized Finite Element Method (GFEM) [38, 40, 89, 105, 106] seem a good alternative for solving this kind of problems while reducing the number of degrees of freedom. This technique is based on the combination of global and locals levels of discretization for capturing the features of interest of the domain.

This combination is carried out by coupling a FEM standard model defined over a coarse meshed domain with a fine-meshed enrichment defined over a patch. This patch is superposed on the zone where the local feature is placed by using the shape functions of the coarse mesh, which satisfy the partition of unity. Thus, a refinement of the coarse mesh can be implemented and an accurate solution of local features of interest can be calculated, without

refining over the whole domain. The local enrichments provide extra degrees of freedom to the corresponding nodes in the domain, without altering the mesh topology.

The ability of this method to capture the solution locally depends on the adequacy of the enrichment function. This is usually carried out by introducing some previous knowledge on the solution, or by setting an auxiliary local problem, whose boundary conditions need to be iterated [41, 45].

All these concepts are taken into consideration in the Global-Local PGD approach proposed in Chapter 3, where the objective is to develop a PGD technique for enriching FEM solutions defined over coarse meshes. Also based on the partition of unity, this PGD uses an appropriate Global-Local scheme that combines local and global levels of discretization, being able to generate accurate approximation spaces, i.e. to provide the pertinent enrichment without the need of solving extra problems or computing *a priori* information of the problem.

2.3.3 PGD for non-Cartesian geometries

One of the most relevant limitations of the PGD is related to the Cartesian framework. The standard PGD approach when addressing space separated representations is associated with discretizations defined over Cartesian geometries, the separability of the solution being unachievable for non-Cartesian domains. This fact represents an important constraint for the applicability of the PGD to some practical contexts, therefore it seems necessary to deal with complex non-Cartesian geometries while keeping the computational benefits of the PGD for building space separated representations.

Some approaches have been proposed to face this issue. In [50], the authors proposed a generic domain embedded into a Cartesian geometry. Moreover, in [47] the authors introduced a parametrisation map for quadrilateral domains.

In this thesis, in order to avoid this limitation of the PGD, the construction of separated representations for non-Cartesians domains is achieved by taking advantage of the Global-Local PGD approach. This is due to the use of a separation scheme based on the partition of the domain, which implies that this technique could be defined over non-structured meshes, independently of the coordinates of the nodes of the problem or the chosen partition.

2.3.4 Intrusiveness of the PGD

The concept of intrusiveness of MOR techniques is related to the fact that these methods involve the manipulation and modification of the operators that reproduce the PDE of interest. These code alterations are sometimes impossible to implement in commercial simulation tools. Consequently, MOR approaches usually require specific codes.

The discretization of each coordinate taken into consideration in the PGD framework and the construction of the associated operators for solving the corresponding PDE imply

that the standard PGD approach is very intrusive. It seems necessary to develop new methodologies in order to reduce the intrusiveness, allowing us to incorporate the PGD into commercial simulation platforms, which are massively used for solving engineering problems of industrial interest

In the PGD framework, some alternatives have been proposed: in [34], the authors suggested that the non-intrusive PGD scheme is workable for shape optimization problems with geometrical parameters as extra-coordinates, and in [119] a non-intrusive PGD scheme with application in biomechanics is introduced.

Regarding other MOR-based techniques, this issue is addressed in [20], where the hierarchical collocation is employed to approximate the numerical solution of parametric models, introducing a non-intrusive approach based on sparse adaptive sampling of the parametric space, which builds a sparse low-rank approximate tensor representation of the solution.

The Global-Local approach based on the partition of unity presented in Chapter 3 generates and combines discrete operators at local and global levels, which implies a very intrusive approach.

In order to avoid this issue, a less intrusive approach based on the Global-Local scheme is proposed in Chapter 4 for building space separated representations. This technique uses some discrete operators as a starting point, these operators being obtained from a previous FEM discretization that can be built by using standard codes. Thus, if the operators are compatible with the desired partition, the Global-Local PGD scheme can be used as an algebraic iterative solver and could be implemented within standard simulation codes.

Chapter 3

Global-Local separated representations based on the Partition of Unity

In this chapter, the Global-Local separated representations are introduced. This approach combines global and local discretization levels based on the partition of unity. It builds a separated representation that provides the local enrichment, without the need for a priori knowledge of the solution, nor the implementation of auxiliary local problems to determine the enrichment.

While in-plane-out-of-plane separated representations achieve a reduction in complexity by splitting a 3D problem into a sequence of problems of lower dimension (2D or 1D), the Global-Local scheme uses the separation of the scales instead. Therefore, the numerical complexity is split into a global problem, defined over a coarse mesh, and a local problem, defined over a reference support with an arbitrarily fine mesh. Both global and local problems are defined in the same physical dimension of the original problem (1D, 2D, or 3D).

Moreover, by using a standard (finite element) isoparametric mapping, arbitrary non-Cartesian domains can be addressed.

Contents

3.1 Introduction

The concept of enriching a finite element formulation with some a priori knowledge on the solution is essentially based on the Partition of Unity Method [8, 76]. This is the case of the Generalized Finite Element Method (GFEM) [38, 40, 89, 105, 106] or the Extended Finite Element Method (XFEM) [12, 82]. These techniques are especially useful for solving problems defined over domains containing local features like cracks [37, 103, 108], edge singularities [40], boundary layers [39], inclusions [107], voids [105, 107], microstructures [104], etc. The main idea is the use of an *a priori* knowledge about the solution of the problem for determining enrichment functions that are coupled to a standard FEM model, in order to capture the solution of local features of interest that would require refined meshes. The conformity is ensured if the enrichment space satisfies the partition of unity.

In some cases, when no a priori knowledge on the solution is available, we can still set an auxiliary problem, defined over a subdomain, or patch, to compute the appropriate local enrichment function. This is usually referred to as a Global-Local GFEM [41, 45].

With respect to the combination of methods based on the partition of unity with MOR approaches, in [23] the PGD was used in the framework of GFEM. This work builds a parametric enrichment function that is able to capture changing simulation conditions, and therefore, to adaptively choose the appropriate enrichment function. The result is a Vademecum-GFEM formulation (V-GFEM).

Inspired by all these techniques, a new point of view is now proposed: a Global-Local PGD based on the Partition of Unity. Instead of using the approach of the methods that combine FEM with the partition of unity for capturing the relevant information of local features of interest, this PGD approach takes advantage of the concept of 'enrichment' to replicate a local solution throughout the whole domain. With this aim, two discretizations are defined throughout the domain: a coarse mesh, associated with the partition of the domain, and a fine mesh, associated with the replication of the enrichment. Thus, with the use of the PGD, the enrichment functions are not previously required: the approximation space is provided by the modes of the PGD as it solves the problem. This new approach is also related to the techniques proposed in [62, 63], but those separation forms are associated with Cartesian geometries.

Thus, this technique represents an adaptation of the point of view of previous methods based on the Partition of Unity to the Model Order Reduction *a priori* approaches, as it does not need previous knowledge of the solution to find an accurate enrichment: the PGD proposes the best possible enrichment without the need of solving an additional local FEM problem.

Section 3.2 is devoted to the Global-Local PGD based on the partition of the unity: the approach is introduced, the combination of global and local levels of discretization is defined and the PGD methodology is intensively described. In Section 3.3, a comparison of this

PGD technique with the GFEM approach is carried out. In Section 3.4 a set of numerical examples is shown and finally, in Section 3.5 the results are discussed and the conclusions are summarised.

3.2 The Global-Local PGD

3.2.1 The concept of Partition of Unity

The use the Partition of Unity Method [8, 38, 76, 103] while addressing high-fidelity approaches allows including in the FEM model *a priori* local knowledge of the PDE being solved. Methods such as GFEM or XFEM are intimately related to the idea of using the Finite Element Method applied to overlapping grids, i.e. to create partitions of a domain into several overlapping regions (the so-called patches) that contain simple generated grids. Thus, domains consisting of complex geometries can be split into subdomains with independent meshes whose refinement can be carried out without altering the rest of the subdomains.

The main idea of these methods is the combination of the partition of unity and an enrichment with local approximation spaces (obtained by taking advantage of the *a priori* knowledge about the behaviour of the solution), which can be used to accurately capture the physics underneath the local features. It results in a simple way to incorporate additional analytical details of the problem while solving in the finite element space, as the refinement is carried out only in the local domains.

There are two key properties that this approach must satisfy:

- The first one is the capability of the method to capture the physics of the local features. To reach this aim, the enrichment functions are accurately built due to the *a priori* knowledge of the configuration of the problem.

- The second one corresponds to conformity when using a standard FEM problem coupled with the enrichment functions. The inter-element C^0 continuity is ensured without losing the approximation properties, by using shape functions that satisfy the partition of unity. For a discretization of a local domain Ω_L, a partition of unity is represented by a collection of global functions N_α whose value sums up to unity at each point of the discretization x_L, which means that the approximation space satisfies the partition of unity if and only if:

$$\sum_{\alpha} N_\alpha(x_L) = 1, \quad \forall x_L \in \Omega_L \tag{3.1}$$

  where $N_\alpha(x_L)$ represents the α-node shape functions and x_L are the coordinates of the discretization of the local domain Ω_L.

Thus, the approximation of the solution field, denoted by u, reads:

$$u = \sum_{i \in I} N_i \, u_i + \sum_{i \in I_{\text{enr}}} N_i \, L \, g_i, \tag{3.2}$$

where N_i are the standard shape functions satisfying the partition of unity, u_i are standard finite element degrees of freedom, L is the enrichment or local function defined over the enrichment patch, and g_i are the extra degrees of freedom. Note that only a single enrichment function per node has been considered. A more general expression could be:

$$u = \sum_{i \in I} N_i \, u_i + \sum_{i \in I_{\text{enr}}} N_i \sum_j L_j \, g_i^j, \tag{3.3}$$

where several enrichment functions L_j have been considered.

3.2.2 Definition of the Global-Local approximation

The Global-Local separated representation is based on the following ideas:

- Both the global variable (the extra degrees of freedom) and the local functions are assumed as unknowns of the problem. Therefore, we will devise a PGD algorithm to compute both g_i^j and L_j in Eq. (3.3).
- Local functions L_j are defined in the reference support of the enriched node i. The support of an enriched node is the union of the elements attached to that node. In practice, the computation of the local function involves the discretization of the support.
- By using standard isoparametric mapping, local functions can be mapped to arbitrary non-Cartesian domains. The isoparametric mapping is given by shape functions N_i.

Under this light, Eq. (3.3) can be reinterpreted to define the Global-Local separated representation over the enriched domain as follows:

$$u_{\text{enr}} \;=\; \sum_{i \in I_{\text{enr}}} N_i \sum_{j=1}^{N_{\text{m}}} L_j \, g_i^j, \;\; \text{by abuse of notation} \rightsquigarrow \;\; \sum_{j=1}^{N_{\text{m}}} L_j G_j, \tag{3.4}$$

where the index j is now understood as the PGD mode j, and N_{m} stands for the number of PGD modes to be computed. In Eq. (3.4), G_j stands for the global function. As it is standard in the PGD framework, the separated representation is computed by adding one mode at a time. Therefore, the separated representation is built progressively by adding pairs (L_j, G_j), for $j = 1, \ldots, N_{\text{m}}$.

The separation is established due to the definition of two different discretization levels, as it is described in Fig. 3.1: the coarse and the fine levels. The global variable is defined over a coarse mesh compatible with the partition of the domain into several macro-elements.

In a connection with GFEM and XFEM techniques, the global shape functions (N) should satisfy the Partition of Unity (see Fig. 3.1).

We denote the discretization of the local functions L_j at the reference support as follows:

$$L_j = \sum_{k \in I_{\text{loc}}} M_k l_j^k, \tag{3.5}$$

where M_k are standard shape functions at node k of the reference support mesh, and l_j^k are the nodal coefficients of the local function. By introducing the above discretization in Eq. (3.4), we can also write the global-local approximation as follows:

$$u_{\text{enr}} = \sum_{i \in I_{\text{enr}}} N_i \sum_{j=1}^{N_{\text{m}}} \sum_{k \in I_{\text{loc}}} M_k l_j^k \, g_i^j. \tag{3.6}$$

Thus, instead of using the refinement for capturing the information of local features of interest as most of the GFEM or XFEM applications do, this technique is used to replicate the fine mesh throughout the whole domain while reducing the computational cost by using a PGD technique. This means that a standard fine FEM discretization of the whole problem is substituted by a coarse mesh that defines the partition and a fine mesh defined over a small support (when compared to the whole domain).

The PGD approximation can be easily replicated by *displacing* the support throughout the whole domain, coupling the distribution obtained for the local variable with the partition of unity applied to the global variable. A scheme representing the combination of both levels for constructing the whole approximation is presented in Fig. 3.2. For a 1D support located over two macro-elements, the local variable distribution l_j^k is multiplied by its shape functions M_k, providing the generic local solution. At the coarse level, the global variable g_i^j associated with the shared node between the macro-elements is interpolated by using its corresponding global shape function N_i (a linear Lagrange shape function, in this example) that satisfy the partition of unity. The coupling of both levels leads to the PGD approximation. In 3.2.2.1 the process of obtaining the approximation throughout the whole domain is more precisely described.

In order to illustrate the global-local approximation, let us consider 1D linear elements, the finite element approximation on a macro-element being defined as follows:

$$u_{\text{fem}} = N_1 g_1 + N_2 g_2 \tag{3.7}$$

where u_{fem} is the approximation of the solution referred to the coordinates over the element. N_1 and N_2 are the shape functions associated with both nodes of the macro-element and g_1 and g_2 are the values associated with those nodes (global variables).

Now, one can consider that this coarse solution can be enriched by adding a single local function. Therefore, we are considering here that $j = 1$. We have at the element level that

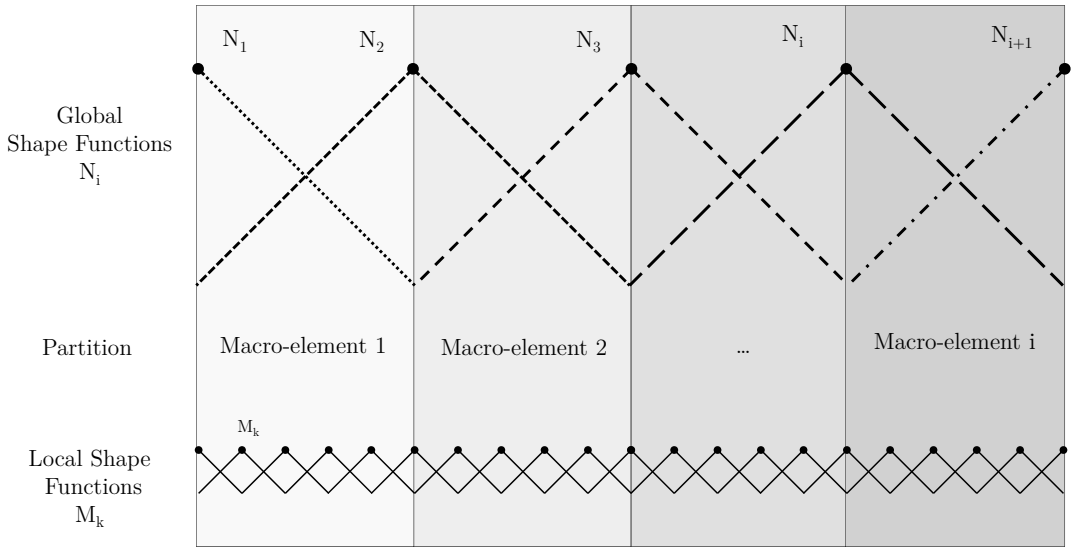

Figure 3.1: Scheme representing the combination of the discretizations of the global and the local levels.

$i = 1, 2$, and the local function, defined over the reference support, is split into its *front* and *back* components: $L_1 = L(\xi \in [-1, 0])$, and $L_2 = L(\xi \in [0, 1])$:

$$u_{\text{enr}} = N_1 L_1 g_1 + N_2 L_2 g_2. \tag{3.8}$$

In turn, these enrichments are discretized using the fine mesh associated with the local level. Thus, if $2n - 1$ nodes are used in the mesh, the enrichments are rewritten as follows:

$$\begin{aligned} L_1 &= M_n l_1^n + \ldots + M_{2n-1} l_1^{2n-1} \\ L_2 &= M_1 l_2^1 + \ldots + M_n l_2^n \end{aligned} \tag{3.9}$$

M_k, with $1 \leq k \leq 2n-1$ are the shape functions associated with the nodes of every element on the fine mesh. The local variable is defined as l_i^k. If Eq. (3.9) is introduced in Eq. (3.8), the Global-Local approximation now reads:

$$u_{\text{enr}} = N_1 \left(\sum_{k=n}^{2n-1} M_k l_1^k \right) g_1 + N_2 \left(\sum_{k=1}^{n} M_k l_2^k \right) g_2, \tag{3.10}$$

or, finally, as follows,

$$u_{\text{enr}} = \sum_{i=1}^{2} N_i \left(\sum_{k=1}^{2n-1} M_k l_i^k \right) g_i. \tag{3.11}$$

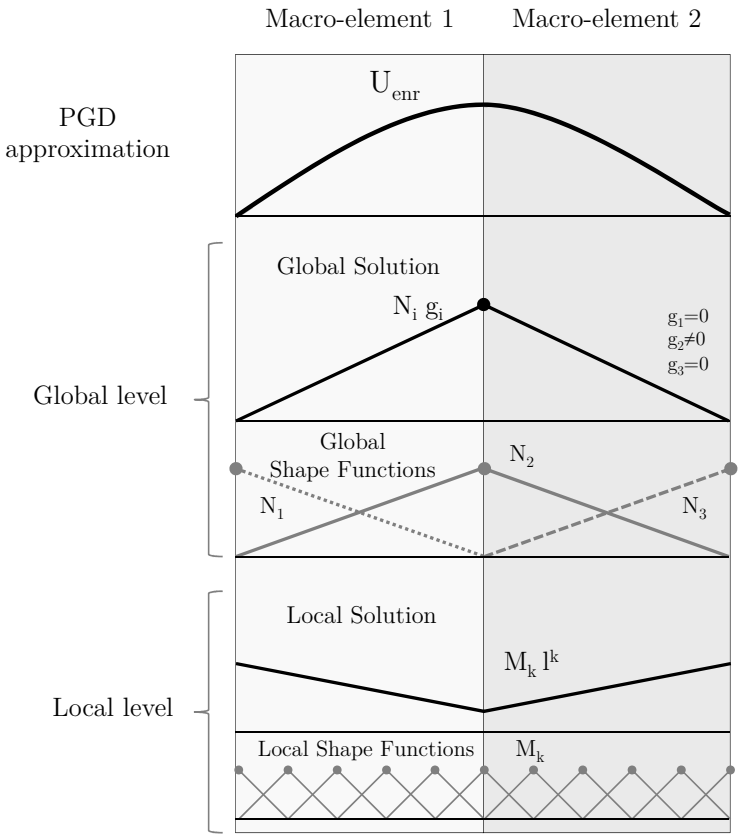

Figure 3.2: Combination of global and local levels to obtain the PGD approximation.

Eq. (3.11) represents the approximation of the solution at every point of the domain, coupling the local and the global variables by satisfying the Partition of Unity. This approximation is used in the framework of the PGD in order to construct a separated representation based on the calculation of the global and the local variable. Nevertheless, before addressing the computation of this PGD, it seems mandatory to carry out a better description of the tools that allows us to couple the global and the local levels: the *support* and the *global shape functions*.

3.2.2.1 Replication of the local solution throughout the domain

Once the strategy of the Global-Local PGD approach combined with the partition of unity has been defined, the process of replication of the fine-meshed approximation throughout

the whole domain is more precisely described. Following the scheme plotted in Fig. 3.2, the objective now is to describe the approximation of the solution provided by the combination of the Global and the Local levels.

When considering the combination of both levels of discretization, the starting point is the concept of support. The support is a generic domain consisting of several fine-meshed macro-elements that share a unique node, i.e. the set of macro-elements where an entire global shape function is defined (see Fig. 3.1 and Fig. 3.2). This means that the support consists of two macro-elements when addressing 1D problems, four macro-elements for 2D problems (when considering squared macro-elements), and eight macro-elements for 3D problems (when considering cubic macro-elements), i.e. 2^d macro-elements, where d is the number of geometric dimensions. These macro-elements are compatible with those resulting from the coarse mesh partition. Consequently, when the shared node of the support is successively located at every node of the global mesh, the whole domain is covered, permitting the overlapping of the support at each macro-element of the partition.

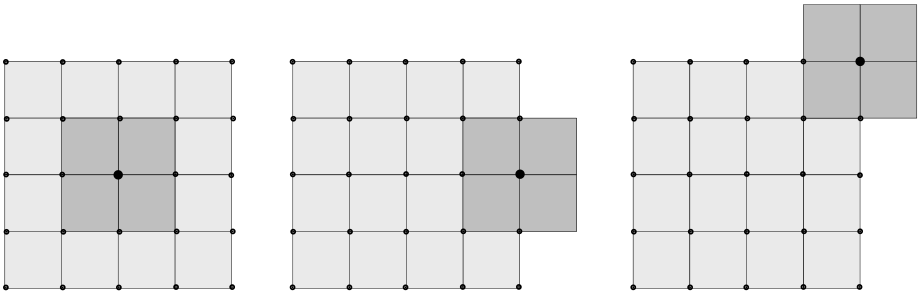

a) Whole support **b) Half-support** **c) Quarter-support**

Figure 3.3: Configuration of the support while covering the whole domain for global linear shape functions.

During the process of covering the domain, the support presents several configurations. For the sake of clarity, Fig. 3.3 represents the three possible configurations of a 2D support (consisting of four squared macro-elements) when it covers the coarse mesh of a domain with linear shape functions. When it is located over an inner node, its four macro-elements cover four macro-elements of the partition. However, when the nodes are located over the domain boundary, only a half or a quarter of the support is used. When the support domain is centred over the position of a node of the coarse mesh, the domain Ω_{loc} covered by the support can be defined as follows:

$$\Omega_{\text{loc}} = \bigcup_e \Omega_e, \tag{3.12}$$

where the index e makes reference to the set of macro-elements that share the coarse-mesh node where the support is centred.

The objective of creating this configuration is the definition of the local variable over the support and the coupling of the local variable with the global variable and its shape functions. For instance, for a 2D support consisting of four squared macro-elements, the distribution of the local enrichment over the support when using linear global shape functions is shown in Fig. 3.4.

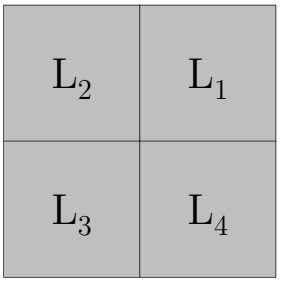

Figure 3.4: Distribution of the Local variable throughout the support.

The configuration of the global shape functions for the linear case for squared 2D meshes is shown in Fig. 3.5. In this case, linear Lagrangian shape functions are applied to a local support whose centre is located at the position of a node of the coarse mesh, involving the four macro-elements Ω_e that share this node. Thus, each part of the shape function is associated with its corresponding set of values of the local enrichment L_i (Fig. 3.4).

The shape functions allow us to interpolate the values of the global variables defined at the nodes of the coarse mesh. Even though the values of the global variable are shared by the macro-elements, reducing the *independence* of the approximation of each subdomain, this fact ensures the continuity of the solution.

3.2.3 Global-Local PGD computation

3.2.3.1 Weak form

After the description of the fundamentals of this Global-Local PGD approach and in order to illustrate this technique, the Poisson equation has been chosen for developing the formulation of the PGD:

$$\Delta u + f = 0. \tag{3.13}$$

The aim of this approach is to enrich a FEM solution previously obtained over a coarse

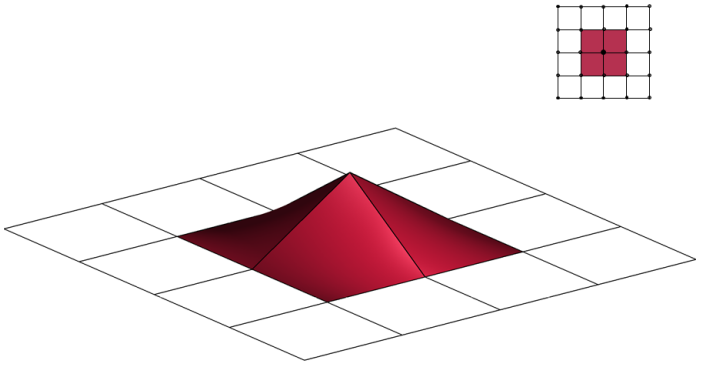

Figure 3.5: Configuration of the global shape functions for the linear case and squared 2D meshes.

mesh, therefore the solution field is defined as the sum of the known coarse solution u_{fem} and the enrichment obtained by using the PGD, u_{enr}:

$$u = u_{\text{fem}} + u_{\text{enr}} \tag{3.14}$$

If we introduce Eq. (3.14) into Eq. (3.13), the Poisson equation now reads

$$\Delta u_{\text{fem}} + \Delta u_{\text{enr}} + f = 0. \tag{3.15}$$

When only considering Dirichlet boundary conditions at the boundary of a generic domain Ω, and for all suitable test functions u^*, the weak form of Eq. (3.15) is defined as follows:

$$\int_\Omega u^* (\Delta u_{\text{fem}} + \Delta u_{\text{enr}} + f)\, d\Omega = 0, \tag{3.16}$$

or integrating by parts,

$$\int_\Omega \nabla u^* \cdot (\nabla u_{\text{fem}} + \nabla u_{\text{enr}})\, d\Omega = \int_\Omega u^* f\, d\Omega \tag{3.17}$$

The global-local approximation has already been defined in Eq. (3.6). Let us suppose that a single mode wants to be computed, i.e. we consider $j = 1$. This represents the greedy PGD algorithm, that adds one term at a time to the separated representation. Consequently, its gradient ∇u_{enr} reads:

$$\nabla u_{\text{enr}} = \sum_{i \in I_{\text{enr}}} \nabla N_i \sum_{k \in I_{\text{loc}}} M_k l^k\, g_i + \sum_{i \in I_{\text{enr}}} N_i \sum_{k \in I_{\text{loc}}} \nabla M_k l^k\, g_i. \tag{3.18}$$

The expression for ∇u_{enr} of Eq. (3.18) can be introduced into Eq. (3.17):

$$\int_\Omega \nabla u^* \cdot \left[\sum_{i \in I_{\text{enr}}} \nabla N_i \sum_{k \in I_{\text{loc}}} M_k l^k \, g_i + \sum_{i \in I_{\text{enr}}} N_i \sum_{k \in I_{\text{loc}}} \nabla M_k l^k \, g_i \right] d\Omega = \\ = \int_\Omega u^* f \, d\Omega - \int_\Omega \nabla u^* \cdot \nabla u_{\text{fem}} \, d\Omega \tag{3.19}$$

where an appropriate choice for the weight function u^* makes possible the calculation of the global and the local variables. This is carried out by following the two-step Alternating Direction Strategy described in Sections 3.2.3.2 and 3.2.3.3 and using a greedy algorithm.

3.2.3.2 Global problem

The definition of u_{enr} and ∇u_{enr} presented above can be rewritten as follows:

$$u_{\text{enr}} = \sum_{i \in I_{\text{enr}}} \left(\sum_{k \in I_{\text{loc}}} N_i M_k l^k \right) g_i, \tag{3.20}$$

and

$$\nabla u_{\text{enr}} = \sum_{i \in I_{\text{enr}}} \left(\sum_{k \in I_{\text{loc}}} \nabla N_i M_k l^k \right) g_i + \sum_{i \in I_{\text{enr}}} \left(\sum_{k \in I_{\text{loc}}} N_i \nabla M_k l^k \right) g_i. \tag{3.21}$$

Introducing $\hat{N}_i$, $\hat{B}^I_{G,i}$ and $\hat{B}^{II}_{G,i}$, the equations Eq. (3.20) and Eq. (3.21) can be rewritten as follows:

$$u_{\text{enr}} = \sum_{i \in I_{\text{enr}}} \hat{N}_i \, g_i, \tag{3.22}$$

and

$$\nabla u_{\text{enr}} = \sum_{i \in I_{\text{enr}}} \left(\hat{B}^I_{G,i} + \hat{B}^{II}_{G,i} \right) g_i \tag{3.23}$$

where $\hat{N}_i$, $\hat{B}^I_{G,i}$ and $\hat{B}^{II}_{G,i}$ represent a sort of *shape functions* composed of products of global shape functions (or their derivatives), local shape functions (or their derivatives) and the local variable.

Similarly, we can choose an appropriate test function, so that u^* and ∇u^* can be defined, at some node $i \in I_{\text{enr}}$:

$$u^*_i = \hat{N}_i \, g^*_i, \tag{3.24}$$

and

$$\nabla u^*_i = \left(\hat{B}^I_{G,i} + \hat{B}^{II}_{G,i} \right) g^*_i. \tag{3.25}$$

Finally, we can substitute Eq. (3.22), Eq. (3.23), Eq. (3.24) and Eq. (3.25) in Eq. (3.17), and obtain a new version of Eq. (3.19) for solving the global problem:

$$\sum_{i\in I_{\text{enr}}} g_j^* \int_\Omega \left(\hat{B}^I_{G,j} + \hat{B}^{II}_{G,j}\right) \cdot \left(\hat{B}^I_{G,i} + \hat{B}^{II}_{G,j}\right) d\Omega\, g_i =$$
$$= g_j^* \int_\Omega \hat{N}_j\, f\, d\Omega - g_j^* \int_\Omega \left(\hat{B}^I_{G,j} + \hat{B}^{II}_{G,j}\right) \cdot \nabla u_{\text{fem}}\, d\Omega, \qquad \forall j \in I_{\text{enr}}, \tag{3.26}$$

where the operators $\hat{N}_i$, $\hat{B}^I_{G,i}$ and $\hat{B}^{II}_{G,i}$ depend on the shape functions and a known value of the local variable at a given enrichment step and its corresponding fixed point iteration. The only unknown is the global variable.

In order to integrate the above equations properly, the standard procedure is to integrate over each macro-element and then assemble the resulting matrices with the global numbering given by the mesh topology. Here the integration needs to be carried out on the reference support, therefore using the Gauss quadrature corresponding to the local discretization. If the Gauss quadrature corresponding to the macro-element discretization were to be used (the one that integrates N_i shape functions), an integration error would be introduced. Fig. 3.6 depicts the situation. In order to avoid that issue, for the solution of the global and the local problems we will consider that the integrals are calculated by using the Gauss quadrature associated with the local discretization, as depicted in Fig. 3.6b.

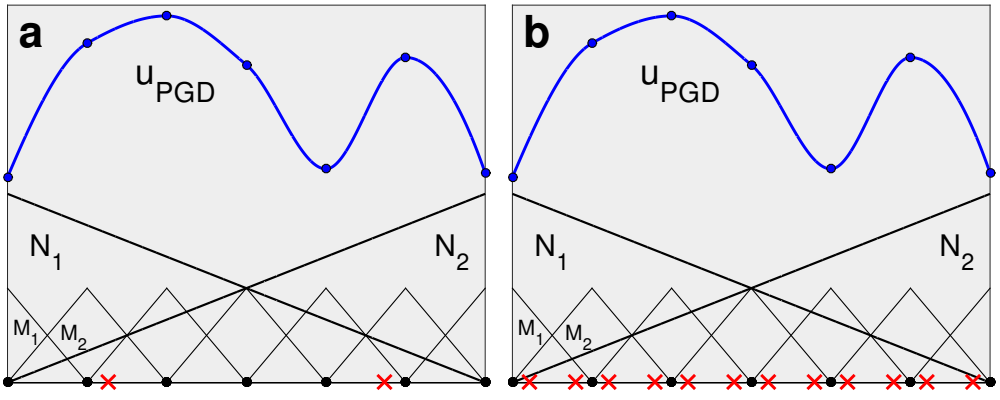

Figure 3.6: Gaussian quadrature associated with the global (a) and the local (b) discretizations.

Now, by performing the integration process, Eq. (3.26) can be turned into the following

set of elemental matrices (here we refer to macro-elements):

$$\begin{aligned}
\boldsymbol{K}_G^{I,e} &\equiv \int_{\Omega^e} \hat{B}_{G,i}^{I} \cdot \hat{B}_{G,j}^{I} \, d\Omega^e, \\
\boldsymbol{K}_G^{II,e} &\equiv \int_{\Omega^e} \hat{B}_{G,i}^{I} \cdot \hat{B}_{G,j}^{II} \, d\Omega^e, \\
\boldsymbol{K}_G^{III,e} &\equiv \int_{\Omega^e} \hat{B}_{G,i}^{II} \cdot \hat{B}_{G,j}^{I} \, d\Omega^e, \\
\boldsymbol{K}_G^{IV,e} &\equiv \int_{\Omega^e} \hat{B}_{G,i}^{II} \cdot \hat{B}_{G,j}^{II} \, d\Omega^e.
\end{aligned} \tag{3.27}$$

The elemental Laplacian matrix at the global level is:

$$\boldsymbol{K}_G^e = \boldsymbol{K}_G^{I,e} + \boldsymbol{K}_G^{II,e} + \boldsymbol{K}_G^{III,e} + \boldsymbol{K}_G^{IV,e}. \tag{3.28}$$

Likewise, on the right-hand side of Eq. (3.26), the integration can be carried out on the initial coarse mesh solution and the source term:

$$\begin{aligned}
\boldsymbol{b}_G^{I,e} &\equiv \int_{\Omega^e} \hat{N}_j \, f \, d\Omega^e, \\
\boldsymbol{b}_G^{II,e} &\equiv \int_{\Omega^e} \left(\hat{B}_{G,i}^{I} + \hat{B}_{G,j}^{II} \right) \cdot \nabla u_{\text{fem}} \, d\Omega^e,
\end{aligned} \tag{3.29}$$

which delivers the vector of nodal equivalent fluxes:

$$\boldsymbol{b}_G^e = \boldsymbol{b}_G^{I,e} - \boldsymbol{b}_G^{II,e}. \tag{3.30}$$

Both the Laplacian matrix and the nodal fluxes vector at the macro-element level can be brought to the global numbering by following a standard finite element assembling process:

$$\boldsymbol{K}_G \, \boldsymbol{g} = \boldsymbol{b}_G, \tag{3.31}$$

where $\boldsymbol{g}$ collects the nodal values g_i, for $i \in I_{\text{enr}}$, of the global function at the macro-mesh.

3.2.3.3 Local problem

The objective of this section is to obtain the local variable from a previously obtained global variable at a given enrichment step. We follow the methodology used in 3.2.3.2. We can write the approximation provided by Eq. (3.6) at the reference support:

$$u_{\text{enr}} = \sum_{k \in I_{\text{loc}}} \left(\sum_{i \in I_{\text{enr}}} N_i M_k g_i \right) l^k, \tag{3.32}$$

that can be interpreted as the contribution of all enriched nodes to the reference support. It can also be written as:

$$u_{\text{enr}} = \sum_{k \in I_{\text{loc}}} \hat{M}_k l^k. \tag{3.33}$$

The gradient is defined as:

$$\nabla u_{\text{enr}} = \sum_{k \in I_{\text{loc}}} \left(\hat{B}^I_{L,k} + \hat{B}^{II}_{L,k} \right) l^k. \tag{3.34}$$

The operators $\hat{M}_k$, $\hat{B}^I_{L,k}$ and $\hat{B}^{II}_{L,k}$ are defined as follows:

$$\hat{M}_k = \sum_{i \in I_{\text{enr}}} N_i M_k g_i, \tag{3.35}$$

$$\hat{B}^I_{L,k} = \sum_{i \in I_{\text{enr}}} N_i \nabla M_k g_i \tag{3.36}$$

$$\hat{B}^{II}_{L,k} = \sum_{i \in I_{\text{enr}}} \nabla N_i M_k g_i. \tag{3.37}$$

Both the test function and its gradient are defined as follows, at the reference support node k:

$$u^*_k = \hat{M}_k l^{k*}, \tag{3.38}$$

and

$$\nabla u^*_k = \left(\hat{B}^I_{L,k} + \hat{B}^{II}_{L,k} \right) l^{k*}. \tag{3.39}$$

Thus, we can replace Eq. (3.33), Eq. (3.34), Eq. (3.38) and Eq. (3.39) in Eq. (3.17), and obtain the weak form for solving the local problem:

$$\begin{aligned} &\sum_{k \in I_{\text{loc}}} l^{j*} \int_\Omega \left(\hat{B}^I_{L,j} + \hat{B}^{II}_{L,j} \right) \cdot \left(\hat{B}^I_{L,k} + \hat{B}^{II}_{L,k} \right) d\Omega \, l^k = \\ &= l^{j*} \int_\Omega \hat{M}_j \, f \, d\Omega - l^{j*} \int_\Omega \left(\hat{B}^I_{L,j} + \hat{B}^{II}_{L,j} \right) \cdot \nabla u_{\text{fem}} \, d\Omega, \qquad \forall j \in I_{\text{loc}}, \end{aligned} \tag{3.40}$$

where the operators $\hat{M}_k$, $\hat{B}^I_{L,k}$ and $\hat{B}^{II}_{L,k}$ depend on the shape functions and a known value of the global variable.

Now, by performing the integration process, Eq. (3.40) can be turned into the following set of elemental matrices (here we refer to elements at the reference local support):

$$\begin{aligned} \boldsymbol{K}^{I,e}_L &\equiv \int_{\Omega^e} \hat{B}^I_{L,j} \cdot \hat{B}^I_{L,k} \, d\Omega^e \\ \boldsymbol{K}^{II,e}_L &\equiv \int_{\Omega^e} \hat{B}^I_{L,j} \cdot \hat{B}^{II}_{L,k} \, d\Omega^e \\ \boldsymbol{K}^{III,e}_L &\equiv \int_{\Omega^e} \hat{B}^{II}_{L,j} \cdot \hat{B}^I_{L,k} \, d\Omega^e \\ \boldsymbol{K}^{IV,e}_L &\equiv \int_{\Omega^e} \hat{B}^{II}_{L,j} \cdot \hat{B}^{II}_{L,k} \, d\Omega^e \end{aligned} \tag{3.41}$$

The elemental Laplacian matrix at the local level is:

$$\boldsymbol{K}^e_L = \boldsymbol{K}^{I,e}_L + \boldsymbol{K}^{II,e}_L + \boldsymbol{K}^{III,e}_L + \boldsymbol{K}^{IV,e}_L. \tag{3.42}$$

Likewise, on the right-hand side, the integration can be carried out:

$$\begin{aligned} \boldsymbol{b}_L^{I,e} &\equiv \int_{\Omega^e} \hat{M}_j \, f \, d\Omega^e \\ \boldsymbol{b}_L^{II,e} &\equiv \int_{\Omega^e} \left(\hat{B}_{L,j}^{I} + \hat{B}_{L,j}^{II} \right) \cdot \nabla u_{\text{fem}} \, d\Omega^e \end{aligned} \tag{3.43}$$

which delivers the vector of nodal equivalent fluxes:

$$\boldsymbol{b}_L^e = \boldsymbol{b}_L^{I,e} - \boldsymbol{b}_L^{II,e}. \tag{3.44}$$

Both the Laplacian matrix and the nodal fluxes vector at the support element level can be brought to the local numbering by following a standard finite element assembly process:

$$\boldsymbol{K}_L \, \boldsymbol{l} = \boldsymbol{b}_L, \tag{3.45}$$

where $\boldsymbol{l}$ collects the nodal values l^k, for $k \in I_{\text{loc}}$, of the local function at the reference support mesh.

3.3 A GFEM interpretation

The partition of unity is a very useful tool for coupling local enrichments to coarse meshes in the framework of some FEM-based techniques. The difference between the methods based on the partition of unity lies in the configuration of the enrichments and how they are obtained. The accuracy is related to the capability of these enrichments for reproducing the solution of the local feature. In this section, the enrichment strategy of one of these techniques, GFEM, is analysed in order to compare it with the Global-Local PGD presented in this work.

3.3.1 Fundamentals of GFEM

In order to describe the enrichment space of GFEM and for the sake of clarity, the scheme of Fig. 3.7 (taken from [94]) is presented. This figure represents the construction of the GFEM shape functions for a 2D domain. The GFEM approximation space (i.e a trial space) is built by means of three components:

- *Patch* ω_α. For GFEM techniques, the patch ω_α is defined by the elements of a standard FEM mesh that share the node α. If we consider that n patches cover the whole local domain of interest Ω_L:

$$\Omega_L = \bigcup_{\alpha=1}^{n} \omega_\alpha \tag{3.46}$$

- *Partition of Unity applied to the patches.* The shape functions satisfying the Partition of Unity are applied to each patch. To illustrate this example, the Lagrangian FEM shape functions N_α are shown in Fig. 3.7 for a patch concerning a generic node α. These shape functions satisfy Eq. (3.1) for the local domain of interest Ω_L, where the enrichments are going to be coupled.

- *Patch approximation spaces* χ_α. For each patch ω_α, there is a m_α-dimensional space of functions defined over ω_α. These functions $L_{\alpha i}$ (see Fig. 3.7) are called *enrichment functions*. Due to these functions, the GFEM is able to capture the information related to the special features of the domain. Functions $L_{\alpha i}$ are calculated in view of the *a priori* knowledge of the problem, which means that the appropriate selection of suitable patch spaces is crucial for obtaining a good GFEM approximation. χ_α is defined as follows:

$$\chi_\alpha = \text{span}\Big\{ L_{\alpha i}, \quad 1 \leq i \leq m_\alpha, L_{\alpha i} \in H^1(\omega_\alpha) \Big\} \tag{3.47}$$

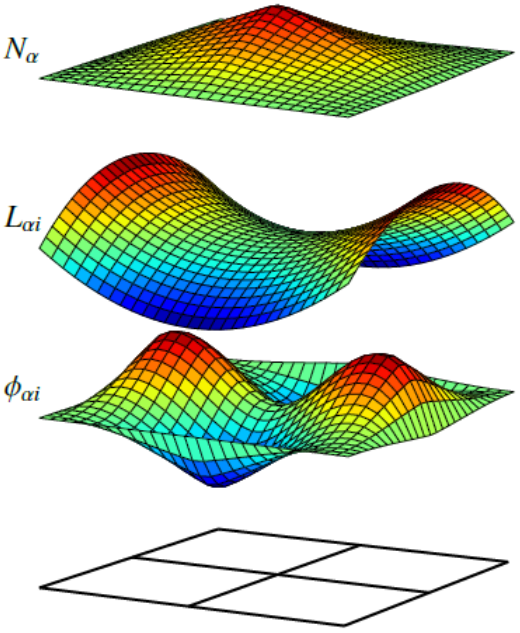

Figure 3.7: Construction of the GFEM shape function $\phi_{\alpha i}$ [94].

Thus, the GFEM trial space can be defined as:

$$S_{\text{GFEM}}(\Omega_L) \equiv \sum_{\alpha=1}^{n} N_\alpha \chi_\alpha = \text{span}\,\{\phi_{\alpha i} := N_\alpha L_{\alpha i}, 1 \leq i \leq m_\alpha, 1 \leq \alpha \leq n\} \tag{3.48}$$

where $\phi_{\alpha i}$ are the GFEM shape functions.

Using Partition of Unity based shape functions N_α as basis functions in a FEM framework, the approximation of the solution of the scalar field Eq. (3.3) at the nodes x of the discretization of a domain Ω is now rewritten as:

$$u_{\text{GFEM}}(x) = \sum_{\alpha \in I} N_\alpha(x)\hat{u}_\alpha + \sum_{e \in I_{\text{enr}} \subset I} N_e(x) \sum_j L_{ej}\tilde{u}_{ej} \tag{3.49}$$

where the two terms represent the standard FEM approximation and the enrichment term. The field $\hat{u}_\alpha$ represents the standard or global degrees of freedom, corresponding to global nodal values related to the basis built by using the shape functions N_α. With respect to the enrichment, which is located in the nodes corresponding to the local feature of interest, $\tilde{u}_{ej}$ represents the extra degrees of freedom. $\tilde{u}_{ej}$ is related to the basis constructed by the local enrichment functions L_{ej} (with $1 \leq j \leq m_\alpha$, j being the number of terms of each enrichment function.

The expression introduced in Eq. (3.49) can also be rewritten in FEM notation, as follows:

$$\boldsymbol{u}_{\text{GFEM}} = \boldsymbol{N}\,\hat{\boldsymbol{u}} + \boldsymbol{N}\,\boldsymbol{L}_e\tilde{\boldsymbol{u}}, \tag{3.50}$$

where $\boldsymbol{u}_{\text{GFEM}}$ is a vector of order p over an n-node full-enriched element. $\boldsymbol{N}$ is a $p \times (p \cdot n)$ matrix representing the standard FEM shape functions. $\boldsymbol{L}_e$ is a $(p \cdot n) \times (p \cdot m \cdot n)$ matrix which provides the extra basis constructed by means of the enrichment functions. The product of $\boldsymbol{N}$ and $\boldsymbol{L}_e$ represents the GFEM shape functions. The degrees of freedom are represented by the standard degrees of freedom vector $\hat{\boldsymbol{u}}$ of size $(p \cdot n) \times 1$ and the enrichment degrees of freedom vector $\tilde{\boldsymbol{u}}$ of size $(p \cdot m \cdot n) \times 1$.

When comparing this enrichment definition with the methodology introduced in this chapter, it can be deduced that the concept of patch is equivalent to the local support presented in 3.2.2.1. In GFEM the union of patches represents the local domain whereas, in the Global-Local PGD approach, the replication of the support over the coarse mesh covers the whole domain. Moreover, the enrichments defined over each patch $L_{\alpha i}$ coincide with the definition of local variable of the Global-Local PGD, but in the PGD approach, these enrichment functions are the same for all the patches.

3.3.2 The enrichment functions

After the definition of the combination of the Partition of the Unity and the enrichments, the main challenge of GFEM is the selection of the enrichment functions, since the accuracy of the method depends on the suitability of the approximation spaces to reproduce the solution. For this purpose, taking advantage of the *a priori* knowledge about the behaviour of the solution, polynomial, exponential, and even discontinuous functions have been employed as enrichments in order to model the local features of interest.

Some analytical approaches have been proposed in [78, 82]. Nevertheless, the use of analytical enrichments has some limitations in terms of applicability as they are not easily available for most of the cases. Model Order Reduction techniques have also been used to face this challenge. More specifically, the modes obtained by using *a posteriori* methods like the POD can be employed as enrichment functions [7]. Nevertheless, this technique presents some limitations, as the GFEM approach does not reproduce the relevant information of the solution when the problem of interest is not very related to the model from which the snapshots were obtained.

One interesting methodology for obtaining enrichment spaces in the framework of GFEM is presented in [37, 41, 45]: GFEM with Global-Local enrichment functions. Among the different techniques for solving detailed FEM models while reducing the numerical complexity without increasing considerably the computational effort required to maintain the accuracy of the results, the Global-Local iterative approach (see [2, 87, 100, 109]) represents a good alternative and has been widely applied to the development of multiple numerical analysis methodologies.

This concept may include a wide amount of techniques, but it basically represents itself a sort of multi-scale method, a hierarchical technique. It is based on the idea that a domain can be globally analysed by means of a coarse mesh in order to obtain suitable boundary conditions that are imposed to a local region of the domain, this local region being reanalysed with a more refined mesh. With respect to GFEM, the enrichments can be obtained by solving a fine local problem with boundary conditions provided by a coarse global solution, implying an iterative problem.

Therefore, this strategy is intimately related to an inheritance concept, since the behaviour of the local fine mesh is governed by the data provided by the global coarse mesh. For the sake of clarity, a scheme representing both discretizations is shown in Fig. 3.8. In order to properly describe the Global-Local approach it is important to carry out the following stages:

1. The accurate characterisation of the Global model is crucial, in order to provide the appropriate information to the Local model.

2. The hierarchical interface: if the data obtained from the coarse mesh (boundary conditions for the Local model) do not exactly match with the fine mesh, it is necessary to establish an interpolation region.

3. The proper Local analysis: the use of a much more refined mesh in order to capture the detailed information of the special features located in the domain.

The process of construction of enrichment functions by using this iterative scheme accounts for possible interactions of local and global behaviours, which represents a considerable improvement with respect to standard Global-Local FEM techniques. Moreover, all

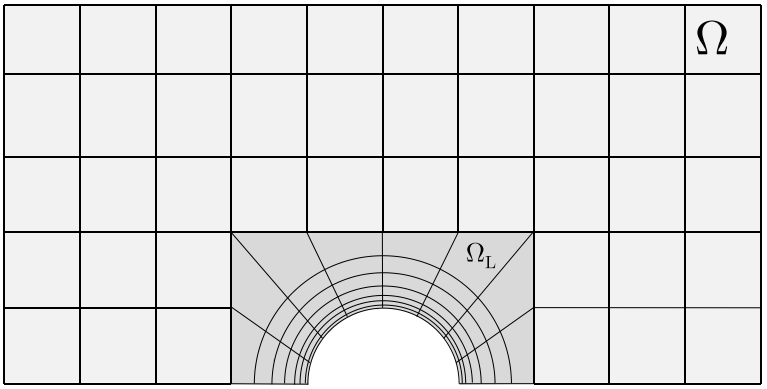

Figure 3.8: Discretization of the Global and Local domains Ω and Ω_L

local problems of the domain can be solved by means of parallel computing, as a domain decomposition technique. However, when addressing time-dependant problems, the iterations must be carried out for each time step.

With respect to *a priori* MOR techniques, the PGD has been employed in [23] to create a computational vademecum in the frame of GFEM (V-GFEM). Parametric solutions computed off-line by means of the PGD are used as enrichment functions, which are employed in the simulation of thermal models related to welding processes.

As it was commented in Chapter 1, considering the variational formulation of a parametric problem Eq. (1.12), the approximation provided by the PGD is expressed as a finite sum of functional products depending on the parameters of the problem (Eq. (1.13)). For the approach presented in [23], the enrichments of the GFEM are obtained by using the PGD, Eq. (3.49) being rewritten as follows:

$$u_{\text{GFEM}} = \sum_{\alpha \in I} N_\alpha \hat{u}_\alpha + \sum_{\epsilon \in I_{\text{enr}} \subset I} N_e \, \phi(\mu_1, \mu_2, ..., \mu_n) \tilde{u}_e \tag{3.51}$$

where $\mu_1, \mu_2, ..., \mu_n$ are the parameters of the solution, and ϕ is the enrichment function that is computed by using the PGD approach. Thus, $\phi(\mu_1, \mu_2, ..., \mu_n)$ reads:

$$\phi(\mu_1, \mu_2, ..., \mu_n) = \sum_{k=1}^{K} \prod_{i=1}^{n} F_i^k(\mu_i). \tag{3.52}$$

In connection with these methods, the PGD presented in this chapter represents an alternative for enriching standard FEM solutions defined over coarse discretizations. Nevertheless, the Global-Local PGD provides the most appropriate enrichment approximation space without *a priori* information of the solution and without solving additional problems, which

represents an important advantage when compared to GFEM approaches. The methodology proposed in this work provides the enrichment as it builds the separated representation of the solution.

3.4 Numerical Examples

3.4.1 One-dimensional cases

3.4.1.1 The steady heat conduction equation

The first example concerns the steady heat conduction equation Eq. (3.13), applied to a 1D domain (with a length $l_x = 2$), with $f = -1$ and homogeneous Dirichlet boundary conditions at $x = 0$ and $x = l_x$. The whole domain is initially partitioned into 2 macro-elements.

The FEM approximation of a coarse mesh described by the partition of the domain, u_{fem}, is defined as the starting point of the method. The mesh size of the support of the local variable corresponds to the size of the elements of the desired fine discretization, which consist in a mesh of 21 nodes per macro-element. Thus, following the formulation described in Section 3.2.3 for the Poisson equation, the Global-Local PGD approach can be applied in order to enrich the initial FEM solution.

The global variable is defined over the coarse discretization (3 nodes) and the local variable is defined over a support domain or patch consisting of 2 macro-elements. This simple example is very particular, as the 1D domain and the support of the local variable match. Due to this fact, the solution can be easily replicated by using Eq. (3.12), imposing the Dirichlet Boundary conditions to the global problem ($G(x = 0) = G(x = l_x) = 0$) and placing the support of the local variable over the domain.

Fig. 3.9, represents the initial coarse FEM solution and the enriched PGD approximation. Thus, by considering one mode, the nodal relative error of the PGD when compared with the FEM approximation (which, in turn, matches the exact solution) is around 10^{-14}.

With regard to the configuration of the PGD solution, the coupling of the local variable and the global shape functions defined over the support is shown in Fig. 3.10, resulting in two similar parabolic distributions. As can be deduced from Fig. 3.9, this configuration is zero for the position of the coarse mesh nodes, resulting in a sort of *bubble* enrichments, since the initial coarse FEM nodal solution is exact (no enrichment is required at the nodes).

This simple configuration where the solution is obtained without overlapping of the support (by making $G = 0$ for the appropriate values of the Global variable) is also maintained when the partition of the domain consists of an ever number of macro-elements, which implies that the solution can be obtained with one mode. Nevertheless, the configuration of the problem, with *bubble* enrichments, makes it impossible to obtain the solution with just one mode for an odd number of macro-elements.

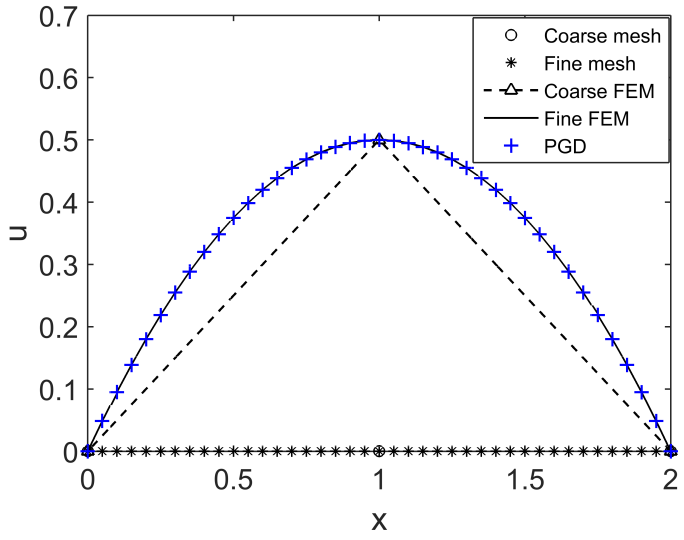

Figure 3.9: PGD approximation of the example 3.4.1.1 for two macro-elements.

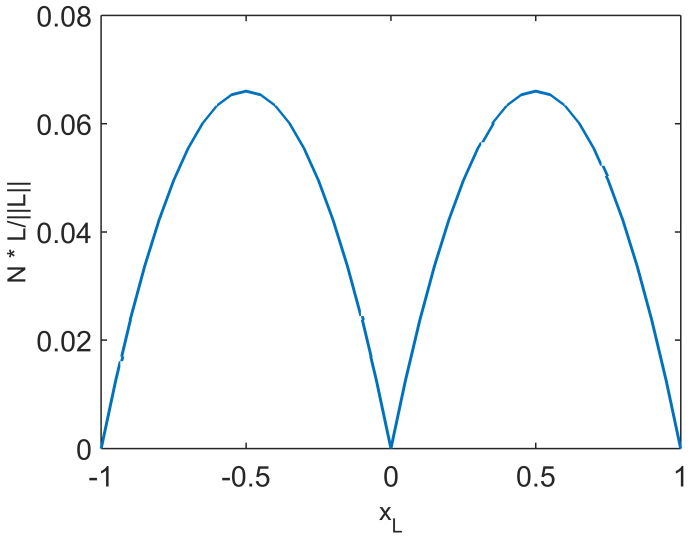

Figure 3.10: Coupling of the local variable and the global shape functions for the example 3.4.1.1 and two macro-elements.

For instance, the same problem is solved with a partition consisting of 3 macro-elements (with a length $l_x = 3$), with the same mesh size of the previous problem (i.e. 21 nodes per subdomain). As can be observed in Fig. 3.11 for one mode, the solution is accurately

obtained for the first and the third macro-elements ($0 \leq x \leq 1$ and $2 \leq x \leq 3$ respectively) but the overlapping of local supports produced in the second subdomain ($1 \leq x \leq 2$) due to non-zero values of the Global variable (G_2 and G_3) makes impossible to obtain the solution for this subdomain. Therefore, a second mode is necessary.

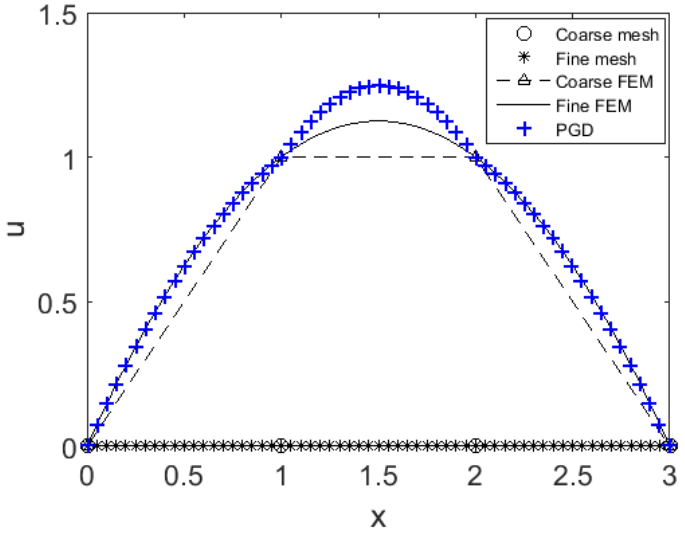

Figure 3.11: PGD approximation of the example 3.4.1.1 for three macro-elements (1 mode).

Fig. 3.12 represents (for two modes), the nodal error when compared to the FEM solution and the coupling of the local variable and the global shape over the local support, respectively. As can be observed, the solution over the second subdomain is corrected by the second mode.

3.4.1.2 The steady reaction-diffusion equation

Another interesting example is related to the steady reaction-diffusion equation, represented as follows:

$$\Delta u - \lambda u + \lambda f = 0, \tag{3.53}$$

where the parameter λ can be modified in order to generate the different cases under consideration.

This equation can be easily applied to a 1D domain, by implementing the approach described in 3.2. For more details, the reader can refer to the formulation of the 1D steady reaction-diffusion equation described in Appendix A.

For instance, this formulation can be applied to a domain consisting of 4 macro-elements with $l_x = 4$ and 26 nodes per subdomain ($h_x = 0.04$). The parameter λ is set to 100. Fig.

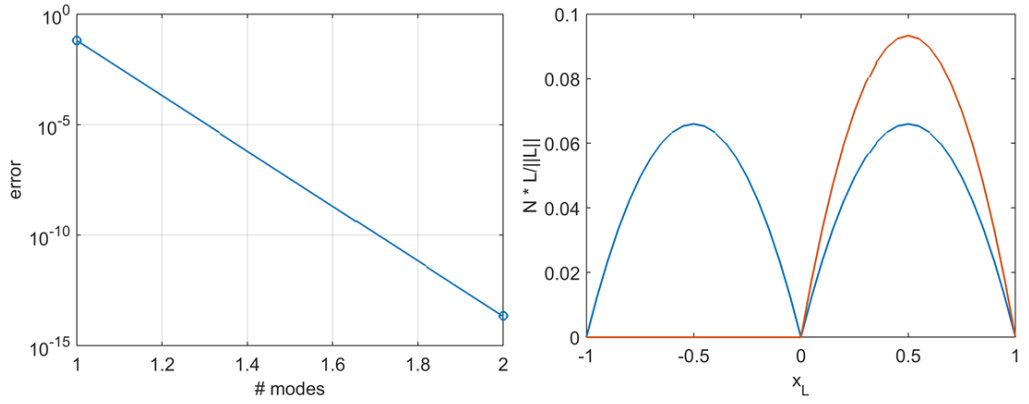

Figure 3.12: Nodal relative error of the PGD when compared with FEM and coupling of the local variable and the global shape functions for the example 3.4.1.1 and three macro-elements.

3.13 represents the coarse and fine FEM solutions of this problem and the PGD approximation when considering the following boundary conditions: $u = 0$ at $x = 0$ and $x = l_x$ for the first case, and $u = 0$ at $x = 0$ and $\frac{du}{dx} = 0$ at $x = l_x$ for the second case; these cases proving the suitability of the method for different types of boundary conditions.

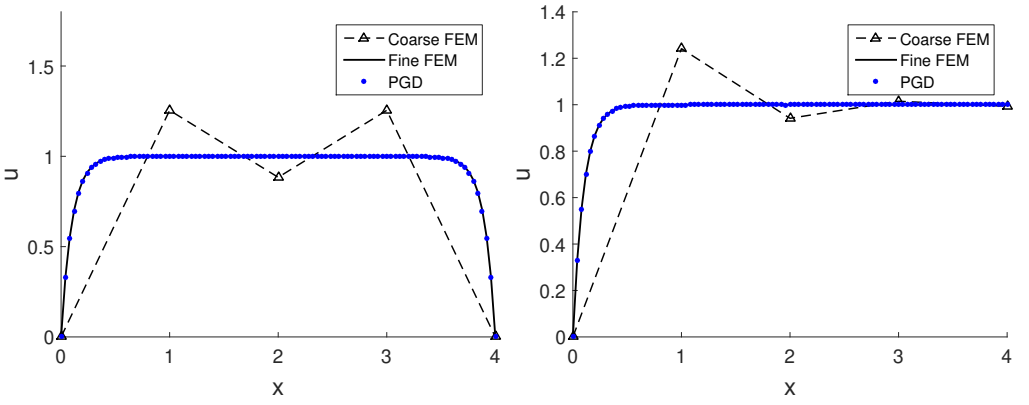

Figure 3.13: Coarse and fine FEM solutions of problem 3.4.1.2 and the PGD approximation for different boundary conditions ($N_s = 4$, $\lambda = 100$ and $h_x = 0.04$).

It is can be easily remarked that, contrary to the examples shown in Section 3.4.1.1, the values of the coarse and the fine FEM solutions do not match the exact solution. Both PGD approximations shown in Fig. 3.13 reveal the potential of this technique for solving fine-meshed problems, with a decrease on the degrees of freedom and consequently, on the computational cost, this decrease becoming more significant as the numbers of macro-

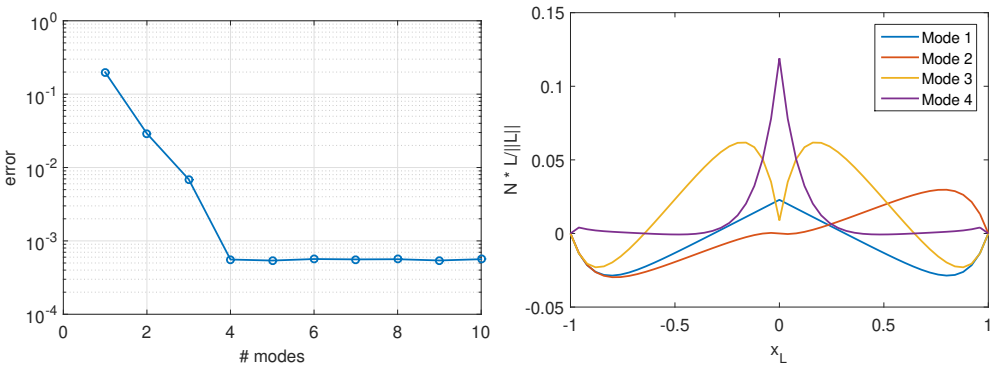

Figure 3.14: Relative L^2-norm error of the PGD when compared with an overkill solution and coupling of the local variable with the global shape functions for the first case shown in Fig. 3.13.

elements of the partition increases. In order to illustrate the performance of the method, in Fig. 3.14 the evolution of the relative L^2-norm error of the PGD when compared with an overkill solution is plotted for the first case. The corresponding coupling of the local variable with the global shape functions is also represented. For this example, the best error is found to be in the order of 10^{-3}, 4 PGD modes being necessary to achieve this value.

In the same way, this technique can be also reproduced for a set of values of the parameter λ. Fig. 3.15 represents the solution of Eq. (3.53) for $\lambda = 1, 10, 100, 1000$, applied to the same domain, partition, and discretization presented in Fig. 3.13 and homogeneous Dirichlet boundary conditions at both sides of the boundary.

As can be observed in Fig. 3.15, this PGD approach reproduces an appropriate approximation of the solution for the set of values of λ, starting from the corresponding coarse mesh FEM solution. As the value of λ increases, the solution is more difficult to approximate, as a higher number of nodes is needed to capture the temperature gradients, as can be deduced from the $\lambda = 1000$ distribution.

Thus, the relative L^2-norm error decreases as λ does, as can be observed in Fig. 3.16 for $\lambda = 10$: the smallest error achieved is now found to be in the order of 10^{-4}, but the method needs a higher number of modes to achieve the best result in terms of relative L^2-norm error when compared to the case $\lambda = 100$.

In order to evaluate and visualise the performance of this approach with regard to the error committed when using the combination of the global and local levels, we propose an analysis of the evolution of the relative L^2-norm error when refining the mesh. The number of nodes per subdomain corresponds to 26, 51, 101, 251 and 501 (h_x=$4 \cdot 10^{-2}$, $2 \cdot 10^{-2}$, $1 \cdot 10^{-2}$, $4 \cdot 10^{-3}$ and $2 \cdot 10^{-3}$). The objective is to compare this PGD error with that obtained when using a standard FEM approximation with a similar mesh size, both errors being calculated

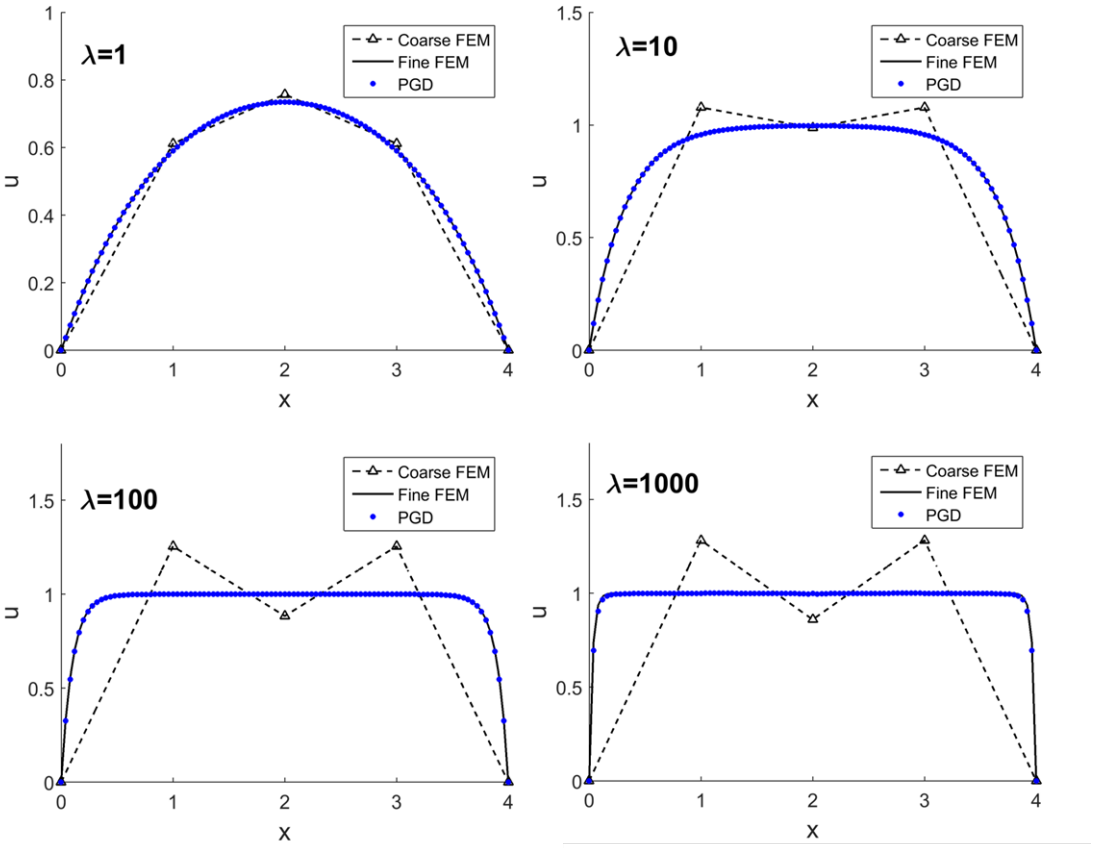

Figure 3.15: Coarse and fine FEM solutions of problem 3.4.1.2 and the PGD approximation for homogeneous Dirichlet boundary conditions ($N_s = 4$, $\lambda = 1, 10, 100, 1000$ and $h_x = 0.04$).

with respect to an overkill solution.

This analysis is plotted in Fig. 3.17 and Fig. 3.18 for $\lambda = 10$ and $\lambda = 1000$ respectively and a partition of the domain consisting of 4 macro-elements. As can be observed, the error is smaller for $\lambda = 10$, as its value achieves $3.33 \cdot 10^{-7}$ for $h_x = 0.002$ (501 nodes per subdomain), in contrast with the case $\lambda = 1000$, where the error is found to be $7.773 \cdot 10^{-6}$.

Regarding the comparison with standard FEM approximations, the evolution of the error of the Global-Local PGD when refining the mesh remains under the results obtained for the FEM solution, which is calculated for the same set of mesh sizes employed for the PGD. The difference between both convergence curves is due to the coupling of both levels of shape functions, which results in a sort of improved FEM operators for solving the global and the local problems (already shown in Eq. (3.31) and Eq. (3.45)). The Global-Local PGD also achieves the FEM optimal convergence, as the slope of the PGD convergence matches with

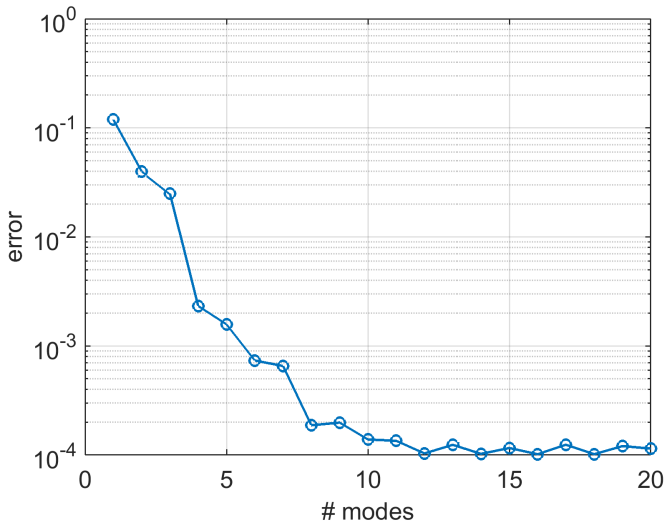

Figure 3.16: Relative L^2-norm error of the PGD when compared with an overkill solution for the problem 3.4.1.2 ($N_s = 4$, $\lambda = 10$ and $h_x = 0.04$)

that of FEM for linear shape functions (i.e. 2).

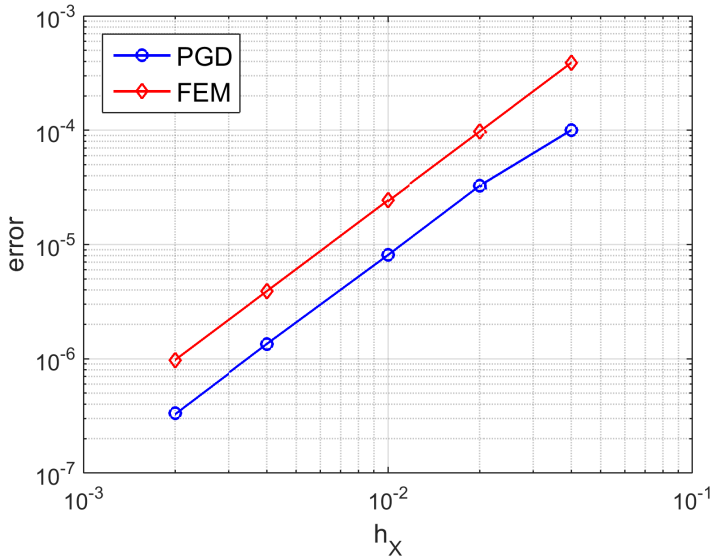

Figure 3.17: Convergence of the relative L^2-norm error of the PGD and FEM when compared to an overkill solution for the problem 3.4.1.2 ($N_s = 4$, $\lambda = 10$)

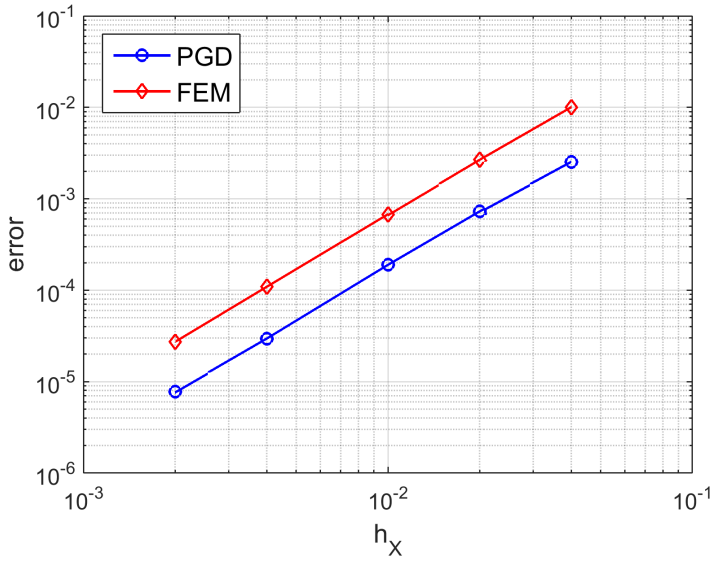

Figure 3.18: Convergence of the relative L^2-norm error of the PGD and FEM when compared to an overkill solution for the problem 3.4.1.2 ($N_s = 4$, $\lambda = 1000$)

As commented before, the relative L^2-norm error corresponding to the Global-Local approach increases as the value of λ does, as the approximation needs a refinement in order to capture the gradient of temperature produced for high values of λ (see $\lambda = 1000$ in Fig. 3.15). This refinement can be carried out without the need of adding more nodes to the discretization, by choosing a pertinent distribution of the macro-elements of the partition. For all the previous examples, the partition resulted in macro-elements that have the same length. But when observing the example $\lambda = 1000$ represented in Fig. 3.15, it seems appropriate to redistribute the configuration of the partition, in order to create two short domains associated with the zone where strong gradients are located. Thus, by using the same number of nodes per subdomain, the approach is able to capture the feature of interest.

This situation is represented in Fig. 3.19, where two of the four macro-elements are made smaller in order to capture the gradients of temperature located at both sides of the domain. The number of nodes is the same that in the case represented in Fig. 3.15, but the configuration of the macro-elements provokes a refinement of the mesh. Moreover, the initial coarse mesh FEM solution is also closer to the reference solution. All these considerations involve a smaller error, as can be observed in Fig. 3.20, where both configurations are compared (Fig. 3.15 and Fig. 3.19). The redistribution of the macro-elements produces a reduction in the error rate by an order of magnitude while maintaining the number of degrees of freedom.

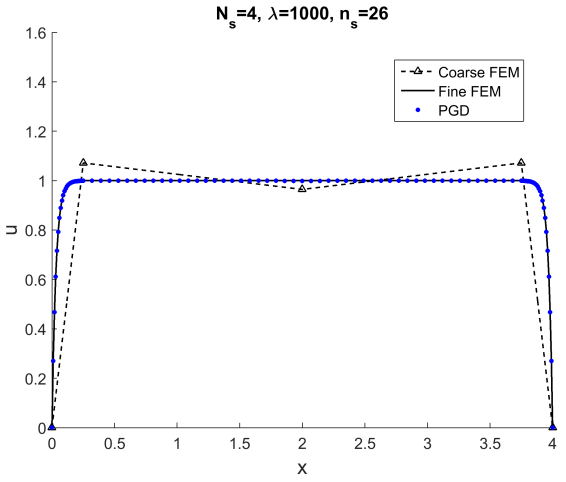

Figure 3.19: Coarse and fine FEM solutions of problem 3.4.1.2 and the PGD approximation for homogeneous Dirichlet boundary conditions ($N_s = 4$, $\lambda = 1000$, and different size meshes throughout the domain).

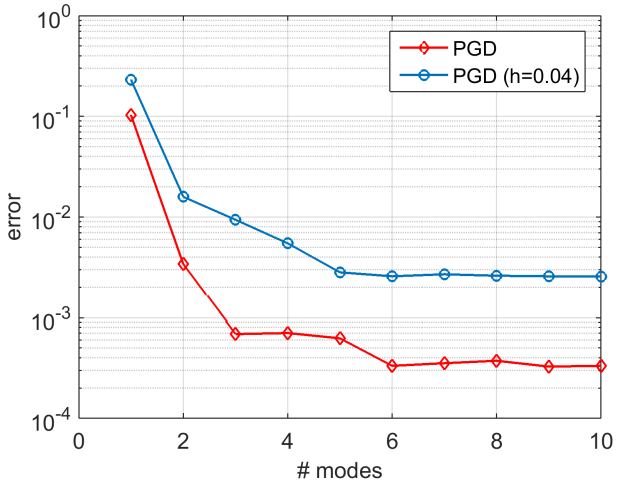

Figure 3.20: Comparison of the relative L^2-norm error of the PGD with respect to an overkill solution for the problem 3.4.1.2 ($N_s = 4$, $\lambda = 1000$) and for $h_x = 0.04$ and different size meshes throughout the domain.

3.4.2 Two-dimensional cases

3.4.2.1 The steady reaction-diffusion equation

The Global-Local approach can be also implemented in 2D geometries for enriching FEM solutions defined over a coarse mesh. The first step corresponds to the partition of the domain into several macro-elements, all macro-elements containing the same number of nodes. For the sake of simplicity, the partitions of the first examples consist of squared macro-elements. The nodes associated with this 2D partition define the coarse mesh where an initial FEM solution is obtained.

In order to enrich this solution, now the coupling of the global level and the local level is carried out by using a 2D support or patch consisting in four subdomains that share a unique node of the coarse mesh. As commented in 3.4.1 the mesh size of the local support is defined by the desired fine mesh configuration of the PGD approximation.

Taking all this into consideration, the steady reaction-diffusion equation (Eq. (3.53)) can be applied to a 2D domain partitioned into 9 squared macro-elements, this configuration being represented in Fig. 3.21.

In addition to the coarse mesh associated with the partition, the approximation is implemented in a fine mesh ($h = 1.33 \cdot 10^{-2}$) which is also represented in Fig. 3.21, this approximation being obtained by replicating the shared node of the patch throughout the coarse mesh.

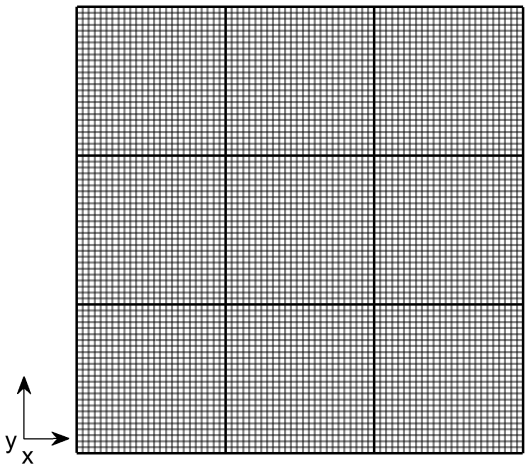

Figure 3.21: Coarse and fine meshes associated with a domain partition into 9 squared macro-elements.

The side length of the squared domain taken into consideration is $l = 1$, and homogeneous Dirichlet boundary conditions are applied at the whole boundary. These boundary conditions

are applied to the Global variable associated with the coarse mesh nodes of the boundary. Fig. 3.22 represents the PGD approximation of Eq. (3.53) for a set of values of λ ($\lambda = 1, 10, 100, 1000$). The partition of the domain is also plotted over the solution in order to visualise the approximation that has to be built at every subdomain.

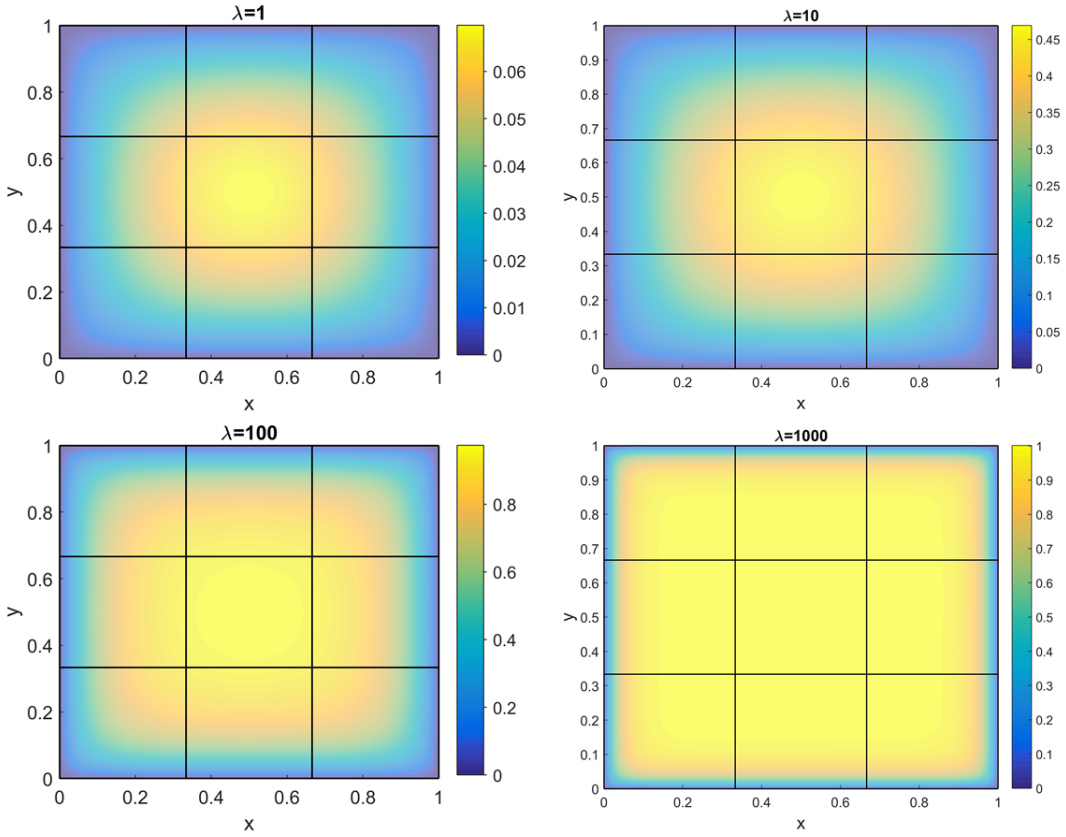

Figure 3.22: PGD approximation of the example associated with Fig. 3.21, Eq. (3.53) with homogeneous Dirichlet boundary conditions at the whole boundary.

As can be observed in Fig. 3.22, while the approximation of the solution does not change remarkably from a qualitative point of view for $\lambda = 1, 10$, as the value of λ increases, a considerable variation of the temperature appears near the boundary of the domain ($\lambda = 100, 1000$). As commented in 3.4.1.2, this gradient is more difficult to be captured and would require a refinement of the mesh of the macro-elements adjacent to the boundary. The regular partition employed in Fig. 3.22 consists in 9 similar macro-elements and, consequently, the relative L^2-norm error is expected to increase as the parameter λ does.

This can be verified by comparing the evolution of the error for all the λ cases under consideration. This comparison is shown in Fig. 3.23. Indeed, the evolution of the relative

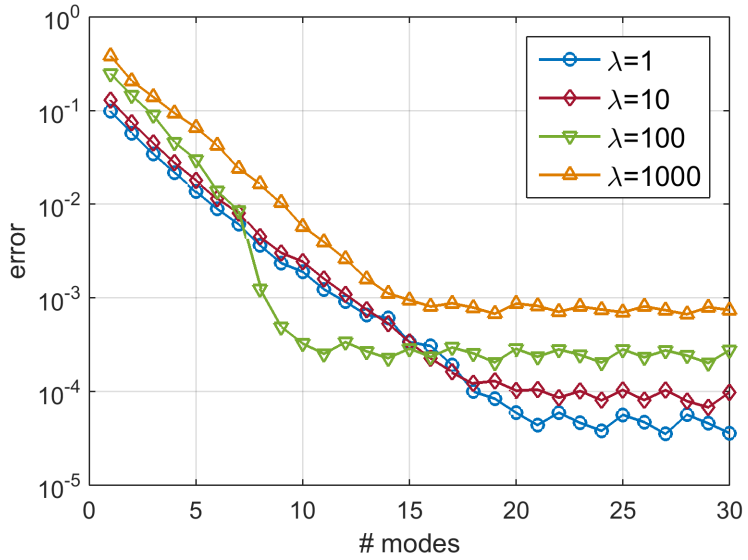

Figure 3.23: Relative L^2-norm error of the PGD when compared with an overkill solution for the examples shown in Fig. 3.22.

L^2-norm error calculated with respect to an overkill solution reveals that the error level decreases as λ does, but a higher number of modes is needed to achieve that error level (as the slope of the convergence is very similar for all the λ cases.

The same strategy employed in 3.4.1.2 is now carried out in order to analyse the performance of the combination of the global and local levels of this PGD in terms of the error convergence when refining. The relative L^2-norm error with respect to an overkill solution is calculated for a fine mesh consisting of squared elements of size $h = 6.67 \cdot 10^{-2}$, $3.33 \cdot 10^{-2}$, $1.67 \cdot 10^{-2}$, and $8.33 \cdot 10^{-3}$. Thus, the performance of the PGD with 9 squared macro-elements is compared with a standard FEM approximation with a similar mesh size.

Fig. 3.24 and Fig. 3.25 represent this convergence for $\lambda = 10$ and $\lambda = 1000$ respectively. As could be expected, the error is considerably smaller for $\lambda = 10$ (by an order of magnitude): it achieves $3.178 \cdot 10^{-5}$ for $h = 8.33 \cdot 10^{-3}$, whereas for $\lambda = 1000$ the error is found to be $3.614 \cdot 10^{-4}$. The convergence of the PGD is similar to the FEM results (the slope is approximately 2). Nevertheless, the combination of the use of global and local shape functions makes the error of the PGD smaller than that obtained with FEM for similar mesh sizes. This fact confirms the results obtained for 1D, as the formulation of the problem by using the global and the local levels represents a sort of improved FEM method.

With respect to the refinement needed to capture the gradient of temperature produced for instance, for the case $\lambda = 100$ (see Fig. 3.22), as commented in 3.4.1.2 for 1D domains, a pertinent redistribution of the macro-elements of the partition can be carried out in order

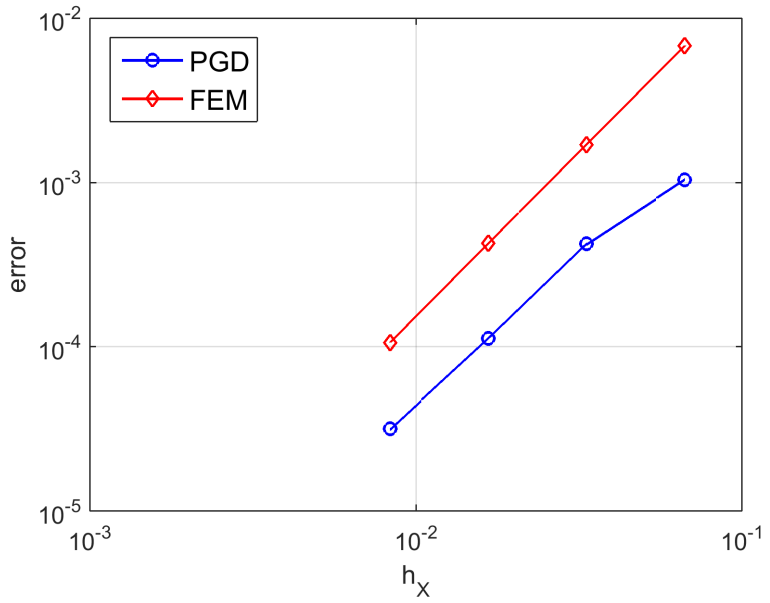

Figure 3.24: Convergence of the relative L^2-norm error of the PGD and FEM when compared to an overkill solution for the problem represented in Fig. 3.22 ($N_s = 9$, $\lambda = 10$).

to obtain a better approximation of the solution. In this case, we can modify the partition for obtaining smaller macro-elements adjacent to the boundary.

As can be observed in Fig. 3.26, a redistribution of the 9 macro-elements can be carried out. This figure represents the partition obtained from the coarse mesh redistribution and the consequent refinement (as all macro-elements have the same number of nodes). In the center of the domain, where no considerable alterations of the solution are expected, a big subdomain is created. The error committed by using this new partition is considerably lower when compared with that obtained with the initial partition (Fig. 3.21). This new partition also needs a smaller number of modes to achieve this level of error, as can be observed in Fig. 3.27.

3.4.3 Non-Cartesian geometry

Once different mesh sizes throughout the same domain have been proposed by changing the distribution of the macro-elements, another interesting example can be implemented concerning non-Cartesian domains. We can assume a quarter annulus and its corresponding coarse discretization consisting of isosceles trapezoid elements. This mesh is represented in Fig. 3.28, with a partition composed of 10 macro-elements. The fine mesh has been obtained by splitting every subdomain into 16 smaller isosceles trapezoids. The objective is to

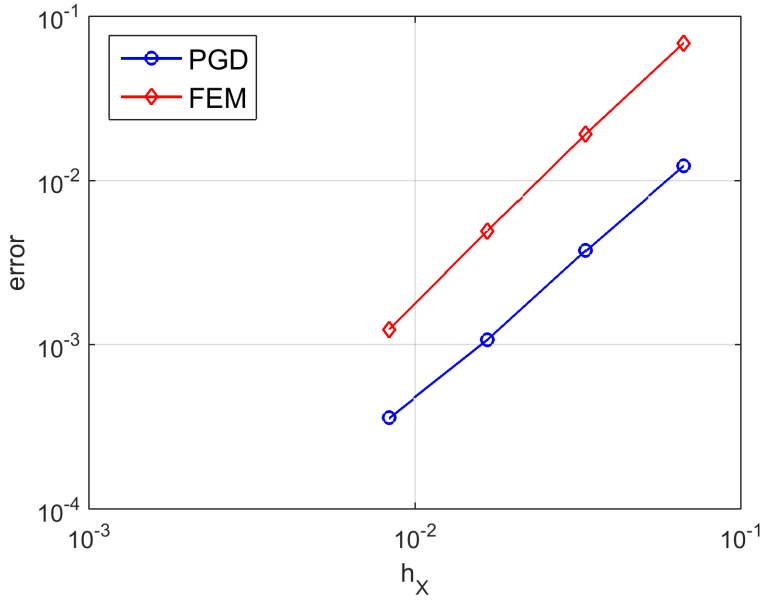

Figure 3.25: Convergence of the relative L^2-norm error of the PGD and FEM when compared to an overkill solution for the problem represented in Fig. 3.22 ($N_s = 9$, $\lambda = 1000$).

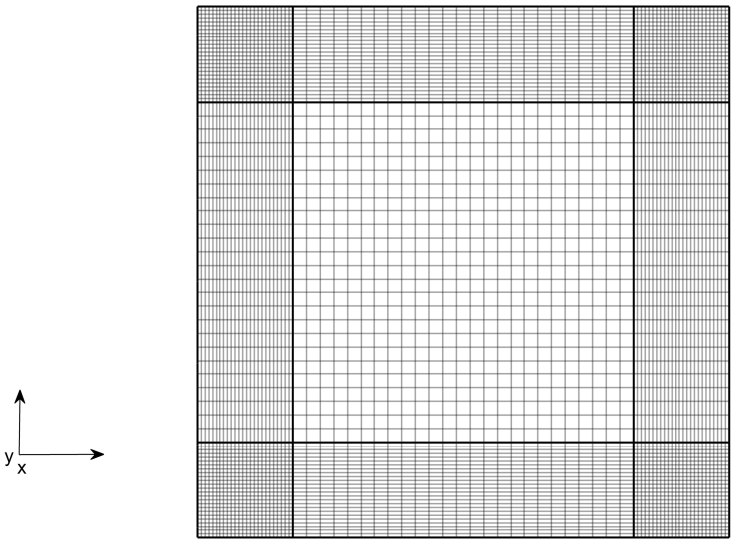

Figure 3.26: Coarse and fine meshes associated with a domain partition into 9 squared macro-elements and different size meshes throughout the domain.

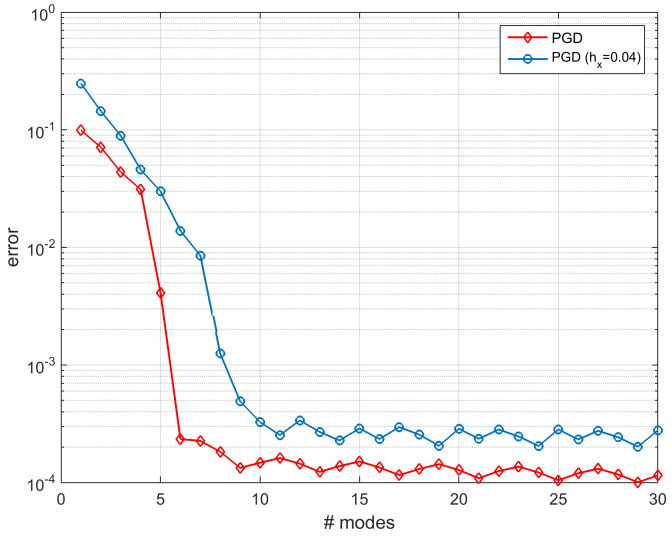

Figure 3.27: Comparison of the relative L^2-norm error of the PGD with respect to an overkill solution for the meshes represented in Fig. 3.21 and Fig. 3.26 ($N_s = 9$, $\lambda = 100$).

obtain the PGD approximation throughout this fine mesh composed of isosceles trapezoidal elements with a different size.

The steady reaction-diffusion equation (Eq. (3.53)) is applied to this domain configuration, for $\lambda = 100$ and homogeneous Dirichlet boundary conditions at $x = 1$ and $y = 0$ as can be seen in Fig. 3.29. The PGD, supported by the combination of different discretization levels and the use of a standard isoparametric mapping of the global shape functions, is able to solve this non-Cartesian example, whose solution is plotted in Fig. 3.29. The error of this approximation evaluated as a comparison with the first mode is represented in Fig. 3.30.

3.5 Discussion, Conclusions and Future Works

The implementation of a PGD method based on the partition of unity has been proposed in this work as an alternative technique for building space separated representations with a Global-Local approach. Inspired by Domain Decomposition and multi-scale approaches, this technique has been constructed by using partitioned domains in order to address a new space separation scheme, not based on the geometric coordinates of the problem. To this aim, this approach is built by carrying out a separation of the scales. It combines different levels of discretization for enriching coarse mesh FEM solutions with a Global-Local PGD scheme.

The main idea of the methodology presented in this chapter is to take advantage of a

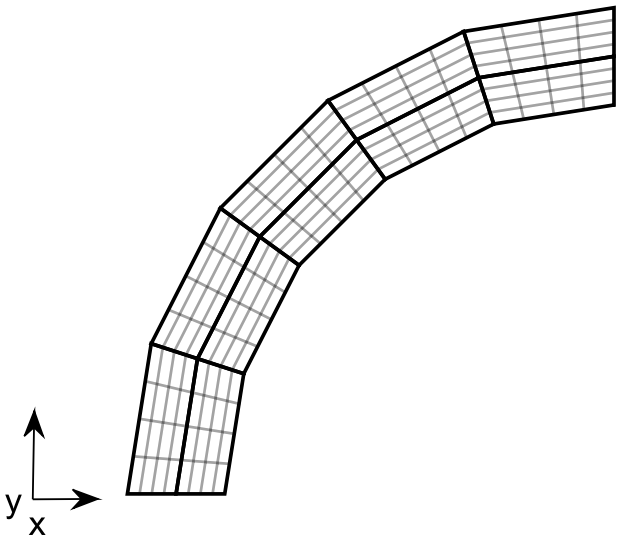

Figure 3.28: Coarse and fine meshes associated with a quarter annulus partitioned into 10 macro-elements.

partition of the domain in order to calculate the approximation as a particularization of a generic solution over each subdomain. More specifically, following the concept of partition of unity, a Global variable is associated with a coarse mesh (defined by the partition into subdomains). This implies that every subdomain is influenced by as many Global variable as nodes of the coarse mesh associated with the subdomain. The enrichment is provided by a Local variable, defined over a fine mesh at the set of macro-elements that share a global node, the so-called local support. This support coincides with the concept of patch presented in other methods based on the partition of unity, such as GFEM. Thus, this local variable and the shape functions associated with the fine mesh can be coupled with the global variable and its shape functions. The approximation of the solution defined over the whole domain is finally obtained by replicating the coupling for every node of the global mesh.

This scheme has allowed addressing the main challenge of the methods based on the partition of unity: the calculation of appropriate enrichment functions for a given problem. The Global-Local PGD provides the enrichment as the separated representation is built. Hence, it proposes the most adapted enrichment to the physics under consideration without the need of previous knowledge of the solution or solving auxiliary problems. Regarding the definition of enrichment proposed by other methods such as GFEM, the main difference lies in the use of the same Local variable for replicating the solution throughout the domain,

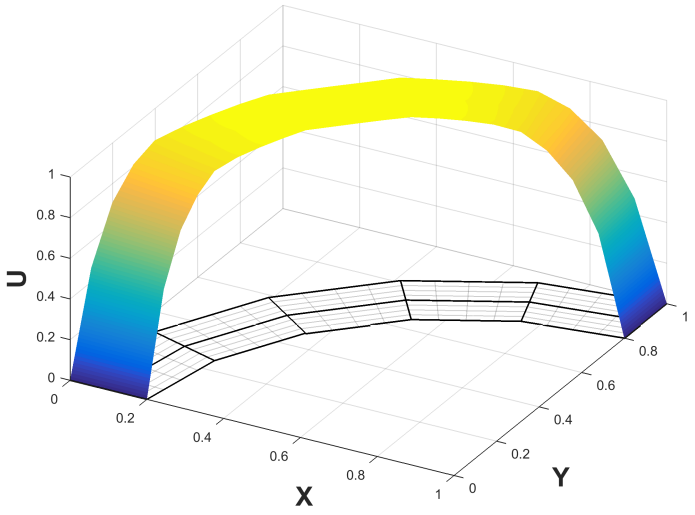

Figure 3.29: PGD approximation of the example associated with Fig. 3.28, Eq. (3.53) with homogeneous Dirichlet boundary conditions at $x = 1$ and $y = 0$ ($N_s = 9$, $\lambda = 100$).

whereas GFEM uses different enrichments at every patch.

For the examples presented in this work for problems defined over 1D and 2D domains, the PGD has been employed to enrich a previously obtained coarse FEM solution over the whole domain, but the scheme can be applied directly in the absence of this coarse approximation or for enriching only a part of the domain in order to capture local features.

Contrary to previous PGD space separated representations, for which the reduction of the complexity was achieved by splitting a problem into a sequence of lower dimension problems, this technique is based on a separation of scales. The global and the local problems are defined in the same physical dimension of the original problem. Due to the fact that the separation is not associated with the coordinates of the domain, a problem defined over an arbitrary non-Cartesian domain has been addressed by using a standard (finite element) isoparametric mapping. This paves the way for future developments of space separated representations for non-Cartesian geometries

Regarding the accuracy of the method, the PGD provides an approximation of the solution with an appropriate error level for the numerical examples proposed in this chapter. Moreover, it has been proved that the convergence of the method is similar to standard FEM schemes for an equivalent fine mesh approximation. When solving the Global and the Local problems, the combination of both levels of shape functions represents a sort of improved FEM problems, the error staying below the FEM error when compared to an overkill FEM solution.

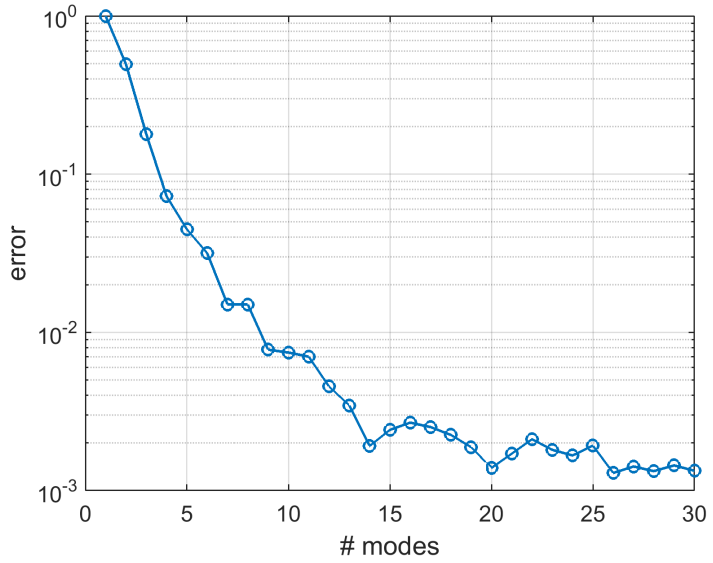

Figure 3.30: Error of the PGD for the example shown in Fig. 3.29.

Furthermore, the use of this technique involves an important reduction in the number of degrees of freedom of the problem. We can consider, for instance, 2D examples defined over a squared domain partitioned into regular squared subdomains, as those presented in Section 3.4.2.1. By increasing the number of subdomains and the number of degrees of freedom of the Local support, we can represent a comparison of the PGD with its corresponding FEM approximation. This comparison is shown in Fig. 3.31.

In view of Fig. 3.31, for a given fine mesh size, the reduction of degrees of freedom is more significant as the number of subdomains increases. This fact reveals the potential application of this approach for solving problems defined over domains containing a big amount of repetitive structures.

Nevertheless, this combination of shape functions defined over global and local levels still represents a very intrusive approach, as standard PGD approximations. This reveals the necessity of taking advantage of the Global-Local scheme for developing a non-intrusive technique. Regarding other future applications of this method, it seems necessary to extend the approach to other physics and time-dependent problems. Moreover, the Global-Local point of view could alleviate the limitations of the PGD when addressing equations with non-symmetric operators (in progress). Finally, with respect to the capability of the method for capturing complex solutions and reducing the number of modes, the use of higher-order global shape functions could improve considerably the performance of this PGD approach (in progress).

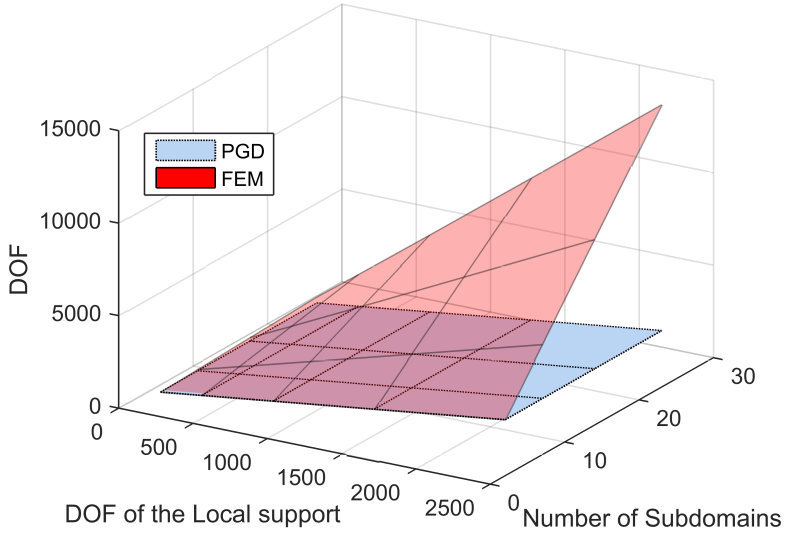

Figure 3.31: Comparison of the number of degrees of freedom of the Globa-Local PGD and its corresponding FEM 2D mesh.

Chapter 4

Towards a non-intrusive Global-Local PGD solver

The Global-Local scheme has been presented in Chapter 3 as a method to build separated representations in arbitrary non-Cartesian domains, where the numerical complexity is split into a global problem, defined over a coarse mesh, and a local problem, defined over a reference support that captures the local scale. However, the approach presented in Chapter 3 is quite intrusive in terms of software implementation, meaning that substantial changes would need to be introduced in a standard simulation platform, based on FEM codes.

In this Chapter, considering a partitioned domain and using its FEM operators as a starting point, the PGD is employed as an algebraic solver that builds global-local separated representations from standard FEM operators. Therefore, standard FEM pre-processing and assembly routines remain unchanged; only the solver is altered. This represents a less intrusive way of building global-local separated representations. Continuity on the boundaries of the domain partition does not need to be imposed explicitly, as it comes as a built-in property of the FEM operators.

Contents

4.1 Introduction

The Global-Local PGD described in Chapter 3 represents a new application when addressing space separations in partitioned domains. It was inspired by the methods based on the partition of unity, combining different discretization levels in order to enrich FEM solutions defined over a coarse mesh. This Global-Local separation scheme allowed us to define a different point of view not based on the Cartesian framework of the standard PGD.

This chapter follows the approach introduced in Chapter 3 in order to build space separated representations: the domain is partitioned in several subdomains and the solution is obtained by particularising a generic local solution for each subdomain. The new approach is also based on the separation of scales, but instead of coupling different discretization levels, this technique uses FEM operators as a starting point, not requiring a specific code and therefore, reducing the algorithmic intrusiveness. Thus, the PGD is presented in this chapter as an iterative algebraic solver.

The main idea is the adaptation of the concept of domain partitioning to the discrete operators that collect the physics applied to the domain. This also allows suppressing the geometrical constraints associated with the use of a standard PGD point of view, and consequently, the approach can be applied to non-Cartesian domains without the need for an isoparametric mapping.

In Section 4.2, the algebraic tensor structure of the standard PGD separated representation is introduced and discussed, using the *in-plane-out-of-plane* case to illustrate this technique and clarify the aim of this chapter. Section 4.3 is devoted to describing the Non-Intrusive Global-Local PGD approach and its formulation. In Section 4.4, some examples are shown in order to highlight the versatility of this method. Finally, the discussion and conclusions are presented in Section 4.5.

4.2 Algebraic tensor structure for separated representations

Let us start this Chapter by reviewing the formulation of the PGD as an algebraic solver. This section is in close connection with Chapter 1, where, starting from a generic weak form, we arrived to formulate the algebraic tensor structure of the problem.

Tensor methods like the PGD build a low-rank tensor subspace for solving multidimensional and multi-parametric models. Thus, the weak form of the model is regarded as an optimization problem where the set of admissible solutions is constrained to a low-rank tensor subspace. The efficiency of tensor methods relies on the tensorization of the model, as it allows dividing a multi-dimensional problem into a series of lower-dimensional ones.

4.2.1 Optimization problem for tensor subspace construction

Consider a multi-dimensional, linear, steady-state model. After discretization (see Chapter 1), it can be written as follows:

$$\boldsymbol{A}\boldsymbol{u} + \boldsymbol{f} = \boldsymbol{0}, \tag{4.1}$$

where $\boldsymbol{u} \in \mathbb{R}^{N_T}$ is a full tensor representation. On the other hand, $\boldsymbol{A} \in \mathbb{R}^{N_T \times N_T}$ represents a linear operator and $\boldsymbol{f} \in \mathbb{R}^{N_T}$ is the independent term. Both $\boldsymbol{A}$ and $\boldsymbol{f}$ are assumed to possess tensor structure, as described in Chapter 1. Tensor methods are designed to build a tensor subspace by turning Eq. (4.1) into an optimization problem. In particular, PGD allows building a tensor subspace progressively by computing rank-one corrections, i.e. by building a series of nested subspaces:

$$T_1 \subset T_2 \subset \cdots \subset T_M \quad \text{where} \quad T_M := T_{M-1} + T_1. \tag{4.2}$$

In practice, the actual rank is driven by some error estimate [4, 66] able to determine when the solution subspace is accurate enough. Assuming that a rank-M tensor approximation of the solution is known, $\boldsymbol{u}_M \in T_M$, we seek a rank-one correction $\delta\boldsymbol{u} \in T_1$ such that:

$$\begin{gathered} \boldsymbol{u}_{M+1} := \boldsymbol{u}_M + \delta\boldsymbol{u} \quad \text{where} \\ \boldsymbol{u}_M = \bigodot_{d=0}^{D} \boldsymbol{W}_d\,\boldsymbol{\alpha} \;\text{ with }\; \boldsymbol{\alpha} \in \mathbb{R}^M,\; \boldsymbol{W}_d \in \mathbb{R}^{N_d \times M} \;\text{ and }\; \delta\boldsymbol{u} = \bigotimes_{d=0}^{D} \boldsymbol{w}_d. \end{gathered} \tag{4.3}$$

Assuming that the operator $\boldsymbol{A}$ is symmetric positive definite (specific formulations of PGD exist for non-symmetric problems), Eq. (4.1) can be regarded as an optimization problem where the set of admissible solutions is constrained to T_1:

$$\delta\boldsymbol{u} := \arg\min_{\boldsymbol{v} \in T_1} \frac{1}{2}\langle \boldsymbol{A}\boldsymbol{v}, \boldsymbol{v}\rangle + \langle \boldsymbol{A}\boldsymbol{u}_M, \boldsymbol{v}\rangle + \langle \boldsymbol{f}, \boldsymbol{v}\rangle, \tag{4.4}$$

where $\langle \bullet, \bullet \rangle$ stands for the scalar product in $\mathbb{R}^{N_T}$. Eq. (4.4) constitutes a non-linear optimization problem due to the tensor multiplicative structure of the subspace. For the efficient solution of Eq. (4.4), tensorization of $\boldsymbol{A}$ and $\boldsymbol{f}$ is essential. Let us suppose that the following tensor representations are known:

$$\begin{aligned} \boldsymbol{A} &= \sum_{r=1}^{R} \bigotimes_{d=0}^{D} \boldsymbol{A}_d^r \qquad \text{with } \boldsymbol{A}_d^r \in \mathbb{R}^{N_d \times N_d} \quad \text{and} \\ \boldsymbol{f} &= \bigodot_{d=0}^{D} \boldsymbol{V}_d\,\boldsymbol{\gamma} \qquad \text{with } \boldsymbol{\gamma} \in \mathbb{R}^S,\; \boldsymbol{V}_d \in \mathbb{R}^{N_d \times S}. \end{aligned} \tag{4.5}$$

By inserting Eq. (4.5) into Eq. (4.4), and after some tedious but conceptually simple manipulations, we see that the scalar product in $\mathbb{R}^N$ can in fact be computed as the product of lower-dimensional scalar products. For instance, the first term in Eq. (4.4) reads:

$$\langle \boldsymbol{A}\boldsymbol{v}, \boldsymbol{v}\rangle \equiv \sum_{r=1}^{R} \prod_{d=0}^{D} \langle \boldsymbol{A}_d^r \boldsymbol{v}_d, \boldsymbol{v}_d\rangle_d, \tag{4.6}$$

where $\langle \bullet, \bullet \rangle_d$ stands for the scalar product in $\mathbb{R}^{N_d}$. Eq. (4.6) defines the separation property of the scalar product. This property suggests applying an alternating directions algorithm in order to optimize each direction $\boldsymbol{w}_d$ alternatively [30]. This can be achieved by simply projecting alternatively the functional in Eq. (4.4) onto each direction. Thus, let $\boldsymbol{w}_*$ the current direction to be optimized, implying that $\boldsymbol{w}_d$, $\forall d \neq *$, are frozen at their most current update. The restriction of Eq. (4.4) onto the current direction yields:

$$\boldsymbol{w}_* := \arg \min_{\boldsymbol{v}_* \in \mathbb{R}^{N_*}} \sum_{r=1}^{R} \left\{ \frac{1}{2} \langle \beta_*^r \boldsymbol{A}_*^r \boldsymbol{v}_*, \boldsymbol{v}_* \rangle_* + \langle \boldsymbol{A}_*^r \boldsymbol{W}_* \tilde{\boldsymbol{\alpha}}_*^r, \boldsymbol{v}_* \rangle_* \right\} + \langle \boldsymbol{V}_* \tilde{\boldsymbol{\gamma}}_*, \boldsymbol{v}_* \rangle_*, \tag{4.7}$$

where $\beta_*^r \in \mathbb{R}$, $\tilde{\boldsymbol{\alpha}}_*^r \in \mathbb{R}^M$ and $\tilde{\boldsymbol{\gamma}}_* \in \mathbb{R}^S$ are coefficients carrying the result of the scalar products in all directions except the current one. See Appendix B for the definition of these coefficients as well as for a detailed solution of Eq. (4.7). In summary, the correction $\delta \boldsymbol{u}$ can be computed by optimizing alternatively each one of its separated factors, using Eq. (4.7), until stagnation [4, 112]. In this way, the algorithm splits a multi-dimensional problem into a series of low-dimensional ones. This has been possible thanks to the tensorization of the problem, introduced in Eq. (4.5). In many cases, tensorization of linear problems can be achieved quite easily. However, when dealing with non-linear models, tensorization is in general lost, thus compromising the overall efficiency of tensor methods.

4.2.2 Cartesian domains

The approach employed in Section 4.2.1, the construction of the tensor structure, can be illustrated for Cartesian geometries. In this case, the *in-plane-out-of-plane* separated representation has been chosen due to its use for addressing problems defined in laminates for composite manufacturing. Fig. 4.1 represents a scheme of a generic model defined in a plate geometry domain Ω. The domain Ω can be decomposed as follows,

$$\Omega = \Omega_\pi \times \Omega_\perp \qquad \text{with} \qquad \begin{array}{l} \Omega_\pi \subset \mathbb{R}^2 \\ \Omega_\perp \subset \mathbb{R} \end{array} \tag{4.8}$$

where Ω_π and $\Omega_\perp$ represent the domains of the plane and the thickness respectively. For the sake of simplicity, the points $(x, y, z) \in \Omega$ are expressed as $(x, y, z) = (\boldsymbol{x}, z)$, with $\boldsymbol{x} = (x, y) \in \Omega_\pi$ and $z \in \Omega_\perp$.

Once the geometry of the model has been described, we consider the steady state heat conduction equation,

$$\nabla \cdot (\boldsymbol{k} \cdot \nabla \boldsymbol{u}) + \boldsymbol{f} = 0 \tag{4.9}$$

where the conductivity is assumed to be constant throughout the domain, $\boldsymbol{k} = \mathbb{1}$, Eq. (4.9) being rewritten as:

$$\Delta \boldsymbol{u} + \boldsymbol{f} = 0 \tag{4.10}$$

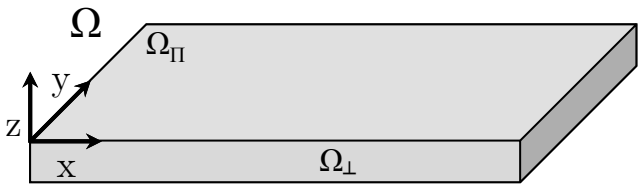

Figure 4.1: Scheme of a plate geometry domain for the *in-plane-out-of-plane* separated representation.

The weak form of Eq. (4.10), when assuming Dirichlet boundary conditions, reads:

$$\langle \nabla \boldsymbol{u}^*, \nabla \boldsymbol{u} \rangle + \langle \boldsymbol{u}^*, \boldsymbol{f} \rangle = 0 \tag{4.11}$$

or

$$\langle \nabla_{\boldsymbol{x}} \boldsymbol{u}^*, \nabla_{\boldsymbol{x}} \boldsymbol{u} \rangle + \langle \nabla_z \boldsymbol{u}^*, \nabla_z \boldsymbol{u} \rangle + \langle \boldsymbol{u}^*, \boldsymbol{f} \rangle = 0 \tag{4.12}$$

Thus, following the approach described in Section 4.2.1, Eq. (4.5) can be particularised for the problem defined by Eq. (4.12) as follows,

$$\boldsymbol{A}\,\boldsymbol{u} = \boldsymbol{b} \qquad \textit{with} \qquad \begin{array}{l} \boldsymbol{A} = \boldsymbol{K}_{\boldsymbol{x}} \otimes \boldsymbol{M}_z + \boldsymbol{M}_{\boldsymbol{x}} \otimes \boldsymbol{K}_z \\ \boldsymbol{b} = \boldsymbol{b}_{\boldsymbol{x}} \otimes \boldsymbol{b}_z \end{array} \tag{4.13}$$

where system $\boldsymbol{A}\,\boldsymbol{u} = \boldsymbol{b}$ is calculated in order to solve the problem using the PGD approach, by means of a greedy algorithm. $\boldsymbol{K}_{\boldsymbol{x}}$,$\boldsymbol{M}_{\boldsymbol{x}}$, $\boldsymbol{K}_z$, and $\boldsymbol{M}_z$ represent the conductivity and mass matrices related to the plane domain Ω_π and the thickness domain $\Omega_\perp$ respectively. The alternating direction strategy needed for the implementation of the PGD for the *in-plane-out-of-plane* decomposition is widely described in [16]. As a result, the *in-plane-out-of-plane* PGD separated representation can be written as:

$$\boldsymbol{u}(\boldsymbol{x}, z) \approx \sum_{j=1}^{N} \boldsymbol{X}_j(\boldsymbol{x}) \otimes \boldsymbol{Z}_j(z) \tag{4.14}$$

where N is the number of enrichments needed to achieve convergence and $\boldsymbol{X}_j$ and $\boldsymbol{Z}_j$ the values of the variables associated with the separated domains Ω_π and $\Omega_\perp$ respectively, for each enrichment step j. Therefore, we can reproduce the solution as a sum of products of functions that depend on the space coordinates of the problem ($\boldsymbol{x}$ and z). Thus, the 3D Poisson equation, Eq. (4.10), defined over the domain Ω has been divided within the PGD framework into two decoupled 2D and 1D problems formulated in Ω_π and $\Omega_\perp$.

4.2.3 Arbitrary domains

The integration of the weak form associated with the thermal problem represented by Eq. (4.9) can be separated in lower-dimensional integrals since the parametric space associated

with the standard PGD framework is assumed to be Cartesian. Therefore, the PGD is suitable for solving problems concerning Cartesian-like geometries mostly, like the mesh shown in Fig. 4.2a, where an X-Y separated representation of problem Eq. (4.10) can be easily carried out.

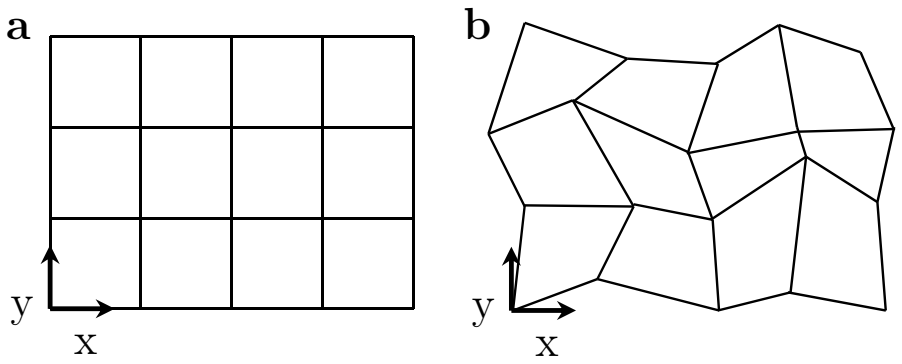

Figure 4.2: (a) Cartesian and (b) Non-Cartesian meshed domains

Nevertheless, when the PGD domain consists of arbitrary geometry, like the domain sketched in Fig. 4.2b, the standard PGD approach described in Section 4.2.2 cannot be used. In order to face this issue, following the Global-Local scheme presented in Chapter 3, a non-intrusive PGD approach is proposed in Section 4.3, using the FEM operators associated with the meshed domain as a starting point.

4.3 Non-Intrusive Global-Local PGD

Compared to the global-local approach presented in Chapter 3, the non-intrusive approach presented here features the following differences:

- The starting point is the algebraic system of equations, which is assembled using completely standard FEM techniques.
- The resulting degrees of freedom (DOFs) are partitioned in what can be identified as subdomains. Note that speaking of partitions is an abuse of language, as standard domain partitioning groups elements, whereas we group degrees of freedom. Moreover, our partition is merely algebraic (a renumbering indeed), and therefore, arbitrary (i.e. does not need to be defined at the geometry nor mesh level).
- The local variable is intrinsically discrete and has the size of the reference partition.

- The global variable, also discrete, can be understood as a piece-wise discontinuous variable that replicates and weights the local variable in each subdomain.
- Because we work directly with assembled variables (including equivalent nodal fluxes), there is no need to address continuity at the partition boundaries; it comes as a built-in property of the FEM operators.

4.3.1 Standard 3D finite element discretization and partition of the domain

Although it will be shown that the partition step is merely algebraic and therefore arbitrary, it is useful to start with a *physical* partition of a generic non-Cartesian domain to fix ideas. Fig. 4.3 depicts the situation.

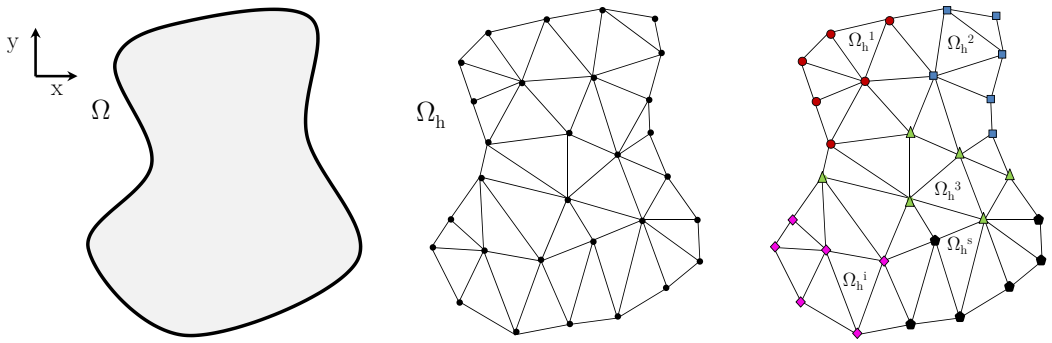

a) Domain b) Mesh c) Partition

Figure 4.3: Scheme of the DOF (or node) partition of the domain Ω.

We can define a generic domain Ω with arbitrary geometry, Fig. 4.3a. The objective of the partition is to eliminate the geometrical constraints associated with the standard PGD framework and thus, to create a new PGD approach, able to be applied to Non-Cartesian geometries. Note that, instead of using the local support presented in Chapter 3, the local domain is fictitious, and it only comprises a collection of degrees of freedom.

When considering a standard Finite Element approximation and discretization on a mesh compatible with the partition of the domain, the resulting matrix form of the model related to the steady state heat conduction equation, Eq. (4.9), reads

$$\boldsymbol{K}\boldsymbol{u} = \boldsymbol{f} \tag{4.15}$$

where vector $\boldsymbol{u}$ represents the nodal temperatures, matrix $\boldsymbol{K}$ is the conductivity matrix related to a Finite Element model of the domain and $\boldsymbol{f}$ contains the essential boundary conditions. By simply employing an adequate nodal re-numbering, Eq. (4.15) can be rewritten as

$$\begin{pmatrix} \boldsymbol{K_{11}} & \boldsymbol{K_{12}} & \dots & \boldsymbol{K_{1s}} \\ \boldsymbol{K_{21}} & \boldsymbol{K_{22}} & \dots & \boldsymbol{K_{2s}} \\ \vdots & \vdots & \ddots & \vdots \\ \boldsymbol{K_{s1}} & \boldsymbol{K_{s2}} & \dots & \boldsymbol{K_{ss}} \end{pmatrix} \begin{pmatrix} \boldsymbol{u_1} \\ \boldsymbol{u_2} \\ \vdots \\ \boldsymbol{u_s} \end{pmatrix} = \begin{pmatrix} \boldsymbol{f_1} \\ \boldsymbol{f_2} \\ \vdots \\ \boldsymbol{f_s} \end{pmatrix} \tag{4.16}$$

where the partition of $\boldsymbol{K}$ into submatrices represents the base for the construction of this Global-Local PGD algorithm, allowing a less-intrusive approach when compared with the standard PGD.

The solution of each subdomain will be provided by replicating the local solution on every subdomain (weighted by the appropriate global function). It is important to remark that the partition does not have to represent a continuous subdomain; in order to use this approach, this partition must satisfy the following requirements: 1) a standard Finite Element discretization of the domain, and 2) the same numbers of degrees of freedom for each subdomain (although this limitation could be overcome).

4.3.2 Separated representation constructor

We simply state that the solution at a given DOF partition can be obtained as:

$$\boldsymbol{u}_i = \boldsymbol{L}_1 \, g_{1,i} + \boldsymbol{L}_2 \, g_{2,i} + \dots \tag{4.17}$$

where the local variable $\boldsymbol{L}$ collects the local solution at the DOFs of a generic fictitious partition, with the same number of degrees of freedom as the real subdomains of the partition. This local variable is scaled at the subdomains by g_i, the i-component of $\boldsymbol{G}$ (the global variable). The separated representation can be expressed as

$$\boldsymbol{u} = \boldsymbol{G} \otimes \boldsymbol{L}, \tag{4.18}$$

that is the form generally considered in the framework of tensor product formats. Thus, if we assume that N terms are required in the separated representation, the Global-Local PGD structure can be rewritten as

$$\boldsymbol{u} = \sum_{j=1}^{N} \boldsymbol{G}_j \otimes \boldsymbol{L}_j. \tag{4.19}$$

Fig. 4.4 represents a scheme of the replication of the solution throughout the whole domain, following Eq. (4.19).

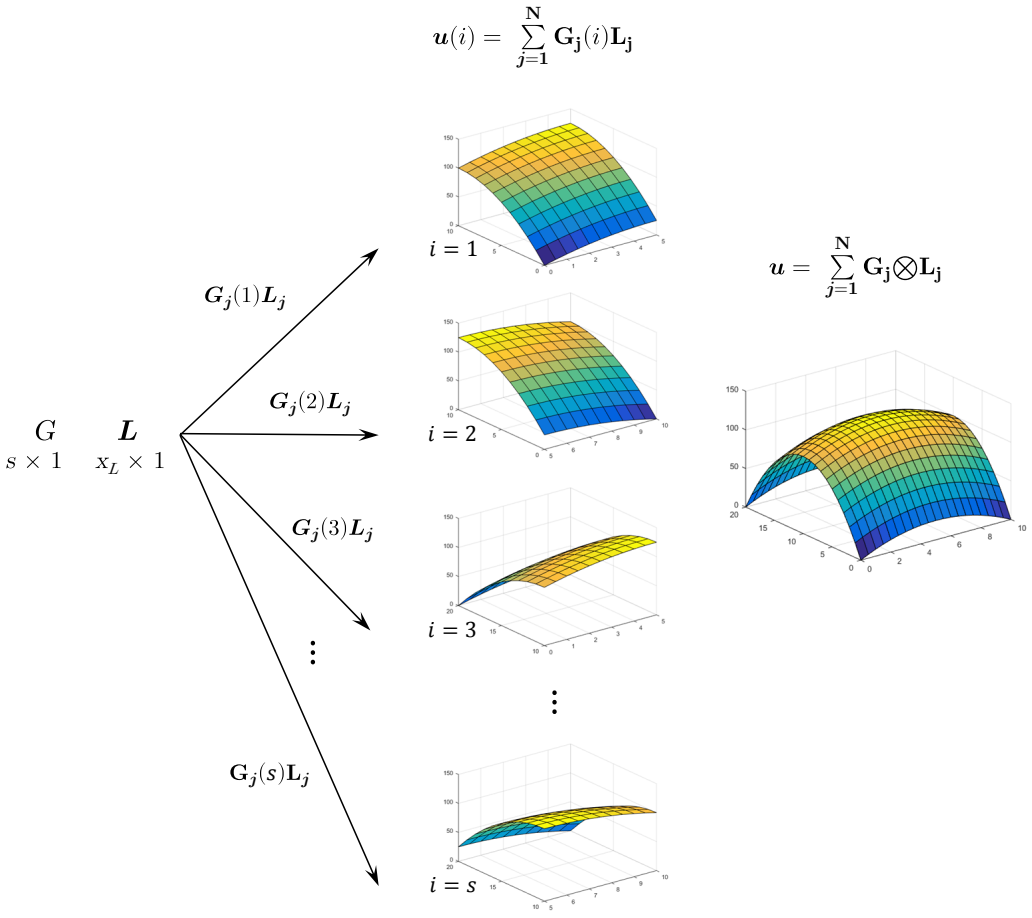

Figure 4.4: Scheme of the replication of the solution throughout the whole domain, using the Global-Local approach.

Following the same approach employed for the *in-plane-out-of-plane* PGD and considering the particularities of the Global-Local technique, the structure shown in Eq. (4.13) is now expressed as:

$$\boldsymbol{A}\,\boldsymbol{u} = \boldsymbol{b} \qquad \text{with} \qquad \begin{aligned} \boldsymbol{A} &= \sum_{m=1}^{s}\sum_{n=1}^{s} \boldsymbol{A}^G_{mn} \otimes \boldsymbol{A}^L_{mn} \\ \boldsymbol{b} &= \sum_{m=1}^{s} \boldsymbol{b}^G_m \otimes \boldsymbol{b}^L_m \end{aligned} \tag{4.20}$$

where $\boldsymbol{A}^G_{mn}$ is the canonical basis in $\mathbb{R}^{s\times s}$, and $\boldsymbol{A}^L_{mn}$ can be identified with the $\boldsymbol{K_{mn}}$ resultant submatrices of the partition of $\boldsymbol{K}$ shown in Eq. (4.16). It is important to remark

that these submatrices, which represent the base of the Global-Local approach, are directly taken from the FEM system, ensuring a less intrusive approach that does not require a specific code and the continuity of the solution across the interfaces between the subdomains. With regard to the right-hand side, $\boldsymbol{b}_m^G$ is the canonical basis in $\mathbb{R}^s$ and $\boldsymbol{b}_m^L$ represents the equivalent nodal fluxes, again, taken from the standard FEM system.

Thus, imposing a test function $\boldsymbol{u}^* = (\boldsymbol{G} \otimes \boldsymbol{L})^*$, Eq. (4.20) can be rewritten as

$$\boldsymbol{u}^{*T} \left(\sum_{m=1}^{s} \sum_{n=1}^{s} \boldsymbol{A}_{mn}^G \otimes \boldsymbol{A}_{mn}^L \right) \boldsymbol{u} = \boldsymbol{u}^{*T} \left(\sum_{m=1}^{s} \boldsymbol{b}_m^G \otimes \boldsymbol{b}_m^L \right) \tag{4.21}$$

or, by considering a single term ($j = 1$) in Eq. (4.19):

$$(\boldsymbol{G} \otimes \boldsymbol{L})^{*T} \left(\sum_{m=1}^{s} \sum_{n=1}^{s} \boldsymbol{A}_{mn}^G \otimes \boldsymbol{A}_{mn}^L \right) (\boldsymbol{G} \otimes \boldsymbol{L}) = (\boldsymbol{G} \otimes \boldsymbol{L})^{*T} \left(\sum_{m=1}^{s} \boldsymbol{b}_m^G \otimes \boldsymbol{b}_m^L \right). \tag{4.22}$$

The expression resulted in Eq. (4.22) allows calculating the PGD variables by using a greedy algorithm. This algorithm consists in the two-step Alternating Direction Strategy that is detailed as follows:

4.3.2.1 The Global problem

The particularisation of Eq. (4.19) for the enrichment step N allows obtaining the Global variable $\boldsymbol{G}$ from the value of the Local variable at the previous iteration, $\boldsymbol{L}$:

$$\boldsymbol{u} = \sum_{j=1}^{N-1} \boldsymbol{G}_j \otimes \boldsymbol{L}_j + \boldsymbol{G} \otimes \boldsymbol{L}, \tag{4.23}$$

where everything is known except the value of the Global variable $\boldsymbol{G}$. Then, introducing Eq. (4.23) and the test function $\boldsymbol{u}^* = \boldsymbol{G}^* \otimes \boldsymbol{L}$ into Eq. (4.21), we obtain:

$$\begin{aligned} (\boldsymbol{G}^* \otimes \boldsymbol{L})^T \left(\sum_{m,n=1}^{s} \boldsymbol{A}_{mn}^G \otimes \boldsymbol{A}_{mn}^L \right) (\boldsymbol{G} \otimes \boldsymbol{L}) = \\ = -(\boldsymbol{G}^* \otimes \boldsymbol{L})^T \left(\sum_{j=1}^{N-1} \sum_{m,n=1}^{s} (\boldsymbol{A}_{mn}^G \otimes \boldsymbol{A}_{mn}^L) \right) (\boldsymbol{G}_j \otimes \boldsymbol{L}_j) + \\ + (\boldsymbol{G}^* \otimes \boldsymbol{L})^T \left(\sum_{m=1}^{s} \boldsymbol{b}_m^G \otimes \boldsymbol{b}_m^L \right). \end{aligned} \tag{4.24}$$

Grouping local and global terms:

$$\sum_{m,n=1}^{s} \left(\boldsymbol{G}^{*T}\boldsymbol{A}^{G}_{mn}\boldsymbol{G}\right)\left(\boldsymbol{L}^{T}\boldsymbol{A}^{L}_{mn}\boldsymbol{L}\right) =$$
$$= -\sum_{j=1}^{N-1}\sum_{m,n=1}^{s} \left(\boldsymbol{G}^{*T}\boldsymbol{A}^{G}_{mn}\boldsymbol{G}_{j}\right)\left(\boldsymbol{L}^{T}\boldsymbol{A}^{L}_{mn}\boldsymbol{L}_{j}\right) +$$
$$+\sum_{m=1}^{s} \left(\boldsymbol{G}^{*T}\boldsymbol{b}^{G}_{m}\right)\left(\boldsymbol{L}^{T}\boldsymbol{b}^{L}_{m}\right). \tag{4.25}$$

Thus, we can obtain the Global variable $\boldsymbol{G}$ as follows:

$$\mathbf{G} = \boldsymbol{A}_{G}^{-1}\cdot\boldsymbol{b}_{G}, \tag{4.26}$$

where

$$\boldsymbol{A}_{G} = \sum_{m,n=1}^{s}\alpha_{mn}\boldsymbol{A}^{G}_{mn} \tag{4.27}$$

and

$$\boldsymbol{b}_{G} = -\sum_{j=1}^{N-1}\sum_{m,n=1}^{s}\beta^{j}_{mn}\boldsymbol{A}^{G}_{mn}\boldsymbol{G}_{j} + \sum_{m=1}^{s}\gamma_{m}\boldsymbol{b}^{G}_{m}. \tag{4.28}$$

The following constants have been introduced:

$$\alpha_{mn} = \boldsymbol{L}^{T}\boldsymbol{A}^{L}_{mn}\boldsymbol{L}, \quad \beta^{j}_{mn} = \boldsymbol{L}^{T}\boldsymbol{A}^{L}_{mn}\boldsymbol{L}_{j}, \quad \gamma_{m} = \boldsymbol{L}^{T}\boldsymbol{b}^{L}_{m}.$$

4.3.2.2 The Local problem

Conversely, by applying the same process (with $\boldsymbol{u}^{*} = \boldsymbol{G}\otimes\boldsymbol{L}^{*}$), we arrive at the solution of the local problem under the form:

$$\boldsymbol{L} = \boldsymbol{A}_{L}^{-1}\cdot\boldsymbol{b}_{L}, \tag{4.29}$$

where

$$\boldsymbol{A}_{L} = \sum_{m,n=1}^{s}\delta_{mn}\boldsymbol{A}^{L}_{mn} \tag{4.30}$$

and

$$\boldsymbol{b}_{L} = -\sum_{j=1}^{N-1}\sum_{m,n=1}^{s}\epsilon^{j}_{mn}\boldsymbol{A}^{L}_{mn}\boldsymbol{L}_{j} + \sum_{m=1}^{s}\kappa_{m}\boldsymbol{b}^{L}_{m}. \tag{4.31}$$

The following constants have been introduced:

$$\delta_{mn} = \boldsymbol{G}^{T}\boldsymbol{A}^{G}_{mn}\boldsymbol{G}, \quad \epsilon^{j}_{mn} = \boldsymbol{G}^{T}\boldsymbol{A}^{G}_{mn}\boldsymbol{G}_{j}, \quad \kappa_{m} = \boldsymbol{G}^{T}\boldsymbol{b}^{G}_{m}.$$

4.3.3 Local permutations

With respect to the basic formulation of the Global-Local technique represented in Eq. (4.20), the application to partitioned domains can be very susceptible (in terms of the number of modes to be computed) to the boundary conditions and its location. This is due to the fact that the solution of every subdomain is calculated with the values of the Local variable associated with the list of nodes of the fictitious subdomain, which are particularised by multiplying by the corresponding value of the Global variable.

In order to alleviate the dependence of the current Global-Local approach on the placement of the boundary conditions, this issue can be solved by adding the use of permutation matrices to the formulation. Thus, Eq. (4.20) can be particularised for the squared subdomains problems as follows

$$\boldsymbol{A}\,\boldsymbol{u} = \boldsymbol{b} \qquad \text{with} \qquad \begin{aligned} \boldsymbol{A} &= \sum_{m,n=1}^{s} \sum_{p,q=1}^{M} \boldsymbol{A}^G_{mn} \otimes (\boldsymbol{P}^T_p \boldsymbol{A}^L_{mn} \boldsymbol{P}_q) \\ \boldsymbol{b} &= \sum_{m=1}^{s} \sum_{p=1}^{M} \boldsymbol{b}^G_m \otimes (\boldsymbol{P}^T_p \boldsymbol{b}^L_m) \end{aligned} \tag{4.32}$$

where $\boldsymbol{P}$ represents the appropriate permutation matrices and M represents the desirable number of permutations for each problem.

4.3.4 Global-Local approach versus standard PGD techniques

In some cases, the use of standard PGD techniques for solving problems defined over Cartesian domains with an evident repetitive structure can be impractical or inefficient. It seems necessary to use a different approach more adapted to this kind of geometries, in order to take advantage of their particularities. The development of the Global-Local separated representation offers not only a new technique for solving non-Cartesian geometries with a PGD-based approach but also a good alternative to the standard PGD for problems consisting of partitioning and regular structures or periodic patterns.

For instance, the use of the PGD for solving 2D thermal problems defined over domains containing regular inclusions (with a different thermal conductivity with respect to the rest of the domain) can be a difficult issue if we want to build a separated representation based on functions depending on both dimensions. This situation is illustrated in Fig. 4.5, where the geometry plotted in Fig. 4.5a represents an eight-inclusion domain, the thermal conductivity at the inclusions being 100 times higher than in the rest of the domain. Then, we can apply Eq. (4.9) to the domain using the PGD and obtain the solution (Fig. 4.5b), which presents a repetitive structure due to the inclusions. The difficulties of the separability when we consider two different values of the thermal conductivity of the domain are confirmed by Fig.

4.6, as the convergence of the PGD when compared to FEM is achieved for an important number of modes (number of terms required to reproduce the solution).

Considering that the domain could be partitioned into eight subdomains containing each inclusion and the solution is the same for all the subdomains, the use of the Global-Local technique seems especially appropriate for obtaining more compact solutions while addressing repetitive structures.

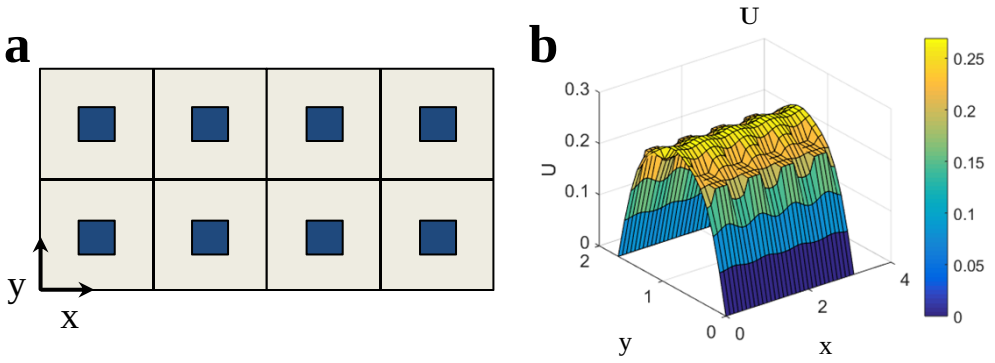

Figure 4.5: Application of the standard PGD to a domain containing regular inclusions.

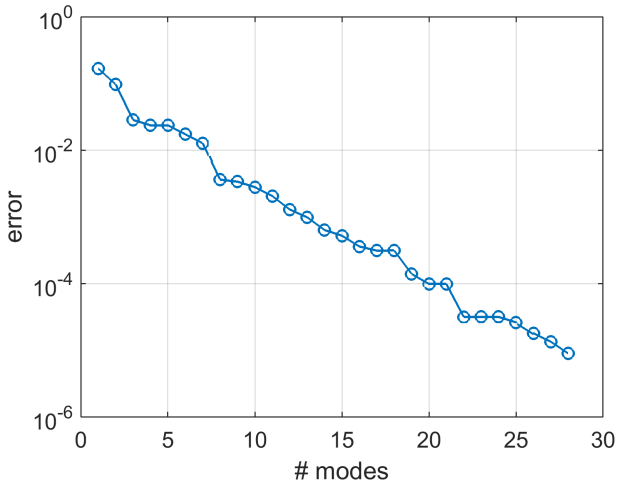

Figure 4.6: Error of the standard PGD when compared to FEM for the example shown in Fig. 4.5.

4.4 Numerical examples

4.4.1 Layered domain

In a connection with the *in-plane-out-of-plane* separated representation, the first academic example consists in a domain representing a 10-ply laminate, in which the plies are associated with subdomains. For the sake of simplicity, a 2D model has been employed, as can be observed in Fig. 4.7, where coordinate x represents the plane and coordinate z is associated with the laminate thickness. As explained in Section 4.3, a standard 2D discretization has been implemented. Thus, by using an adequate nodal re-numbering, the Finite Element equations can be rewritten and the Global-Local PGD formulation can be applied.

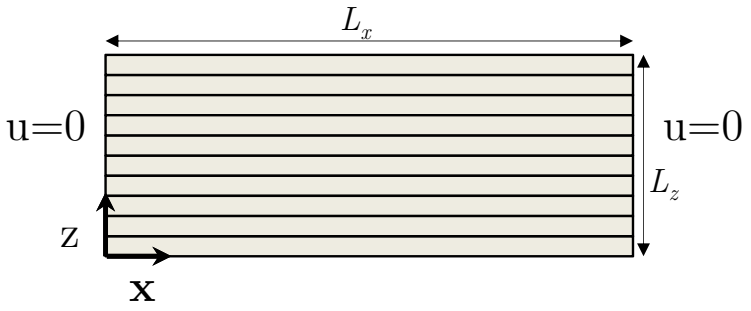

Figure 4.7: Layered domain Ω with $s = 10$ and homogeneous Dirichlet boundary conditions at $x = 0$ a and $x = L_x$.

The steady heat conduction equation, Eq. (4.10), is applied to the domain, particularly considering that the independent term is set to $\boldsymbol{f} = \mathbb{1}$ and defining homogeneous Dirichlet boundary conditions at $x = 0$ a and $x = L_x$, these boundary conditions ensuring that all the subdomains consist of the same number of degrees of freedom. Taking all these considerations into account, in Fig. 4.8 the FEM solution is plotted for this first example.

Once the example has been described and the FEM solution has been obtained, the Global-Local PGD technique can be applied, solved, and compared with the FEM results, as it can be also observed in Fig. 4.8, where the PGD temperature distribution is represented, also plotting the nodal temperature corresponding to each of the 10 plies.

For all the examples of this study, the nodal relative error has been computed with respect to the FEM solution, and the stop criterion is set to make the procedure ends when an appropriate measure of the error becomes small enough (in this case, 10^{-5}). For this problem, only one enrichment step is necessary for the Global-Local approach to converge to the FEM solution; the relative error is found to be in the order of 10^{-8}. The solution of the Global and Local variables are represented in Fig. 4.9; this Local solution L is particularised

in each subdomain by multiplying the nodal temperatures by its corresponding value of the Global variable $G(i)$.

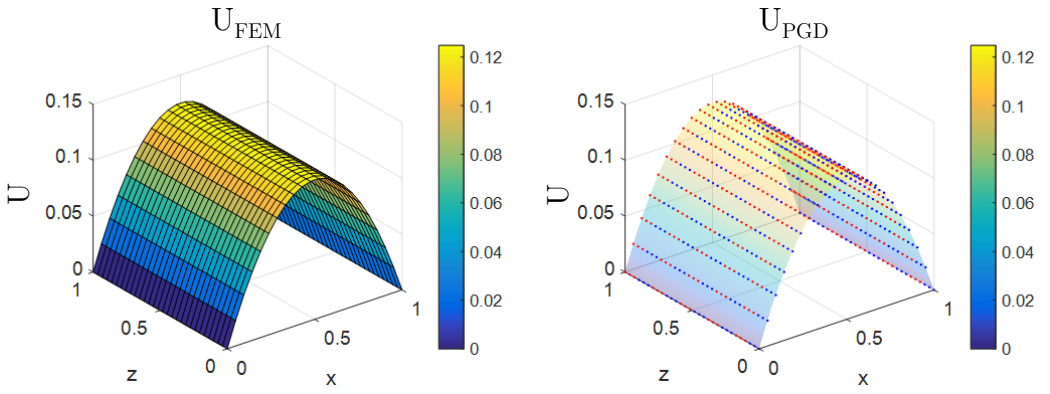

Figure 4.8: FEM and Global-Local PGD solutions of the example 4.4.1 for the layered domain Ω with $s = 10$.

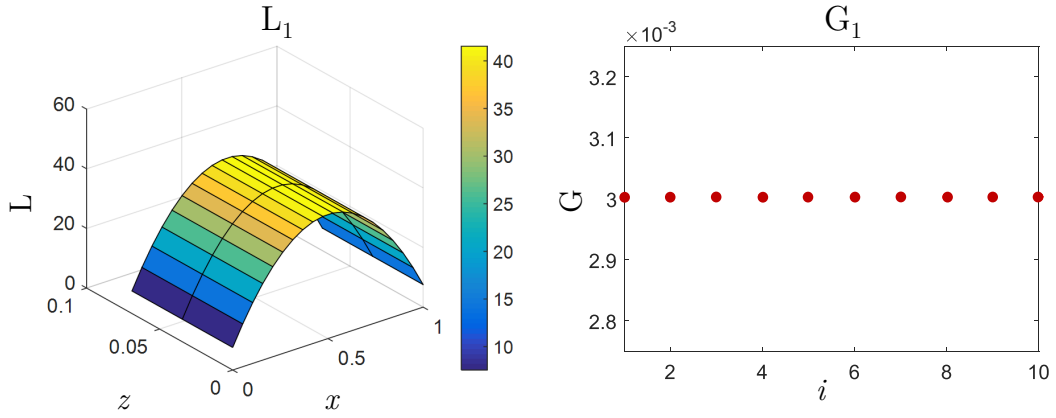

Figure 4.9: Representation of the Local variable L and the values of the Global variable G for the example 4.4.1.

4.4.2 L-shaped domain

With regard to the configuration of domains consisting of squared subdomains, a new example is proposed. The second example represents an 'L-shaped' domain with $s = 3$. A representation of this example is plotted in Fig. 4.10. Eq. (4.10) is also applied, considering

$\boldsymbol{f} = \mathbb{1}$ and homogeneous Dirichlet boundary conditions at $x = 0$, $x = L_x$, $y = 0$ and $y = L_y$ (all the subdomains having the same number of degrees of freedom).

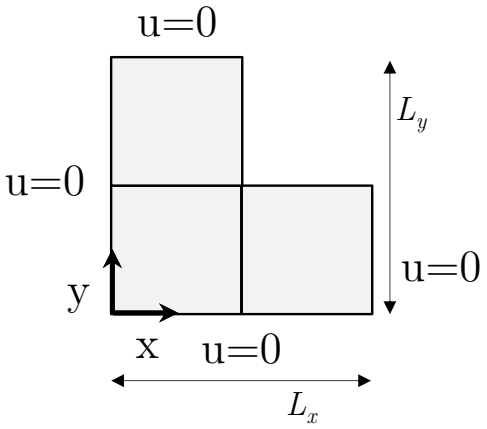

Figure 4.10: 'L-shaped' domain Ω divided into $s = 3$ squared subdomains and homogeneous Dirichlet boundary conditions at $x = 0$, $x = L_x$, $y = 0$ a and $y = L_y$.

Fig. 4.11 represents the discretization employed and the solution obtained by using the Global-Local PGD. When observing the error made with reference to the FEM solution (Fig. 4.12) we can remark that, with reference to the example presented in 4.4.1, the number of modes obtained is considerably higher (about 60) due to the different configurations of the orientations of the subdomains and their corresponding boundary conditions. After the post-compression techniques the number of modes corresponds to the number of subdomains of the partition (Fig. 4.12).

4.4.3 Squared subdomains

The third academic example consists in a domain Ω containing four squared subdomains ($s = 4$); the heat conduction equation Eq. (4.10) is applied, considering that the source term is set to $\boldsymbol{f} = \mathbb{1}$ and the thermal conductivity tensor is constant through the whole domain ($\boldsymbol{k} = \mathbb{1}$). For this example, the current configuration of the partition allows the homogeneous Dirichlet boundary conditions to be applied at the whole boundary, i.e. $x = 0$, $x = L_x$, $y = 0$, and $y = L_y$. A scheme representing the partition employed and the boundary conditions is shown in Fig. 4.13.

Fig. 4.14 shows the FEM and the Global-Local PGD results and Fig. 4.15 represents the evolution of the error made by using the Global-Local separated representation with respect to the FEM results, both figures corresponding to the example of the four squared subdomains. As observed in 4.4.2, the increase in the complexity of the distribution of the

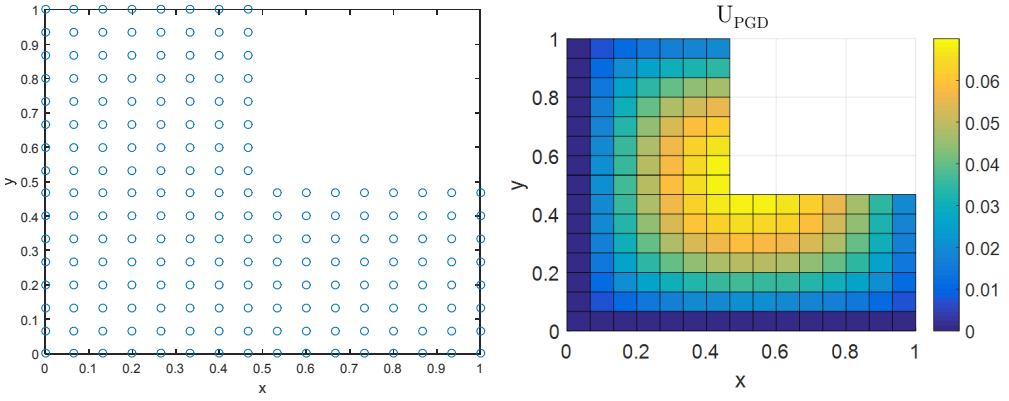

Figure 4.11: Meshed 'L shaped' domain and Global-Local PGD solution of 4.4.2.

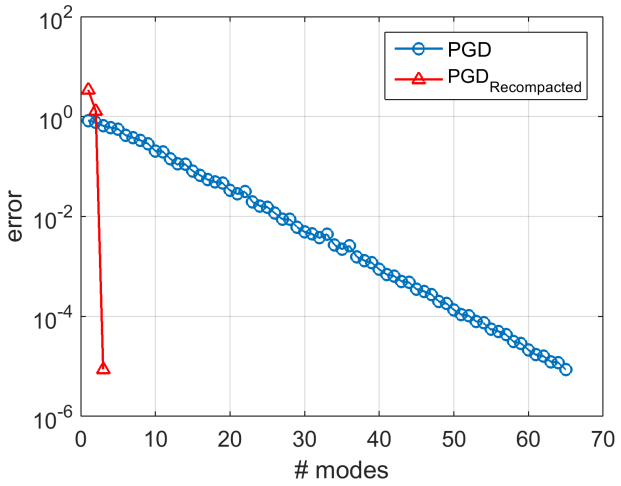

Figure 4.12: Evolution of the Global-Local PGD error with reference to the FEM solution of 4.4.2 for $s = 3$ squared subdomains.

boundary conditions with respect to the configuration of the partition involves an increase in the number of enrichments needed to achieve convergence (about 90), as can be observed in Fig. 4.15. This issue is due to the fact that the Local solution, calculated at a generic fictitious subdomain, is common to all the subdomains, whereas the boundary conditions are applied in different sides of the squares for each subdomain ($x = 0$, $x = L_x$, $y = 0$ and $y = L_y$).

Nevertheless, this fact is solved by using a post-compression technique as can be observed

in Fig. 4.15; we can obtain a four-mode separated representation as could be expected in view of the double symmetry of the temperature distribution obtained with FEM. The Local and Global variables obtained with these four enrichments are represented in Fig. 4.16 and Fig. 4.17 respectively. The first mode is common to all the subdomains, as the values of Global variable are equal, whereas for the rest of the modes the Global variable reaches different values, in order to obtain the solution of each subdomain, depending on the orientation of the subdomain with respect to the boundary conditions.

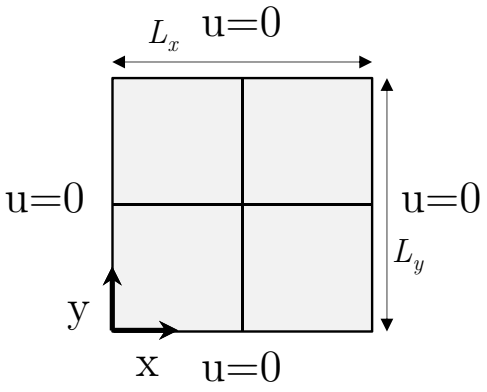

Figure 4.13: Domain Ω divided into $s = 4$ squared subdomains and homogeneous Dirichlet boundary conditions at $x = 0$, $x = L_x$, $y = 0$ a and $y = L_y$.

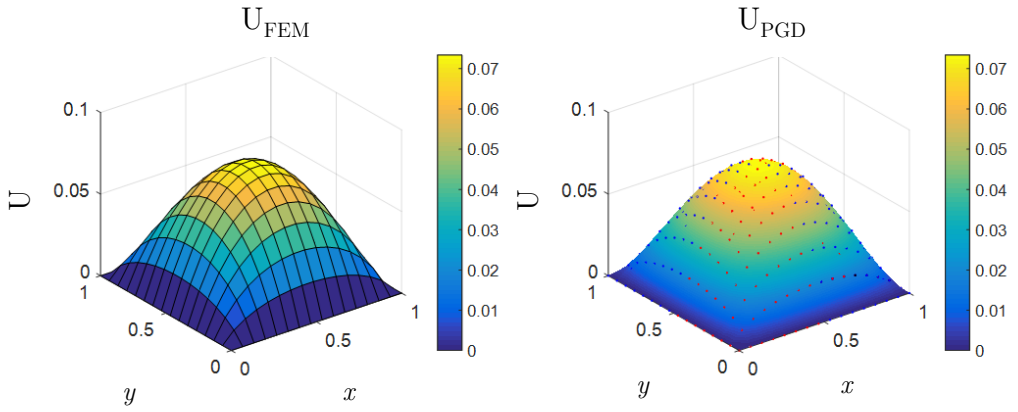

Figure 4.14: FEM and Global-Local PGD solutions of 4.4.3 for $s = 4$ squared subdomains.

As can be observed, the use of the Global-Local PGD approach for this example is not as efficient as its application for the example presented in 4.4.1 (layered domain). In the

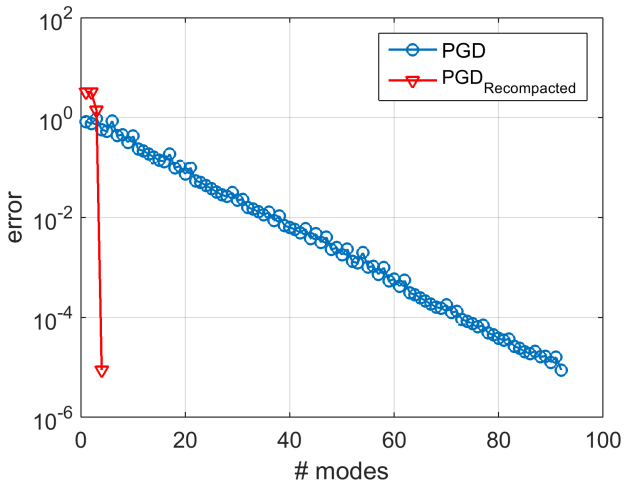

Figure 4.15: Evolution of the Global-Local PGD error with reference to the FEM solution of 4.4.3 for $s = 4$ squared subdomains.

squared subdomains case, all the subdomains achieve the same temperature distribution, as in 4.4.1. However, in this example, we cannot reach the convergence with just one enrichment. This situation reveals the dependence of the Global-Local approach on the placement of the boundary conditions. This issue is alleviated by adding permutation matrices to the formulation, as it was explained in Eq. (4.32). For instance, in view of the configuration of this problem, four permutations are expected in order to make the Local variable fit for reproducing the solution of the four subdomains. Thus, the corresponding boundary conditions could be satisfied for each subdomain by using a rotation of the temperature distribution obtained for the Local variable. Indeed, following this approach the solution can be obtained with just one enrichment, as can be observed in Fig. 4.18, where the Local distribution and the values of the Global variables are shown.

4.4.4 Randomly selected subdomains

With regard to the selection and distribution of the subdomains, the Non-Intrusive Global-Local formulation allows a wide variety of configurations to be implemented. The only requirement is to establish the same numbers of degrees of freedom for all subdomains. It could be possible, for example, to solve Eq. (4.10) (with $\boldsymbol{f} = \mathbb{1}$) applied with homogeneous Dirichlet boundary conditions at the whole domain boundary of a squared domain by using randomly selected subdomains, i.e. the nodes associated with the degrees of freedom are randomly assigned to the subdomains, all these subdomains consisting of the same number of nodes.

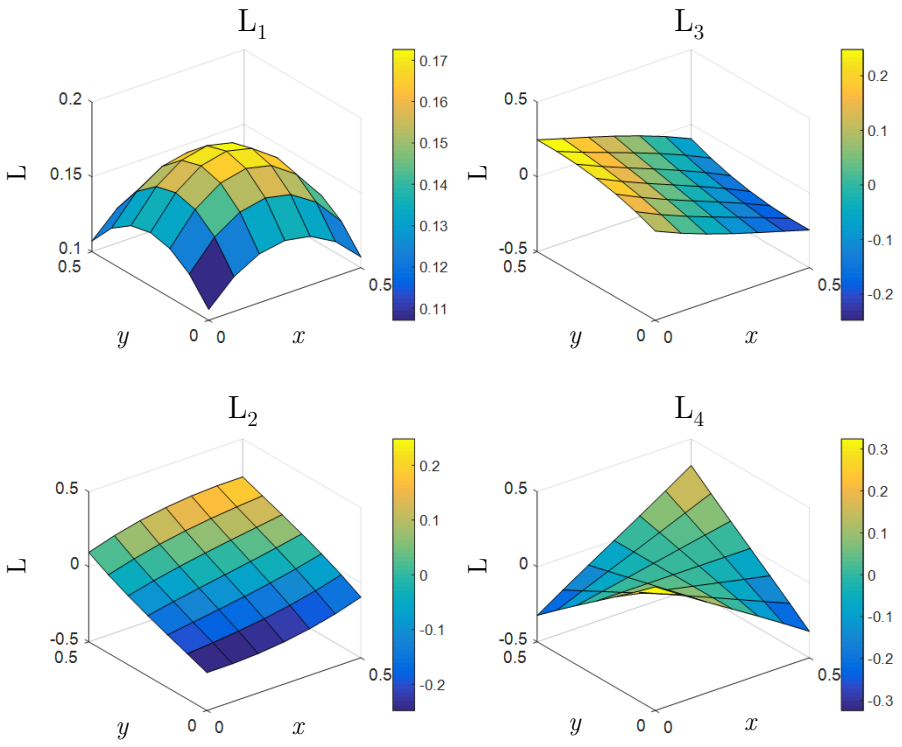

Figure 4.16: Representation of the Local variable L_j for 4.4.3 ($j = 1, \ldots, 4$).

This example makes no sense from the physical point of view, but it reveals the versatility of the Global-Local approach and its possible application to Non-Cartesian domains, which represents an important contribution with respect to the standard PGD techniques. Fig. 4.19 shows this situation: the nodes of the discretization of a Cartesian domain with four randomly assigned subdomains (Non-Cartesian partition, represented in different colours) and the representation of the randomly selected subdomains on its corresponding FEM solution.

The errors made by the Global-Local PGD method and the post-compression approach for this example, are plotted in Fig. 4.20. The randomly selected subdomains involve a considerably greater number of modes than the examples shown in the previous sections. Nevertheless, the post-compression approaches obtain a similar decrease in the number of modes as the example shown in 4.4.3, confirming that this reduction is related to the number of subdomains established.

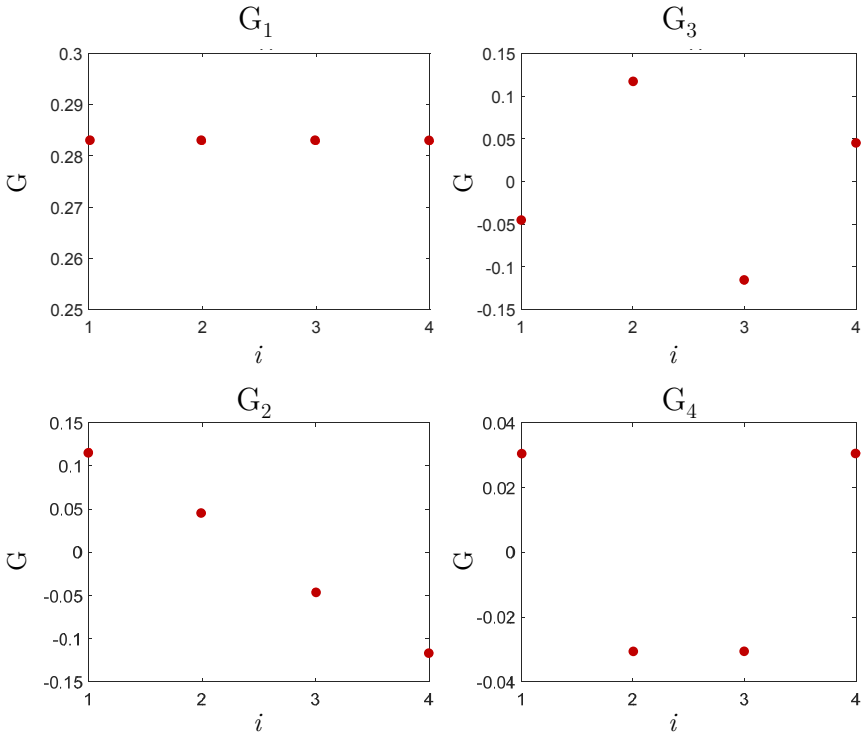

Figure 4.17: Values of the Global variable for each subdomain G_j for 4.4.3 ($j = 1, \ldots, 4$).

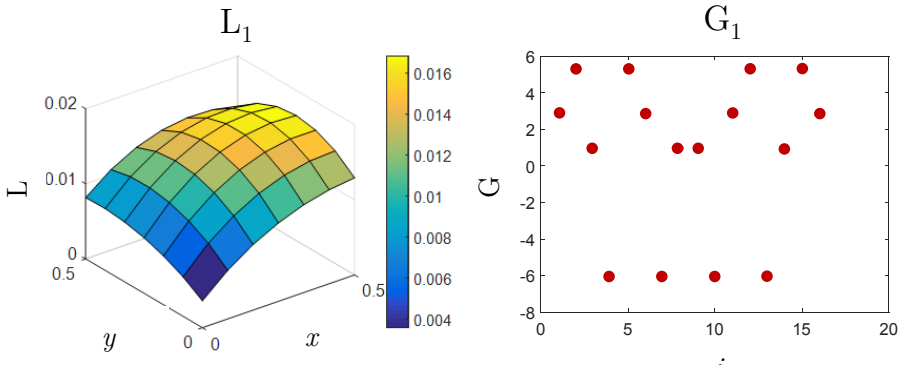

Figure 4.18: Representation of the Local variable L_j and the values of the Global variable for each subdomain G_j for 4.4.3 ($j = 1$), by using permutation matrices.

4.4.5 Non-Cartesian domain

In order to verify the versatility of the Global-Local PGD, we can implement this approach to a Non-Cartesian geometry. The example is defined over the domain shown in Fig. 4.21,

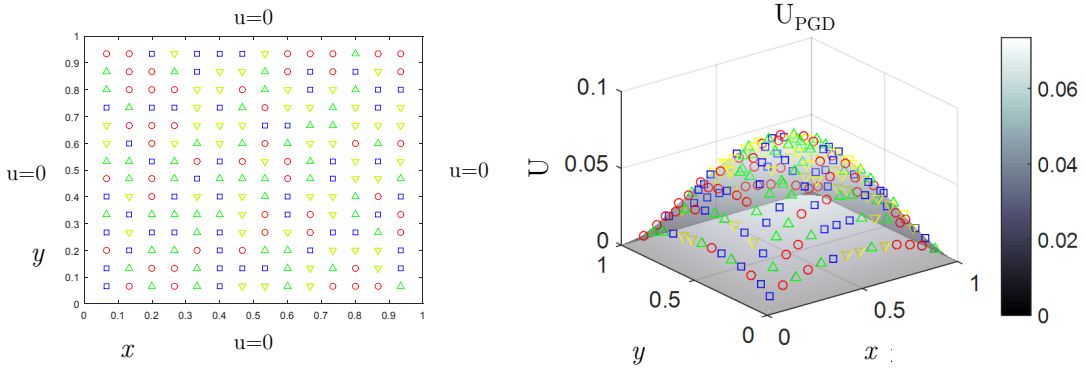

Figure 4.19: Randomly selected partition and Global-Local PGD solution of 4.4.4.

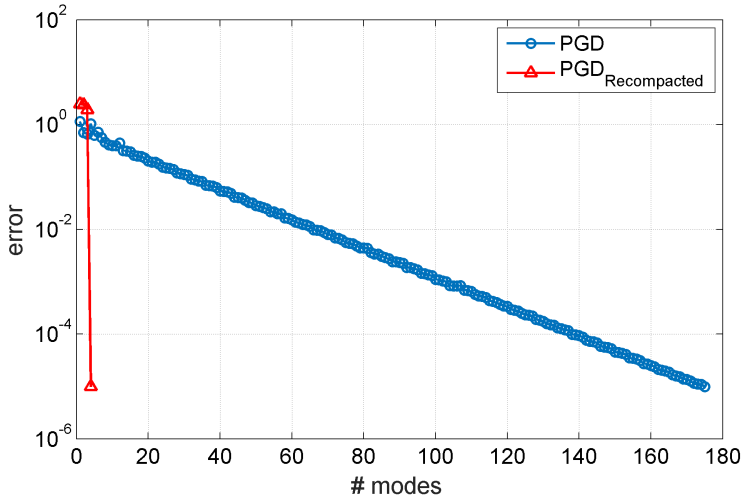

Figure 4.20: Evolution of the Global-Local PGD error with reference to the FEM solution of 4.4.4.

where Eq. (4.10) is also applied (with $\boldsymbol{f} = \mathbb{1}$) and the homogeneous Dirichlet boundary conditions are applied at the whole boundary of a triangle meshed Non-Cartesian domain. The nodes of the discretization are grouped into four subdomains, as can be observed in Fig. 4.22.

As can be observed in Fig. 4.23, the PGD solution can also be reproduced for a Non-Cartesian configuration. The evolution of the error, when compared with the FEM solution, is also plotted in Fig. 4.23. The Global-Local separated representation needs an important number of enrichments to achieve convergence, but the use of post-compression techniques

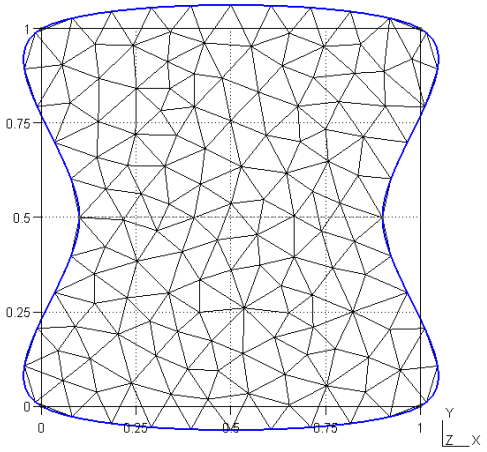

Figure 4.21: Non-Cartesian meshed domain.

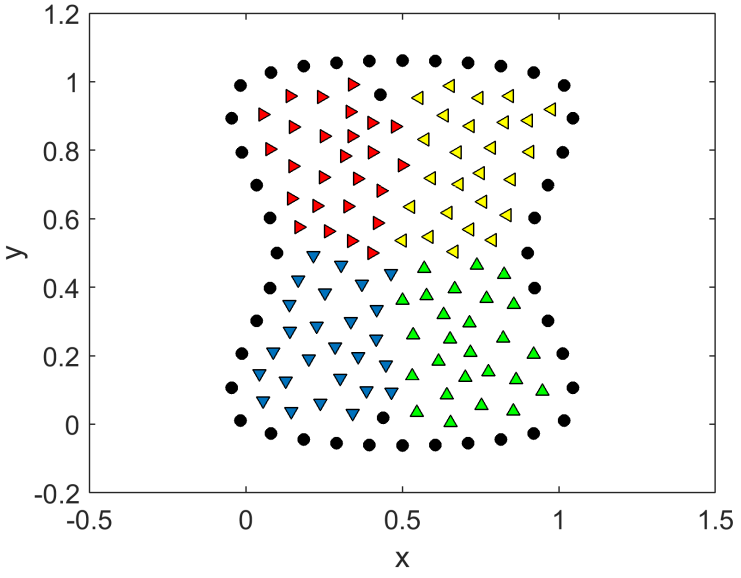

Figure 4.22: Partition of the non-Cartesian domain into $s = 4$ subdomains.

reveals that we can just obtain four modes to build the accurate solution (the number of subdomains of the partition).

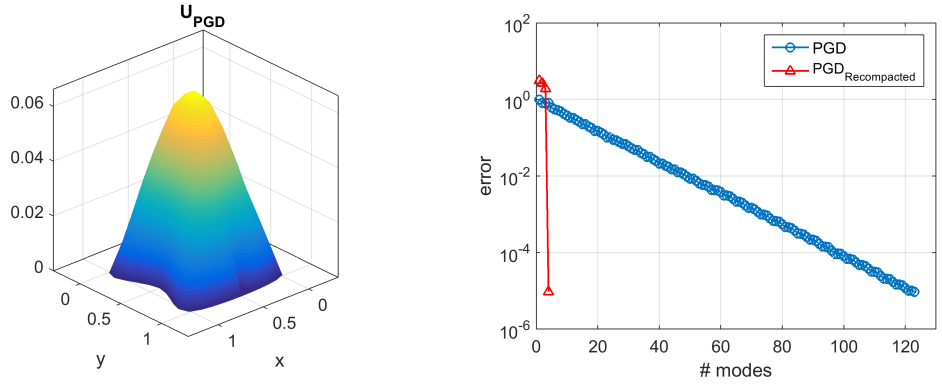

Figure 4.23: Global-Local PGD solution and evolution of the Global-Local PGD error with reference to the FEM solution of 4.4.5 for $s = 4$ subdomains.

4.4.6 Regular-inclusions domain

Finally, in order to illustrate the most appropriate application for the Non-Intrusive Global-Local PGD, a new example concerning a regular-inclusions domain is presented. A scheme representing this example is shown in Fig. 4.24. It represents a squared subdomains partition consisting of eight squared inclusions, where the thermal conductivity is 100 times higher than in the rest of the domain, the thermal conductivity being $\boldsymbol{k} = \mathbb{1}$ out of the inclusions.

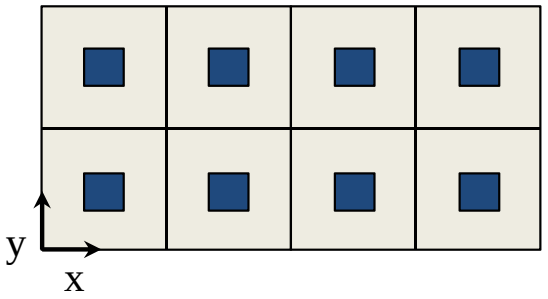

Figure 4.24: 8-inclusion domain.

In order to apply the Global-Local approach to this problem, a FEM manufactured solution is imposed. This manufactured solution has been obtained by solving Eq. (4.10) for a two-inclusion domain as can be observed in Fig. 4.25a. Homogeneous Dirichlet Boundary Conditions are imposed at $y = 0$ and $y = L_y$. The FEM solution of this two-inclusion problem is replicated in order to obtain an eight-inclusion manufactured solution (Fig. 4.25b). Thus, by using this solution and the matrix $\boldsymbol{K}$ associated with the eight-inclusion partition (Fig. 4.24), Eq. (4.15) allows us to obtain $\boldsymbol{f}$, the vector that contains the essential bound-

ary conditions. Finally, the partition associated with the eight-subdomain problem can be carried out, following Eq. (4.16).

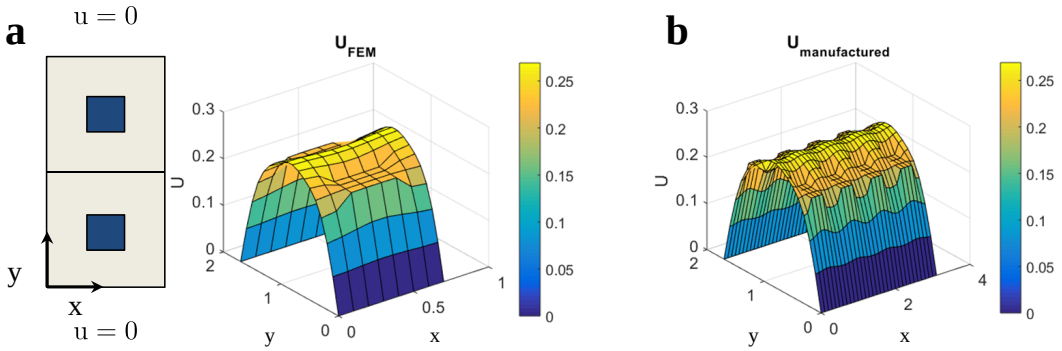

Figure 4.25: (a)Two-inclusion FEM solution and (b) Eight-inclusion manufactured solution for 4.4.6.

The application of the Global-Local PGD approach to the partition of the domain into eight subdomains containing inclusions, along with the use of two permutation matrices (Eq. (4.32)), allows us to obtain the PGD approximation of the solution with just one mode, (Fig. 4.26) as the same solution is replicated throughout each subdomain, with two different orientations. As we can see, the error achieved is around 10^{-8} with respect to the manufactured solution. This result is considerably better than the approximation provided by a standard PGD X-Y separated representation, as the solution is obtained by adding about 30 modes due to the presence of the inclusions (see Fig. 4.26). The use of post-compression techniques allows us to obtain a recompacted solution consisting of four modes. Consequently, we can confirm that the use of a Global-Local approach is especially appropriate for solving problems related to repetitive configurations concerning inclusions.

A more complex problem is presented in Fig. 4.27, it represents a squared domain partitioned into 16 squared subdomains containing the same kind of inclusions taken into consideration in Fig. 4.24. The same strategy of Fig. 4.25 for obtaining the manufactured solution from Eq. (4.10) has been used. Homogeneous Dirichlet boundary bonditions are also imposed at $y = 0$ and $y = L_y$.

In this case, as shown in Fig. 4.28 the approximation of the solution is achieved by adding around six modes (for an error around 10^{-5}) using two permutation matrices. This number of modes is much lower than in the standard PGD case (around 32), but higher than the number of different solutions that are observed in Fig. 4.27 for each subdomain (two different solutions are replicated throughout the subdomains with two different orientations). This fact suggests a need for improvement of the Global-Local PGD in terms of versatility

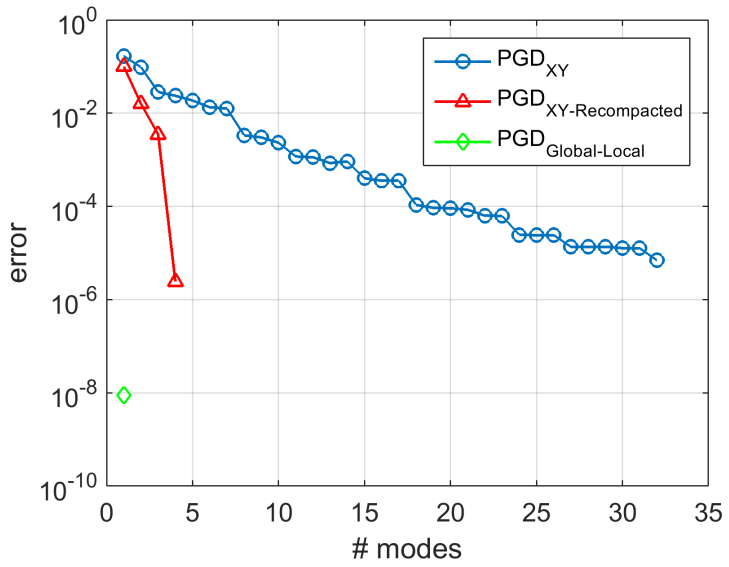

Figure 4.26: Evolution of the Global-Local PGD error and the Standard PGD error with reference to the FEM solution of 4.4.6 for $s = 8$ subdomains.

and efficiency.

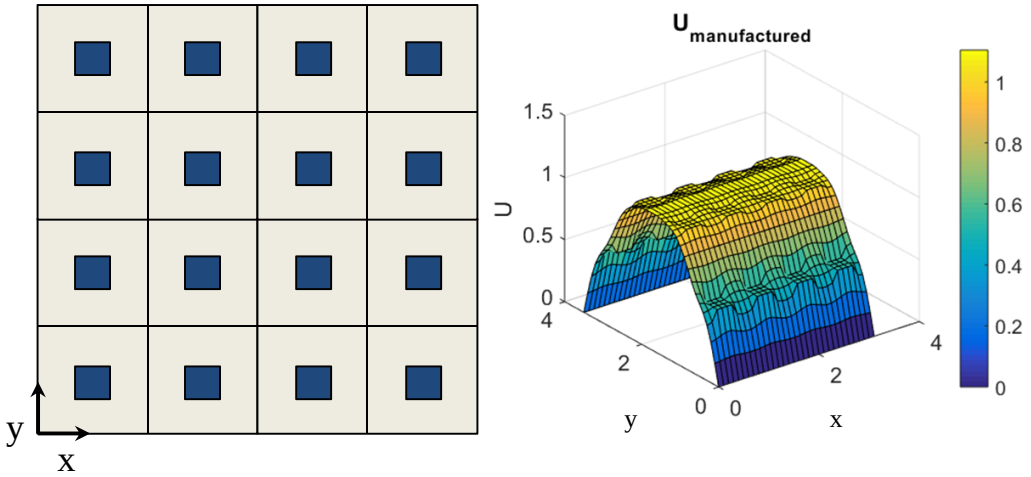

Figure 4.27: Sixteen-inclusion domain and manufactured solution.

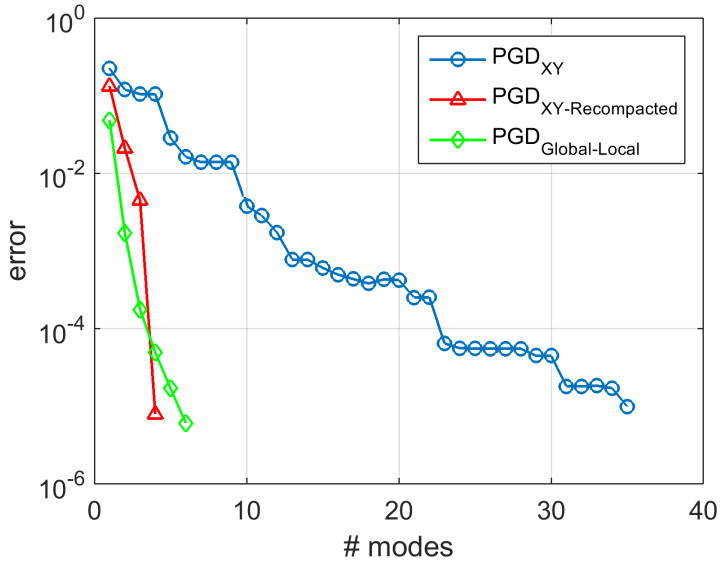

Figure 4.28: Evolution of the Global-Local PGD error and the Standard PGD error with reference to the FEM solution of 4.4.6 for $s = 16$ subdomains.

4.5 Discussion and Conclusions

The methodology introduced in this chapter follows the Global-Local concept explained in Chapter 2, in the framework of PGD-based space separated representations: a separation scheme not based on the geometric coordinates of the problem, but built from a partition of the domain that takes advantage of the particularities of the problem (repetitive structures of patterns).

In order to alleviate the intrusiveness of the PGD, the approach is constructed by using previously obtained discrete operators as a starting point, these operators being compatible with the partition of the domain. After the algebraic description of the PGD in Section 1.3, this implementation of the PGD as an iterative algebraic solver allows obtaining the approximation of the solution over each subdomain by particularising a unique Local solution for all the subdomains, multiplying the Local variable by the Global variable (a constant value for each subdomain).

This procedure deserves the following important comments:

- The partition of $\boldsymbol{K}$ and $\boldsymbol{f}$ is obtained with any FEM code using any type of finite element. In this sense, the just-described technique is much less intrusive than the separated representation described in Section 2 for standard PGD procedures. The application of other physics only affects the contents of the discrete operators.

- The proposed strategy could be viewed as an iterative linear solver able to produce a separated representation of the nodal solution.
- The Global-Local PGD only involves matrix products and linear systems solutions of reduced sizes that can be efficiently performed using massively parallel computing architectures.
- The solution procedure can also be viewed as a domain decomposition technique where continuity conditions are implicitly enforced by the use of the discrete operators and in which the information spreads all along the whole domain at each iteration.
- In contrast to the standard PGD approaches, this technique is not restricted to Cartesian geometries, it can be used in any partition of the vector containing the nodal unknowns with the only restriction that all subdomains consist of the same number of nodes. Thus, the Global-Local PGD eliminates the geometrical constraints of the standard PGD scheme.
- This technique is very sensitive to the relative location of the boundary conditions for each subdomain. Besides this issue, the fact of using FEM operators in order to minimize the intrusiveness of the approach could result in continuity problems, as the non-intrusive approach makes it impossible to split the nodal components of the FEM matrices, not permitting the presence of shared nodes between the subdomains. Moreover, the boundary conditions are imposed in the Local solution, which involves that all the subdomains of the partition have the same numbers of degrees of freedom.

In conclusion, this new study is particularly attractive when addressing regular geometries, as they can be easily solved, replacing the complexity of full models. Moreover, the Global-Local PGD allows facing two important challenges of the standard PGD techniques: the algorithm intrusiveness and the geometrical limitations.

Conclusions

The use of MOR techniques such as the PGD has involved a relevant advance for building space separated representations. Nevertheless, there is an important need for new approaches in terms of adaptation of these techniques to complex geometries in order to extend the application of *a priori* MOR to problems defined over any physical domain.

These cases include problems for which a full separated representation is not possible or is not the most appropriate because of the geometry of the domain or the physics applied. Some advances have been previously proposed for degenerated domains, for which some of the coordinates of the problem are clustered for building the separated representation. One example is the *in-plane-out-of-plane* PGD, which has been extensively analysed.

In this thesis, a new space separation scheme has been presented: the Global-Local PGD. This separated representation is not built according to the space coordinates of the problem; it is based on a partition of the domain, and it represents a first step for applying the PGD to non-Cartesians geometries. The main idea is the construction of the PGD based on two variables: the local variable, a fine-mesh solution defined over a generic domain (much smaller than the original one), and the global variable, which represents the particularization of that solution over the subdomains of the partition.

With regard to this new point of view, two different approaches are proposed in this work:

The Global-Local PGD based on the Partition of Unity. This PGD approach, presented in Chapter 3, is based on the application of the Global-Local scheme to the PGD by combining two levels of discretization: a coarse mesh and a fine mesh. The method is used to enrich an initial coarse-meshed FEM solution. For this chapter, the main concepts and remarks are summarised next:

- *The construction of the Global-Local scheme.* The global variable is defined over the coarse mesh associated with the partition of the domain into several subdomains. The local variable is defined over a fine-meshed set of subdomains that share a unique global node. This set is called support and, when it is centred over a node of the coarse mesh, its position coincides with the entire global shape function associated with that node. As this shape function satisfy the partition of unity, the global variable, the local

variable and their corresponding shape functions are coupled. When the local variable support is replicated over each node of the coarse mesh, the solution is obtained along the whole domain.

- *Comparison with other methods based on the partition of unity.* The use of the partition of unity is similar to other methods such as GFEM. The main idea of GFEM is to enrich the coarse solution over a part of the domain. To this aim, this local domain is covered by a set of patches that is equivalent to our concept of support. However, the GFEM enrichment is different for each patch whereas the local variable is the same for every position of the support. The principal advantage of the Global-Local PGD is that, using this MOR approach, the enrichment is proposed by the PGD as the problem is solved, without *a priori* knowledge of the solution or solving additional problems, as GFEM requires.

- *Errors and rate of convergence.* The combination of both discretization levels achieves the optimal convergence rate of FEM when using linear shape functions. The error committed is slightly smaller than that of FEM when compared to an overkill solution.

The Non-Intrusive Global-Local PGD. This approach is presented in Chapter 4 and it emerges at an alternative for reducing the intrusiveness of the PGD. The partition of the domain of the Global-Local approach is also applied to previously obtained discrete operators that will be used as the starting point of the technique. Thus, the technique can be considered as a non-intrusive algebraic solver. Its main characteristics are summarised next:

- *Adaptation of the Global-Local scheme.* In this case, the PGD is also built by considering two variables. The local variable now is defined over a generic subdomain with the same number of degrees of freedom than all the subdomains of the partition. The global variable is a constant value per subdomain. The particularization of the solution for every subdomain is obtained by multiplying the local solution for each corresponding global variable.

- *Non-intrusive algebraic solver.* When considering the aforementioned scheme of variables, and taking previously obtained discrete operators, no modifications of these operators are needed (except the partition of the operators according to the set of subdomains). Since this technique does not implement any discretization over the geometric coordinates, the PGD is used as an iterative algebraic solver. This could allow incorporating the PGD to pre-existing simulation platforms. Moreover, the use of the operators ensures the continuity of the solution on the internal boundaries between subdomains without imposing extra boundary conditions.

- *A new approach for non-Cartesian domains.* The fact of using this separation based on the partition involves that this technique can be implemented over non-Cartesian

domains, without any restriction concerning the form of the subdomains or the mesh employed.

In summary, both techniques involve a relevant advance on the implementation of new space separated representations and its application in science and engineering. They represent two different interpretations of the Global-Local point of view, but share the concept of constructing the PGD approximation based on the partition of the domain. This produces a considerable reduction of the degrees of freedom of the problem and consequently, of the computational cost. This reduction becomes more important when increasing the number of subdomains and decreasing the nodes of the local support. Moreover, the configuration of the partition can be chosen in order to take advantage of the geometry and its particularities or the physics applied.

Regarding the numerical results, the approach presented in Chapter 3 achieved better results in terms of applicability and performance when compared to the results obtained in Chapter 4. This technique based on the partition of unity is less sensitive to the configuration and distribution of the boundary conditions, and therefore, easier to adapt to other cases. Nevertheless, it is very intrusive and includes the calculation of an important amount on operators with respect to the non-intrusive PGD. Moreover, the results shown in Chapter 4 involve a more evident reduction of the geometric limitations. Consequently, the advantages of each technique will depend on the requirements of the problem to be solved.

With respect to the future perspectives of this thesis, it paves the way for new advances based on non-Cartesian geometries. The concept of mapping used on recent studies in space separated representations for hardly separated geometries [46] could be very useful for the development of Global-Local PGD approaches applied to more complex geometries or problems. The implementation of the Global-Local scheme to other physics, especially for the problems where the standard PGD approaches fail, is also another major challenge to be addressed, as well as the adaptation of this scheme to time-dependent and parametric problems.

Bibliography

[1] Aguado, J. V. (2015). *Advanced strategies for the separated formulation of problems in the Proper Generalized Decomposition framework*. Phd thesis, Ecole Centrale Nantes, France. *cited on page 6 and 11*

[2] Alaimo, A., Milazzo, A., and Orlando, C. (2008). Global/local fem-bem stress analysis of damaged aircraft structures. *CMES - Computer Modeling in Engineering and Sciences*, 36(1):23–42. *cited on page 47*

[3] Ammar, A., Chinesta, F., and Cueto, E. (2011). Coupling Finite Elements and Proper Generalized Decompositions. *International Journal for Multiscale Computational Engineering*, 9(1):17–33. *cited on page 25*

[4] Ammar, A., Chinesta, F., Diez, P., and Huerta, A. (2010). An error estimator for separated representations of highly multidimensional models. *Computer Methods in Applied Mechanics and Engineering*, 199(25-28):1872–1880. *cited on page 72 and 73*

[5] Ammar, A., Mokdad, B., Chinesta, F., and Keunings, R. (2006). A new family of solvers for some classes of multidimensional partial differential equations encountered in kinetic theory modeling of complex fluids. *Journal of Non-Newtonian Fluid Mechanics*, 139(3):153–176. *cited on page 5 and 9*

[6] Ammar, A., Mokdad, B., Chinesta, F., and Keunings, R. (2007). A new family of solvers for some classes of multidimensional partial differential equations encountered in kinetic theory modelling of complex fluids. Part II: Transient simulation using space-time separated representations. *Journal of Non-Newtonian Fluid Mechanics*, 144(2-3):98–121. *cited on page 13*

[7] Aquino, W., Brigham, J. C., Earls, C. J., and Sukumar, N. (2009). Generalized finite element method using proper orthogonal decomposition. *International Journal for Numerical Methods in Engineering*, 79(7):887–906. *cited on page 47*

[8] Babuška, I. and Melenk, J. M. (1997). The partition of unity method. *International Journal for Numerical Methods in Engineering*, 40(4):727–758. *cited on page 31 and 32*

[9] Badías, A., Curtit, S., González, D., Alfaro, I., Chinesta, F., and Cueto, E. (2019). An augmented reality platform for interactive aerodynamic design and analysis. *International Journal for Numerical Methods in Engineering*, 120(1):125–138. *cited on page 5*

[10] Badías, A., González, D., Alfaro, I., Chinesta, F., and Cueto, E. (2017). Local proper generalized decomposition. *International Journal for Numerical Methods in Engineering*, 112(12):1715–1732. *cited on page 25*

[11] Bellman, R. (1954). The Theory of Dynamic Programming. *Bulletin of the American Mathematical Society*, 60(6):503–515. *cited on page 4*

[12] Belytschko, T. and Black, T. (1999). Elastic crack growth in finite elements with minimal remeshing. *International Journal for Numerical Methods in Engineering*, 45(5):601–620. *cited on page 31*

[13] Ben Dhia, H. (1998). Multiscale mechanical problems: the arlequin method. *Comptes Rendus de l'Academie des Sciences Series IIB Mechanics Physics Astronomy*, 326(12):899–904. *cited on page 25*

[14] Bialecki, R. A., Kassab, A. J., and Fic, A. (2005). Proper orthogonal decomposition and modal analysis for acceleration of transient FEM thermal analysis. *International Journal for Numerical Methods in Engineering*, 62(6):774–797. *cited on page 6*

[15] Bird, R. B., Curtiss, F. C., Amstrong, C. R., and Ole, H. (1987). *Dynamics of polymeric liquids, second edition volume 2: Kinetic theory*, volume 2. John Wiley & Sons. *cited on page 4*

[16] Bognet, B., Bordeu, F., Chinesta, F., Leygue, A., and Poitou, A. (2012). Advanced simulation of models defined in plate geometries: 3D solutions with 2D computational complexity. *Computer Methods in Applied Mechanics and Engineering*, 201-204:1–12. *cited on page 19 and 74*

[17] Bognet, B., Ghnatios, C., Lurot, R., Barasinski, A., Leygue, A., Binetruy, C., and Chinesta, F. (2014a). Models defined in stratified-plate domains. A review on efficient 3D PGDbased solution procedures. *Revue des Composites et des Materiaux Avances*, 24(1):97–109. *cited on page 19*

[18] Bognet, B., Leygue, A., and Chinesta, F. (2014b). Separated representations of 3d elastic solutions in shell geometries. *Advanced Modeling and Simulation in Engineering Sciences*, 1:1–34. *cited on page 19*

[19] Bordeu, F., Ghnatios, C., Boulze, D., Carles, B., Sireude, D., Leygue, A., and Chinesta, F. (2015). Parametric 3D elastic solutions of beams involved in frame structures. *Advances in aircraft and spacecraft science*, 2(3):233–248. *cited on page 20*

[20] Borzacchiello, D., Aguado, J. V., and Chinesta, F. (2019). Non-intrusive Sparse Subspace Learning for Parametrized Problems. *Archives of Computational Methods in Engineering*, 26(2):303–326. *cited on page 4 and 28*

[21] Burkardt, J., Gunzburger, M., and Lee, H. C. (2006). POD and CVT-based reduced-order modeling of Navier-Stokes flows. *Computer Methods in Applied Mechanics and Engineering*, 196(1-3):337–355. *cited on page 6*

[22] Canales, D., Leygue, A., Chinesta, F., Alfaro, I., González, D., Cueto, E., Feulvarch, E., and Bergheau, J.-M. (2016a). In-plane/out-of-plane separated representations of updated lagrangian descriptions of viscoplastic flow models in plate domains. *Comptes Rendus Mécanique*, 344(4):225–235. *cited on page 20*

[23] Canales, D., Leygue, A., Chinesta, F., González, D., Cueto, E., Feulvarch, E., Bergheau, J. M., and Huerta, A. (2016b). Vademecum-based GFEM (V-GFEM): optimal enrichment for transient problems. *International Journal for Numerical Methods in Engineering*, 108(9):971–989. *cited on page 31 and 48*

[24] Cancès, E., Defranceschi, M., Kutzelnigg, W., Le Bris, C., and Maday, Y. (2003). Computational quantum chemistry: a primer. In *Handbook of Numerical Analysis X. Special volume: Computational chemistry.*, pages 3–270. Amsterdam: North-Holland. *cited on page 4*

[25] Carroll, J. D. and Chang, J.-J. (1970). Analysis of individual differences in multidimensional scaling via an n-way generalization of "eckart-young" decomposition. *Psychometrika*, 35(3):283–319. *cited on page 9*

[26] Chatterjee, A. (2000). An introduction to the proper orthogonal decomposition. *Current Science*, 78(7):808–817. *cited on page 5*

[27] Chen, Y., Hesthaven, J. S., Maday, Y., and Rodríguez, J. (2009). Improved successive constraint method based a posteriori error estimate for reduced basis approximation of 2D Maxwell's problem. *ESAIM - Mathematical Modelling and Numerical Analysis*, 43(6):1099–1116. *cited on page 8*

[28] Chinesta, F., Ammar, A., Leygue, A., and Keunings, R. (2011a). An overview of the proper generalized decomposition with applications in computational rheology. *Journal of Non-Newtonian Fluid Mechanics*, 166(11):578–592. *cited on page 20*

[29] Chinesta, F., Keunings, R., and Leygue, A. (2014a). The proper generalized decomposition for advanced numerical simulations: A primer. In *SpringerBriefs in Applied Sciences and Technology*. *cited on page 5, 9 and 21*

[30] Chinesta, F., Ladevèze, P., and Cueto, E. (2011b). A Short Review on Model Order Reduction Based on Proper Generalized Decomposition. *Archives of Computational Methods in Engineering*, 18:395–404. *cited on page 5, 9 and 73*

[31] Chinesta, F., Leygue, A., Bognet, B., Ghnatios, C., Poulhaon, F., Bordeu, F., Barasinski, A., Poitou, A., Chatel, S., and Maison-Le-Poec, S. (2014b). First steps towards an advanced simulation of composites manufacturing by automated tape placement. *International Journal of Material Forming*, 7(1):81–92. *cited on page 20*

[32] Chinesta, F., Leygue, A., Bordeu, F., Aguado, J. V., Cueto, E., González, D., Alfaro, I., Ammar, A., and Huerta, A. (2013). PGD-Based Computational Vademecum for Efficient Design, Optimization and Control. *Archives of Computational Methods in Engineering*, 20(1):31–59. *cited on page 5 and 9*

[33] Cotin, S., Delingette, H., and Ayache, N. (1999). Real-time elastic deformations of soft tissues for surgery simulation. *IEEE Transactions on Visualization and Computer Graphics*, 5(1):62–73. *cited on page 5*

[34] Courard, A., Néron, D., Ladevèze, P., and Ballere, L. (2016). Integration of PGD-virtual charts into an engineering design process. *Computational Mechanics*, 57(4):637–651. *cited on page 28*

[35] Digonnet, H., Coupez, T., Laure, P., and Silva, L. (2019). Massively parallel anisotropic mesh adaptation. *International Journal of High Performance Computing Applications*, 33(1):3–24. *cited on page 4*

[36] Digonnet, H., Silva, L., and Coupez, T. (2015). Using full tier supercomputers for finite element computations with adaptive meshing. *Civil-Comp Proceedings*, 107. *cited on page 4*

[37] Duarte, C., Hamzeh, O., Liszka, T., and Tworzydlo, W. (2001). A generalized finite element method for the simulation of three-dimensional dynamic crack propagation. *Computer Methods in Applied Mechanics and Engineering*, 190(15-17):2227–2262. *cited on page 31 and 47*

[38] Duarte, C. and Oden, J. (1996). An h-p adaptive method using clouds. *Computer Methods in Applied Mechanics and Engineering*, 139(1-4):237–262. *cited on page 26, 31 and 32*

[39] Duarte, C. A. and Babuška, I. (2002). Mesh-independent p-orthotropic enrichment using the generalized finite element method. *International Journal for Numerical Methods in Engineering*, 55(12):1477–1492. *cited on page 31*

[40] Duarte, C. A., Babuška, I., and Oden, J. T. (2000). Generalized finite element methods for three-dimensional structural mechanics problems. *Computers and Structures*, 77(2):215–232. *cited on page 26 and 31*

[41] Duarte, C. A. and Kim, D. J. (2008). Analysis and applications of a generalized finite element method with global-local enrichment functions. *Computer Methods in Applied Mechanics and Engineering*, 197(6):487–504. *cited on page 27, 31 and 47*

[42] Falcó, A. and Nouy, A. (2011). A Proper Generalized Decomposition for the solution of elliptic problems in abstract form by using a functional Eckart-Young approach. *Journal of Mathematical Analysis and Applications*, 376(2):469–480. *cited on page 11 and 13*

[43] Gagliardi, M., Lenarda, P., and Paggi, M. (2017). A reaction-diffusion formulation to simulate eva polymer degradation in environmental and accelerated ageing conditions. *Solar Energy Materials and Solar Cells*, 164:93 – 106. *cited on page 5*

[44] Gallimard, L., Vidal, P., and Polit, O. (2013). Coupling finite element and reliability analysis through proper generalized decomposition model reduction. *International Journal for Numerical Methods in Engineering*, 95(13):1079–1093. *cited on page 20*

[45] Garzon, J., Gupta, V., Simone, A., and Duarte, C. (2012). Bridging Scales with a Generalized Finite Element Method. *Procedia IUTAM*, 3:172–191. *cited on page 27, 31 and 47*

[46] Ghnatios, C., Abisset, E., Ammar, A., Cueto, E., Duval, J.-L., and Chinesta, F. (2019). Advanced separated spatial representations for hardly separable domains. *Computer Methods in Applied Mechanics and Engineering*, 354:802 – 819. *cited on page 101*

[47] Ghnatios, C., Ammar, A., Cimetiere, A., Hamdouni, A., Leygue, A., and Chinesta, F. (2013). First Steps in the Space Separated Representation of Models Defined in Complex Domains. pages 37–42. ASME International. *cited on page 27*

[48] Ghnatios, C., Chinesta, F., and Binetruy, C. (2015). 3D Modeling of squeeze flows occurring in composite laminates. *International Journal of Material Forming*, 8:73–83. *cited on page 20*

[49] Giner, E., Bognet, B., Ródenas, J., Leygue, A., Fuenmayor, J., and Chinesta, F. (2013). The Proper Generalized Decomposition (PGD) as a numerical procedure to solve 3D cracked plates in linear elastic fracture mechanics. *International Journal of Solids and Structures*, 50(10):1710–1720. *cited on page 20*

[50] González, D., Ammar, A., Chinesta, F., and Cueto, E. (2010). Recent advances on the use of separated representations. *International Journal for Numerical Methods in Engineering*, 81(5):637–659. *cited on page 17 and 27*

[51] Grasedyck, L., Kressner, D., and Tobler, C. (2013). A literature survey of low-rank tensor approximation techniques. *GAMM-Mitteilungen*, 36(1):53–78. *cited on page 9*

[52] Hackbusch, W. and Kühn, S. (2009). A new scheme for the tensor representation. *Journal of Fourier Analysis and Applications*, 15(5):706–722. *cited on page 9*

[53] Hamdaoui, M., Le Quilliec, G., Breitkopf, P., and Villon, P. (2014). POD surrogates for real-time multi-parametric sheet metal forming problems. *International Journal of Material Forming*, 7(3):337–358. *cited on page 6*

[54] Haouchine, N., Cotin, S., Peterlik, I., Dequidt, J., López, M. S., Kerrien, E., and Berger, M. (2015). Impact of soft tissue heterogeneity on augmented reality for liver surgery. *IEEE Transactions on Visualization and Computer Graphics*, 21(5):584–597. *cited on page 5*

[55] Haouchine, N., Dequidt, J., Berger, M.-O., and Cotin, S. (2015). Monocular 3d reconstruction and augmentation of elastic surfaces with self-occlusion handling. *IEEE Transactions on Visualization and Computer Graphics*, 21(12):1363–1376. *cited on page 5*

[56] Harshman, R. A. (1970). Foundations of the parafac procedure: Models and conditions for an "explanatory" multi-model factor analysis. *UCLA working papers in phonetics*, 16(12):1–84. *cited on page 9*

[57] Heyberger, C., Boucard, P.-A., and Néron, D. (2012). Multiparametric analysis within the proper generalized decomposition framework. *Computational Mechanics*, 49:277–289. *cited on page 4*

[58] Hotelling, H. (1933). Analysis of a complex of statistical variables into principal components. *Journal of Educational Psychology*, 24(6):417–441. *cited on page 6*

[59] Huerta, A., Nadal, E., and Chinesta, F. (2018). Proper generalized decomposition solutions within a domain decomposition strategy. *International Journal for Numerical Methods in Engineering*, 113(13):1972–1994. *cited on page 25*

[60] Huynh, D. B., Knezevic, D. J., Chen, Y., Hesthaven, J. S., and Patera, A. T. (2010). A natural-norm Successive Constraint Method for inf-sup lower bounds. *Computer Methods in Applied Mechanics and Engineering*, 199:1963–1975. *cited on page 8*

[61] Huynh, D. B., Rozza, G., Sen, S., and Patera, A. T. (2007). A successive constraint linear optimization method for lower bounds of parametric coercivity and inf-sup stability constants. *Comptes Rendus Mathématique*, 345(8):473–478. *cited on page 8*

[62] Ibáñez, R., Ammar, A., Cueto, E., Huerta, A., Duval, J.-L., and Chinesta, F. (2019). Multiscale proper generalized decomposition based on the partition of unity. *International Journal for Numerical Methods in Engineering*, 120(6):727–747. *cited on page 25 and 31*

[63] Ibáñez, R., Abisset-Chavanne, E., Chinesta, F., Huerta, A., and Cueto, E. (2019). A local multiple proper generalized decomposition based on the partition of unity. *International Journal for Numerical Methods in Engineering*, 120(2):139–152. *cited on page 25 and 31*

[64] Jia, W., Helenbrook, B. T., and Cheng, M. C. (2016). Fast thermal simulation of FinFET circuits based on a multiblock reduced-order model. *IEEE Transactions on Computer-Aided Design of Integrated Circuits and Systems*, 35(7):1114–1124. *cited on page 23*

[65] Jin, J. (2014). *The Finite Element Method in Electromagnetics*. Wiley-IEEE Press, 3rd edition. *cited on page 5*

[66] Ladevèze, P. and Chamoin, L. (2011). On the verification of model reduction methods based on the proper generalized decomposition. *Computer Methods in Applied Mechanics and Engineering*, 200(23-24):2032–2047. *cited on page 72*

[67] Ladevèze, P. and Germain, P. (1989). La méthode à grand incrément de temps pour l'analyse de structures à comportement non linéaire décrit par variables internes. *Comptes rendus de l'Académie des sciences. Série 2, Mécanique, Physique, Chimie, Sciences de l'univers, Sciences de la Terre*, 309(11):1095–1099. *cited on page 9 and 25*

[68] Ladevèze, P., Passieux, J. C., and Néron, D. (2010). The LATIN multiscale computational method and the Proper Generalized Decomposition. *Computer Methods in Applied Mechanics and Engineering*, 199(21-22):1287–1296. *cited on page 9 and 25*

[69] Le Bris, C. and Lions, P. (2005). From atoms to crystals: A mathematical journey. *Bulletin (New Series) of the American Mathematical Society*, 42(3):1287–1296. *cited on page 4*

[70] León, Á., Barasinski, A., Abisset-Chavanne, E., Cueto, E., and Chinesta, F. (2018). Wavelet-based multiscale proper generalized decomposition. *Comptes Rendus Mécanique*, 346(7):485–500. *cited on page 25*

[71] Liang, Y. C., Lee, H. P., Lim, S. P., Lin, W. Z., Lee, K. H., and Wu, C. G. (2002). Proper orthogonal decomposition and its applications - Part I: Theory. *Journal of Sound and Vibration*, 252(3):527–544. *cited on page 5*

[72] Loève, M. (1965). *Fonctions aléatoires du second ordre, in: Processus stochastiques et mouvement Brownien*. Gauthier-Villars, Paris, 2nd edition. *cited on page 6*

[73] Løvgren, A. E., Maday, Y., and Rønquist, E. M. (2006). A reduced basis element method for the steady Stokes problem. *ESAIM: Mathematical Modelling and Numerical Analysis*, 40(3):529–552. *cited on page 23*

[74] Maday, Y. and Rønquist, E. M. (2002). A reduced-basis element method. *Comptes Rendus Mathématique*, 335(2):195–200. *cited on page 5 and 23*

[75] Maday, Y. and Ronquist, E. M. (2004). The Reduced Basis Element Method: Application to a Thermal Fin Problem. *SIAM Journal on Scientific Computing*, 26:240–258. *cited on page 7 and 23*

[76] Melenk, J. and Babuška, I. (1996). The partition of unity finite element method: Basic theory and applications. *Computer Methods in Applied Mechanics and Engineering*, 139(1-4):289–314. *cited on page 31 and 32*

[77] Mena, A., Bel, D., Alfaro, I., González, D., Cueto, E., and Chinesta, F. (2015). Towards a pancreatic surgery simulator based on model order reduction. *Advanced Modeling and Simulation in Engineering Sciences*, 2(1). *cited on page 5*

[78] Merle, R. and Dolbow, J. (2002). Solving thermal and phase change problems with the eXtended finite element method. *Computational Mechanics*, 28(5):339–350. *cited on page 47*

[79] Metoui, S., Prulière, E., Ammar, A., Dau, F., and Iordanoff, I. (2014). The proper generalized decomposition for the simulation of delamination using cohesive zone model. *International Journal for Numerical Methods in Engineering*, 99(13):1000–1022. *cited on page 20*

[80] Meyer, D. S., Helenbrook, B. T., and Cheng, M. C. (2017). Proper orthogonal decomposition-based reduced basis element thermal modeling of integrated circuits. *International Journal for Numerical Methods in Engineering*, 112(5):479–500. *cited on page 23*

[81] Michel, J., Moulinec, H., and Suquet, P. (1999). Effective properties of composite materials with periodic microstructure: a computational approach. *Computer Methods in Applied Mechanics and Engineering*, 172(1-4):109–143. *cited on page 5*

[82] Moës, N., Dolbow, J., and Belytschko, T. (1999). A finite element method for crack growth without remeshing. *International Journal for Numerical Methods in Engineering*, 46:131–150. *cited on page 31 and 47*

[83] Nazeer, S. M., Bordeu, F., Leygue, A., and Chinesta, F. (2014). Arlequin based PGD domain decomposition. *Computational Mechanics*, 54:1175–1190. *cited on page 25*

[84] Néron, D., Dhia, H., and Cottereau, R. (2016). A decoupled strategy to solve reduced-order multimodel problems in the pgd and arlequin frameworks. *Computational Mechanics*, 57(4):509–521. *cited on page 25*

[85] Néron, D. and Ladevèze, P. (2010). Proper Generalized Decomposition for Multiscale and Multiphysics Problems. *Archives of Computational Methods in Engineering*, 17(4):351–372. *cited on page 9 and 25*

[86] Niroomandi, S., Alfaro, I., González, D., Cueto, E., and Chinesta, F. (2012). Real-time simulation of surgery by reduced-order modeling and x-fem techniques. *International Journal for Numerical Methods in Biomedical Engineering*, 28(5):574–588. *cited on page 5*

[87] Noor, A. K. (1986). Global-local methodologies and their application to nonlinear analysis. *Finite Elements in Analysis and Design*, 2(4):333–346. *cited on page 47*

[88] Nouy, A. and Ladevèze, P. (2005). Multiscale Computational Strategy With Time and Space Homogenization: A Radial-Type Approximation Technique for Solving Micro-problems. *International Journal for Multiscale Computational Engineering*, 2(4):557–574. *cited on page 9 and 25*

[89] Oden, J. T., Duarte, C. A., and Zienkiewicz, O. C. (1998). A new cloud-based hp finite element method. *Computer Methods in Applied Mechanics and Engineering*, 153(1):117–126. *cited on page 26 and 31*

[90] Paillet, C., Néron, D., and Ladevèze, P. (2018). A door to model reduction in high-dimensional parameter space. *Comptes Rendus Mécanique*, 346(7):524–531. *cited on page 4*

[91] Park, H. M. and Cho, D. H. (1996). The use of the Karhunen-Loève decomposition for the modeling of distributed parameter systems. *Chemical Engineering Science*, 51:81–98. *cited on page 6*

[92] Passieux, J. C., Ladevèze, P., and Néron, D. (2010). A scalable time-space multiscale domain decomposition method: Adaptive time scale separation. *Computational Mechanics*, 46(4):621–633. *cited on page 9 and 25*

[93] Pinnau, R. (2008). *Model Reduction via Proper Orthogonal Decomposition*, pages 95–109. Springer Berlin Heidelberg, Berlin, Heidelberg. *cited on page 5*

[94] Plews, J. and Duarte, C. A. (2015). Generalized finite element approaches for analysis of localized thermo-structural effects: Gfem for analysis of localized thermo-structural effects. *International Journal for Numerical Methods in Engineering*, 104:1–50. *cited on page ix, 44 and 45*

[95] Quarteroni, A. (2017). *Domain decomposition methods*, pages 555–612. Springer International Publishing, Cham. *cited on page 23 and 24*

[96] Quarteroni, A., Manzoni, A., and Negri, F. (2015). *Reduced Basis Methods for Partial Differential Equations: An Introduction*. Springer International Publishing. *cited on page 5 and 7*

[97] Quarteroni, A. and Valli, A. (1999). *Domain Decomposition Methods for Partial Differential Equations*. Numerical mathematics and scientific computation. Clarendon Press. *cited on page 23 and 24*

[98] Quesada, C., Alfaro, I., González, D., Chinesta, F., and Cueto, E. (2018). Haptic simulation of tissue tearing during surgery. *International Journal for Numerical Methods in Biomedical Engineering*, 34(3). *cited on page 5*

[99] Quesada, C., González, D., Alfaro, I., Cueto, E., and Chinesta, F. (2016). Computational vademecums for real-time simulation of surgical cutting in haptic environments. *International Journal for Numerical Methods in Engineering*, 108(10):1230–1247. *cited on page 5*

[100] Ransom, J. and Knight, N. (1990). Global/local stress analysis of composite panels. *Computers & Structures*, 37(4):375 – 395. *cited on page 47*

[101] Rautio, J. (1992). Some comments on electromagnetic dimensionality. *IEEE M-TTS Newsl*, page 23. *cited on page 5*

[102] Silva, L., Coupez, T., and Digonnet, H. (2016). Massively parallel mesh adaptation and linear system solution for multiphase flows. *International Journal of Computational Fluid Dynamics*, 30(6):431–436. *cited on page 4*

[103] Simone, A. (2007). Partition of unity-based discontinuous finite elements: Gfem, pufem, xfem. *Revue Européenne de Génie Civil*, 11(7-8):1045–1068. *cited on page 31 and 32*

[104] Simone, A., Duarte, C., and Van der Giessen, E. (2006). A generalized finite element method for polycrystals with discontinuous grain boundaries. *International Journal for Numerical Methods in Engineering*, 67(8):1122–1145. *cited on page 31*

[105] Strouboulis, T., Babuška, I., and Copps, K. (2000). The design and analysis of the Generalized Finite Element Method. *Computer Methods in Applied Mechanics and Engineering*, 181(1-3):43–69. *cited on page 26 and 31*

[106] Strouboulis, T., Copps, K., and Babuška, I. (2001). The generalized finite element method. *Computer Methods in Applied Mechanics and Engineering*, 190(32-33):4081–4193. *cited on page 26 and 31*

[107] Sukumar, N., Chopp, D., Moës, N., and Belytschko, T. (2001). Modeling holes and inclusions by level sets in the extended finite-element method. *Computer Methods in Applied Mechanics and Engineering*, 190(46-47):6183–6200. *cited on page 31*

[108] Sukumar, N., Moës, N., Moran, B., and Belytschko, T. (2000). Extended finite element method for three-dimensional crack modelling. *International Journal for Numerical Methods in Engineering*, 48(11):1549–1570. *cited on page 31*

[109] Sun, C. and Mao, K. (1988). A global-local finite element method suitable for parallel computations. *Computers & Structures*, 29(2):309–315. *cited on page 47*

[110] Tertrais, H., Ibáñez, R., Barasinski, A., Ghnatios, C., and Chinesta, F. (2019). On the proper generalized decomposition applied to microwave processes involving multilayered components. *Mathematics and Computers in Simulation*, 156:347 – 363. *cited on page 5*

[111] Tucker, L. R. (1964). The extension of factor analysis to three-dimensional matrices. In Gulliksen, H. and Frederiksen, N., editors, *Contributions to mathematical psychology.*, pages 110–127. Holt, Rinehart and Winston, New York. *cited on page 9*

[112] Uschmajew, A. (2012). Local convergence of the alternating least squares algorithm for canonical tensor approximation. *SIAM Journal on Matrix Analysis and Applications*, 33(2):639–652. *cited on page 73*

[113] Vidal, P., Gallimard, L., and Polit, O. (2012). Composite beam finite element based on the Proper Generalized Decomposition. *Computers & Structures*, 102-103:76–86. *cited on page 20*

[114] Vidal, P., Gallimard, L., and Polit, O. (2013). Proper Generalized Decomposition and layer-wise approach for the modeling of composite plate structures. *International Journal of Solids and Structures*, 50(14-15):2239–2250. *cited on page 20*

[115] Vidal, P., Gallimard, L., and Polit, O. (2014a). Explicit solutions for the modeling of laminated composite plates with arbitrary stacking sequences. *Composites Part B: Engineering*, 60:697–706. *cited on page 20*

[116] Vidal, P., Gallimard, L., and Polit, O. (2014b). Shell finite element based on the Proper Generalized Decomposition for the modeling of cylindrical composite structures. *Computers & Structures*, 132:1–11. *cited on page 20*

[117] Vidal, P., Gallimard, L., and Polit, O. (2015). Assessment of variable separation for finite element modeling of free edge effect for composite plates. *Composite Structures*, 123:19–29. *cited on page 20*

[118] Wang, P., Becker, A., Jones, I., Glover, A., Benford, S., Greenhalgh, C., and Vloeberghs, M. (2007). Virtual reality simulation of surgery with haptic feedback based on the boundary element method. *Computers and Structures*, 85(7):331 – 339. *cited on page 5*

[119] Zou, X., Conti, M., DÃez, P., and Auricchio, F. (2018). A non-intrusive proper generalized decomposition scheme with application in biomechanics. *International Journal for Numerical Methods in Engineering*, 113(2):230–251. *cited on page 28*

Appendices

Appendix A

Formulation for the 1D steady reaction-diffusion equation

We can consider the equation:

$$\Delta u - \lambda u + \lambda f = 0 \tag{A.1}$$

The aim is to enrich a FEM solution obtained over a coarse FEM mesh, therefore the temperature field is defined as the sum of the coarse solution u_{fem} and the enrichment obtained by using the PGD, u_{enr}:

$$u = u_{\text{fem}} + u_{\text{enr}} \tag{A.2}$$

If we introduce Eq. (A.2) into Eq. (A.1), the steady reaction-diffusion equation equation now reads

$$\Delta u_{\text{fem}} + \Delta u_{\text{enr}} - \lambda u_{\text{fem}} - \lambda u_{\text{enr}} + \lambda f = 0. \tag{A.3}$$

When only considering Dirichlet boundary conditions at a 1D generic domain Ω and for all suitable test functions u^*, the weak form of Eq. (3.15) is defined as follows:

$$\int_\Omega u^* (\Delta u_{\text{fem}} + \Delta u_{\text{enr}} - \lambda u_{\text{fem}} - \lambda u_{\text{enr}} + \lambda f)\, d\Omega = 0, \tag{A.4}$$

or more specifically,

$$\int_\Omega \nabla u^* \cdot (\nabla u_{\text{fem}} + \nabla u_{\text{enr}})\, d\Omega + \int_\Omega u^* (\lambda u_{\text{fem}} + \lambda u_{\text{enr}})\, d\Omega = \int_\Omega u^* \lambda f\, d\Omega \tag{A.5}$$

A.1 Global problem

When considering the definition of u_{enr} and ∇u_{enr} used in Eq. (3.20) and Eq. (3.21), their simplification Eq. (3.22) and Eq. (3.23) (after introducing the operators $\hat{N}_i$, $\hat{B}^I_{G,i}$ and $\hat{B}^{II}_{G,i}$)

and the expressions concerning the test function u^* (Eq. (3.24)) and ∇u^* (Eq. (3.25)), the weak form Eq. (3.19) now reads:

$$\sum_{i\in I_{\text{enr}}} g_j^* \int_\Omega \left(\hat{B}_{G,j}^I + \hat{B}_{G,j}^{II}\right) \cdot \left(\hat{B}_{G,i}^I + \hat{B}_{G,i}^{II}\right) d\Omega\, g_i + \lambda \sum_{i\in I_{\text{enr}}} g_j^* \int_\Omega \hat{N}_j\, \hat{N}_i\, d\Omega\, g_i =$$
$$= \lambda\, g_j^* \int_\Omega \hat{N}_j\, (f - u_{\text{fem}})\, d\Omega - g_j^* \int_\Omega \left(\hat{B}_{G,j}^I + \hat{B}_{G,j}^{II}\right) \cdot \nabla u_{\text{fem}}\, d\Omega, \qquad \forall j \in I_{\text{enr}}, \tag{A.6}$$

where the operators $\hat{N}_i$, $\hat{B}_{G,i}^I$ and $\hat{B}_{G,i}^{II}$ depend on the shape functions and a known value of the local variable at a given enrichment step and its corresponding fixed point iteration. The only unknown is the global variable.

Now, by performing the integration process and considering that the integrals are calculated by using the Gauss quadrature associated with the local discretization (as commented in Section 3.2.3.2), Eq. (A.6) can be turned into the following set of elemental matrices (here we refer to macro-elements):

$$\begin{aligned}
\boldsymbol{K}_G^{I,e} &\equiv \int_{\Omega^e} \hat{B}_{G,i}^I \cdot \hat{B}_{G,j}^I\, d\Omega^e, \\
\boldsymbol{K}_G^{II,e} &\equiv \int_{\Omega^e} \hat{B}_{G,i}^I \cdot \hat{B}_{G,j}^{II}\, d\Omega^e, \\
\boldsymbol{K}_G^{III,e} &\equiv \int_{\Omega^e} \hat{B}_{G,i}^{II} \cdot \hat{B}_{G,j}^I\, d\Omega^e, \\
\boldsymbol{K}_G^{IV,e} &\equiv \int_{\Omega^e} \hat{B}_{G,i}^{II} \cdot \hat{B}_{G,j}^{II}\, d\Omega^e \\
\boldsymbol{K}_G^{V,e} &\equiv \int_{\Omega^e} \hat{N}_i\, \hat{N}_j\, d\Omega^e.
\end{aligned} \tag{A.7}$$

The elemental Laplacian matrix at the global level is:

$$\boldsymbol{K}_G^e = \boldsymbol{K}_G^{I,e} + \boldsymbol{K}_G^{II,e} + \boldsymbol{K}_G^{III,e} + \boldsymbol{K}_G^{IV,e} + \lambda\, \boldsymbol{K}_G^{V,e}. \tag{A.8}$$

Likewise, for the right hand side term, the following operators are introduced, including the computation of the initial coarse mesh solution and the source term:

$$\begin{aligned}
\boldsymbol{b}_G^{I,e} &\equiv \int_{\Omega^e} \hat{N}_j\, (f - u_{\text{fem}})\, d\Omega^e, \\
\boldsymbol{b}_G^{II,e} &\equiv \int_{\Omega^e} \left(\hat{B}_{G,j}^I + \hat{B}_{G,j}^{II}\right) \cdot \nabla u_{\text{fem}}\, d\Omega^e,
\end{aligned} \tag{A.9}$$

which delivers the vector of nodal equivalent fluxes:

$$\boldsymbol{b}_G^e = \lambda\, \boldsymbol{b}_G^{I,e} - \boldsymbol{b}_G^{II,e}. \tag{A.10}$$

Both the Laplacian matrix and the nodal fluxes vector at the macro-element level can be brought to the global numbering by following a standard finite element assembling process. Finally, the global problem can be solved by following Eq. (3.31) where $\boldsymbol{g}$ collects the nodal values g_i, for $i \in I_{\text{enr}}$, of the global function at the macro-mesh.

A.2 Local problem

Likewise, now the objective is to obtain the local variable from a previously obtained global variable at a given enrichment step and its corresponding fixed point iteration. When considering the expressions of u_{enr} and ∇u_{enr} used in Eq. (3.33) and Eq. (3.34) (after introducing the operators $\hat{M}_k$, $\hat{B}^I_{L,k}$ and $\hat{B}^{II}_{L,k}$) and the expressions concerning the test function u^* (Eq. (3.38)) and ∇u^* (Eq. (3.39)), the weak form Eq. (3.19) now reads:

$$\sum_{k\in I_{\text{loc}}} l^{j*} \int_\Omega \left(\hat{B}^I_{L,j} + \hat{B}^{II}_{L,j}\right) \cdot \left(\hat{B}^I_{L,k} + \hat{B}^{II}_{L,k}\right) d\Omega\, l^k + \lambda \sum_{k\in I_{\text{loc}}} l^{j*} \int_\Omega \hat{M}_j\, \hat{M}_k\, d\Omega\, l^k =$$
$$= l^{j*} \int_\Omega \hat{M}_j\, (f - u_{\text{fem}})\, d\Omega - l^{j*} \int_\Omega \left(\hat{B}^I_{L,j} + \hat{B}^{II}_{L,j}\right) \cdot \nabla u_{\text{fem}}\, d\Omega, \qquad \forall j \in I_{\text{loc}}, \quad \text{(A.11)}$$

where the operators $\hat{M}_k$, $\hat{B}^I_{L,k}$ and $\hat{B}^{II}_{L,k}$ depend on the shape functions and a known value of the global variable.

Now, by performing the integration process, Eq. (A.11) can be turned into the following set of elemental matrices (here we refer to elements at the reference local support):

$$\begin{aligned}
\boldsymbol{K}^{I,e}_L &\equiv \int_{\Omega^e} \hat{B}^I_{L,j} \cdot \hat{B}^I_{L,k}\, d\Omega^e \\
\boldsymbol{K}^{II,e}_L &\equiv \int_{\Omega^e} \hat{B}^I_{L,j} \cdot \hat{B}^{II}_{L,k}\, d\Omega^e \\
\boldsymbol{K}^{III,e}_L &\equiv \int_{\Omega^e} \hat{B}^{II}_{L,j} \cdot \hat{B}^I_{L,k}\, d\Omega^e \\
\boldsymbol{K}^{IV,e}_L &\equiv \int_{\Omega^e} \hat{B}^{II}_{L,j} \cdot \hat{B}^{II}_{L,k}\, d\Omega^e \\
\boldsymbol{K}^{V,e}_L &\equiv \int_{\Omega^e} \hat{M}_j\, \hat{M}_k\, d\Omega^e.
\end{aligned} \quad \text{(A.12)}$$

The elemental Laplacian matrix at the local level is:

$$\boldsymbol{K}^e_L = \boldsymbol{K}^{I,e}_L + \boldsymbol{K}^{II,e}_L + \boldsymbol{K}^{III,e}_L + \boldsymbol{K}^{IV,e}_L + \lambda\, \boldsymbol{K}^{V,e}_L. \quad \text{(A.13)}$$

Likewise on the right-hand side, integration can be carried out:

$$\begin{aligned}
\boldsymbol{b}^{I,e}_L &\equiv \int_{\Omega^e} \hat{M}_j\, (f - u_{\text{fem}})\, d\Omega^e \\
\boldsymbol{b}^{II,e}_L &\equiv \int_{\Omega^e} \left(\hat{B}^I_{L,j} + \hat{B}^{II}_{L,j}\right) \cdot \nabla u_{\text{fem}}\, d\Omega^e
\end{aligned} \quad \text{(A.14)}$$

which delivers the vector of nodal equivalent fluxes:

$$\boldsymbol{b}_L^e = \lambda\, \boldsymbol{b}_L^{I,e} - \boldsymbol{b}_L^{II,e}. \tag{A.15}$$

Both the Laplacian matrix and the nodal fluxes vector at the support element level can be brought to the local numbering by following a standard finite element assembly process. Finally, the local problem can be solved following 3.45, where $\boldsymbol{l}$ collects the nodal values l^k, for $k \in I_{\text{loc}}$, of the local function at the reference support mesh.

Appendix B

Coefficients definition for alternating directions optimization

Coefficients $\beta_*^r \in \mathbb{R}$, $\tilde{\boldsymbol{\alpha}}_*^r \in \mathbb{R}^M$ and $\tilde{\boldsymbol{\gamma}}_* \in \mathbb{R}^S$ in Eq. (4.7) are defined as follows:

$$\beta_*^r := \prod_{d=0, d\neq *}^{D} \langle \boldsymbol{A}_*^r \boldsymbol{v}_*, \boldsymbol{v}_* \rangle_* \,,$$

$$\tilde{\boldsymbol{\alpha}}_*^r := \boldsymbol{\alpha} \circ \left(\bigodot_{d=0, d\neq *}^{D} \langle \boldsymbol{A}_*^r \boldsymbol{W}_*, \boldsymbol{v}_* \rangle_* \right)^T \quad \text{and}$$

$$\tilde{\boldsymbol{\gamma}}_* := \boldsymbol{\gamma} \circ \left(\bigodot_{d=0, d\neq *}^{D} \langle \boldsymbol{V}_*, \boldsymbol{v}_* \rangle_* \right)^T ,$$

where "$\bullet^T$" denotes the transpose and "$\circ$" stands for the Hadamard (component-wise) product. Recall that $\boldsymbol{\alpha}$ contains the representation coefficients of the rank-M approximation of the solution, while $\boldsymbol{\gamma}$ are the representation coefficients of the rank-S representation of the non-linear term. See Eq. (4.3) and Eq. (4.5), respectively.

Using the coefficients defined above, we can define the following quantities:

$$\tilde{\boldsymbol{A}}_* := \sum_{r=1}^{R} \beta_*^r \boldsymbol{A}_*^r \quad \text{and} \quad \tilde{\boldsymbol{b}}_* := -\sum_{r=1}^{R} \boldsymbol{A}_*^r \boldsymbol{W}_* \tilde{\boldsymbol{\alpha}}_*^r - \boldsymbol{V}_* \tilde{\boldsymbol{\gamma}}_*,$$

that can be introduced in Eq. (4.7), leading to the following minimization problem:

$$\boldsymbol{w}_* = \arg \min_{\boldsymbol{v}_* \in \mathbb{R}^{N_*}} \frac{1}{2} \langle \tilde{\boldsymbol{A}}_* \boldsymbol{v}_*, \boldsymbol{v}_* \rangle_* + \langle \tilde{\boldsymbol{b}}_*, \boldsymbol{v}_* \rangle_*, \tag{B.1}$$

whose solution is $\boldsymbol{w}_* = \tilde{\boldsymbol{A}}_*^{-1}\,\tilde{\boldsymbol{b}}_*$.

UNIVERSITE BRETAGNE SCIENCES LOIRE POUR L'INGENIEUR

CENTRALE NANTES

Titre : Développement de représentations séparées de type global-local dans le cadre de la méthode « Proper Generalized Decomposition »

Mots clés : PGD, Global-Local, Représentations Séparées, Non-Intrusif, Partition de l'Unité.

Résumé : L'un des principaux avantages de la méthode «Proper Generalized Decomposition», par rapport à d'autres méthodes de réduction de modèles, réside dans son adéquation pour calculer des représentations séparées dans l'espace pour des domaines dégénérés de type cartésien, tels que des plaques ou des coques. L'objectif principal de cette thèse est de généraliser les représentations séparées dans l'espace aux domaines non cartésiens, en introduisant la notion de représentations séparées. Les représentations séparées de type global-local peuvent être comprises comme une décomposition multiplicative dans laquelle les modes locaux capturent la solution à une échelle fine, tandis que les modes globaux résolvent une échelle grossière.

Pour ce faire, deux stratégies sont proposées. La première proposition est basée sur la partition de l'unité et combine les niveaux de discrétisation globale et locale, basés sur une partition du domaine. Cette approche construit une représentation séparée qui fournit l'enrichissement local, sans qu'il soit nécessaire de connaître a priori la solution, ni de mettre en œuvre des problèmes locaux auxiliaires pour déterminer l'enrichissement.

La deuxième stratégie est consacrée à la construction de représentations séparées de type global-local de manière moins intrusive, compatible avec le standard des éléments finis.
Par conséquent, nous nous basons sur l'assemblage FEM standard des opérateurs et utilisons la PGD comme résolveur algébrique itératif. La continuité sur les limites de la partition du domaine n'a pas besoin d'être imposée explicitement, car elle constitue une propriété intégrée dans les opérateurs FEM.

Title : Global-local separated representations based on the Proper Generalized Decomposition

Keywords : PGD, Global-Local, Separated Representations, Non-Intrusive, Partition of Unity.

Abstract : One of the main advantages of the Proper Generalized Decomposition method, when compared to other model reduction methods, lies in its adequacy to compute space separated representations in Cartesian-like degenerated domains, such as plates or shells. The main objective of this thesis is to generalize space separated representations to non-Cartesian domains, by introducing the notion of Global-Local separated representations. Global-Local separated representations can be understood as a multiplicative decomposition in which the local modes capture the solution at the finer scale, while the global modes solve the coarser scale.

To this aim, two strategies are proposed. The first proposal is based on the partition of unity, and combines the global and local discretization levels, based on a partition of the domain. It builds a separated representation that provides the local enrichment, without the need for a priori knowledge of the solution, nor the implementation of auxiliary local problems to determine the enrichment.

The second strategy is devoted to the construction of Global-Local separated representations in a less intrusive manner, compatible with the finite element standard. Therefore, we rely on standard FEM assembly of the operators and use the PGD as an algebraic iterative solver. Continuity on the boundaries of the domain's partition does not need to be imposed explicitly, as it comes as a built-in property of the FEM operators.